Thiatriazines: Building Blocks towards Molecular Materials

Elizabeth Kleisath

A thesis submitted to the
Faculty of Graduate and Postdoctoral Studies
In partial fulfillment of the requirements for the
Master's degree in Science

Department of Chemistry and Biomolecular Sciences
Faculty of Science
University of Ottawa

Abstract

Post-functionalization of 3,5-*bis*(2-pyridyl)-4-hydro-1,2,4,6-thiatriazine (**Py$_2$TTAH**) and its synthetic precursors have been explored through alkylation, arylation, and coordination. While alkylation was initially pursued at the central nitrogen atom of **Py$_2$TTAH**, functionalization instead occurred on the sulfur atom. Consequently, the proclivity of the sulfur towards alkylation and arylation was studied. Neutral 3,5-*bis*(2-pyridyl)-*S*-methyl-1,2,4,6-thiatriazine (***S*-Me-Py$_2$TTA**) and 3,5-*bis*(2-pyridyl)-*S*-ethyl-1,2,4,6-thiatriazine were achieved *via* either anionic or cationic intermediates, and all isolable species were fully characterized. In addition, an aromatic derivative, 3,5-*bis*(2-pyridyl)-*S*-phenyl-1,2,4,6-thiatriazine was obtained through reactions using hypervalent iodide as an electrophile.

Functionalization of **Py$_2$TTAH** and ***S*-Me-Py$_2$TTA** was also explored through coordination with iron. The synthesis and crystal structures of two different iron complexes are described. The incorporation of boron with **Py$_2$TTAH** and its precursor, *N*-2-pyridylimidoyl-2-pyridylamidine was also considered. Both compounds afforded the same boratriazine ring.

Overall, this thesis describes the groundwork for future functionalization of the **Py$_2$TTA** framework, and its potential for molecular materials applications.

This thesis is dedicated to my parents, Chris and Barb

who taught me to keep on dreaming and never give up.

Acknowledgements

First, I would like to thank my supervisor, Jaclyn Brusso. Thank you so much for everything that you have taught me both in the lab as well as out! Thank you for the guidance and support you have provided over the past two years, and for being an inspiring mentor!

To my parents, Chris and Barb, the words "Thank You" do not even begin to describe my appreciation for all of the support you have given me throughout my entire life. Thank you for encouraging me to pursue my dreams!

My sisters, Susan and Theresa, and my brother Matthew, you guys are awesome! Thank you for always being there with me, enjoying life, and understanding my craziness like only a family can! I can't imagine my life without you guys!

To my friends in chemistry, you have become like a second family to me (I know that's cliché, but it's true). Katie, I'm so glad for all our wine nights, and because I probably wouldn't be where I am today without you; Nathan, you are an inspiration in the lab, and I'm so glad I can count you as my dear friend; Andrew, you are a healthy dose of salt in an otherwise bland dish, and the lab would not be the same without you; François, you have showed me that wizard status is achievable; Irina, I miss our chats and spending time with you, I will be coming to visit you soon; Tom, you were always

able to tell when I needed a break, be it beer, coffee, board games, or just a chat; Terry, for worldly conversations and fun times; Tom, for being a great friend and lab TA partner.

Lauren, Ben, and everyone else at the OHRI, even though you guys aren't in chemistry, you're still pretty awesome! Grad school would not have been the same without you.

To my friends Angela, Rachele, and Lacey, you have always been just a text or a visit away when I needed you, and I am so glad we are friends! Thank you for always being there for me whenever I needed to talk.

Finally, I have to thank Jaclyn, Katie, Nathan, Frank, Andrew, Ben and Susan for taking the time to edit and provide me with feedback on various parts of my thesis during the writing process, as well as Ilia Korobkov and Bulat Gabidullin for collecting and solving my crystal structures.

Table of Contents

Table of Schemes

Chapter 1 — Introduction

Chapter 2 — Progress Towards the Formation of *bis*-*N*-bridgehead-1,2,5-thiadiazolyl Biradicals

Chapter 3 — Sulfur Functionalization of 3,5-*bis*(2-pyridyl)-1,2,4,6-thiatriazine *via* Alkylation and Arylation

Chapter 4 — Iron Coordination with Thiatriazine Ligands

Table of Charts

Table of Figures

Chapter 4 — Iron Coordination with Thiatriazine Ligands

Chapter 5 — Incorporation of Boron into Thiatriazine Precursor Frameworks

Table of Tables

Appendix

List of Abbreviations

$(SN)_x$	Polythiazyl
$[Et_3O][BF_4]$	Triethyloxonium Tetrafluoroborate
[Fe(Py$_2$TTA)$_2$]·THF	An iron compound surrounded by two Py$_2$TTA ligands
[Fe(Py$_2$TTA)Cl$_2$]	An iron compound surrounded by a Py$_2$TTA ligand and two chloride ions
[Fe(Py$_2$TTA)Br$_2$]/	An iron compound surrounded by a Py$_2$TTA ligand and two bromide ions
[Fe(μ-F)(1-oxo-Py$_2$TTA)F]$_\infty$	1D polymer consisting of an iron compound surrounded by an oxidized Py$_2$TTA ligand and three fluoride ions
[Na(μ-I)(*S*-Me-Py$_2$TTA)]$_\infty$	Coordination polymer intermediate to *S*-Me-Py$_2$TTA
$[NH_4][Cl]$	Ammonium chloride
[*S*-Et-Py$_2$TTAH][BF$_4$]	Cationic intermediate to *S*-Et-Py$_2$TTA with counterion
[*S*-Et-Py$_2$TTAH]$^+$	Cationic intermediate to *S*-Et-Py$_2$TTA
[*S*-Me-Py$_2$TTAH][OTf]	Cationic intermediate to *S*-Me-Py$_2$TTA with counterion
[*S*-Me-Py$_2$TTA]$^+$	Cationic intermediate to *S*-Me-Py$_2$TTA
°C	Degrees Celsius
Å	Angstroms
aza-BODIPY	4,4-difluoro-4-bora-3a,4a,8-triaza-s-indacene
B3LYP/6-311+G(2d,p)	A computational level of theory
BF_3	Boron trifluoride
$BF_3{\cdot}OEt_2$	Boron trifluoride diethyl etherate
BF_4^-	Tetrafluoroborate anion
BODIPY	4,4-difluoro-4-bora-3a,4a-diaza-s-indacene
$CDCl_3$	Deuterated chloroform
$Cl(NO_2)_2Ph$	1-chloro-2,4-dinitrobenzene
cm^{-1}	Reciprocal centimetres
COSY	Correlation Spectroscopy NMR
cp	Cyclopentadienyl
DCE	Dichloroethane
DCM	Dichloromethane
DFT	Density functional theory
DMAP	4-Dimethylaminopyridine
DMSO	Dimethylsulfoxide
EPR	Electron paramagnetic resonance (spectroscopy)

Et_2O	Diethyl ether
EtI	Ethyl iodide
EtOH	Ethanol
eV	Electron volts
Fe(*S*-Me-Py$_2$TTA)Cl$_3$	An iron compound surrounded by an *S*-Me-Py$_2$TTA ligand and three chloride ions
$FeBr_3$	Iron(III) bromide
$FeCl_3$	Iron(III) chloride
FETs	Field Effect Transistors
g	Grams
H_2O	Water
HOMO	Highest Occupied Molecular Orbital
*i*Pro	Isopropyl group
IR	Infrared (spectroscopy)
K	Kelvin
$KMnO_4$	Potassium permanganate
KOH	Potassium hydroxide
LCDs	Liquid crystal displays
LUMO	Lowest Unoccupied molecular orbital
MeCN	Acetonitrile
MeCN-d_3	Deuterated acetonitrile
MeI	Methyl iodide
MeOH	Methanol
MeOTf	Methyl triflate
$MgSO_4$	Magnesium sulfate
mmol	Millimoles
NaH	Sodium hydride
NaOMe	Sodium methoxide
$NaSO_4$	Sodium sulfate
NCS	*N*-chlorosuccinimide
***N*-Et-Py$_2$TTA**	3,5-*bis*(2-pyridyl)-*N*-ethyl-1,2,4,6-thiatriazine
NH_3	Ammonia
nm	Nanometers
***N*-Me-Py$_2$TTA**	3,5-*bis*(2-pyridyl)-*N*-methyl-1,2,4,6-thiatriazine
NMR	Nuclear magnetic resonance
OLEDs	Organic light emitting devices

Ph_3Sb	Triphenylantimony
PhCl	Chlorobenzene
ppm	Parts per million
Prm_2TTA	3,5-*bis*(2-pyrimidyl)-1,2,4,6-thiatriazine framework
Py_2TTA	3,5-*bis*(2-pyridyl)-1,2,4,6-thiatriazine framework
Py_2TTA^-	3,5-*bis*(2-pyridyl)-1,2,4,6-thiatriazine anion
$Py_2TTA^\cdot$	3,5-*bis*(2-pyridyl)-1,2,4,6-thiatriazinyl radical
Py_2TTAH	3,5-*bis*(2-pyridyl)-4-hydro-1,2,4,6-thiatriazine
RT	Room temperature
S_2Cl_2	Sulfur monochloride
SCl_2	Sulfur dichloride
***S*-Et-Py_2TTA**	3,5-*bis*(2-pyridyl)-*S*-ethyl-1,2,4,6-thiatriazine
***S*-Me-Py_2TTA**	3,5-*bis*(2-pyridyl)-*S*-methyl-1,2,4,6-thiatriazine
S_N1	Unimolecular nucleophilic substitution
S_N2	Bimolecular nucleophilic substitution
S_NArylation	Nucleophilic arylation
***S*-Ph-Py_2TTA**	Neutral *S*-Phenyl derivative of Py_2TTA
TD DFT	Time dependant density functional theory
terpy	Terpyridine
THF	Tetrahydrofuran
TMS OTf	Trimethylsilyl triflate
TTA	Thiatriazine
TTA^-	Thiatriazine anion
TTA^+	Thiatriazine cation
$TTA^\cdot$	Thiatriazinyl radical
UV	Ultraviolet
UV-Vis	Ultraviolet/visible spectroscopy
XRD	X-ray diffraction

Summary of Chemical Structures

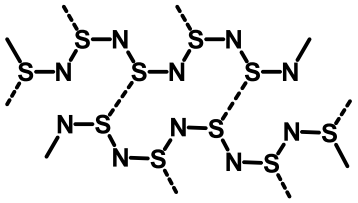

1.1
$(SN)_x$

1.2

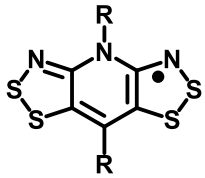

1.3

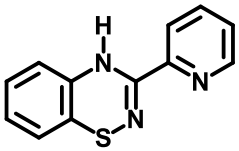

1.4

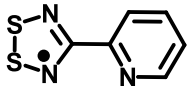

1.5

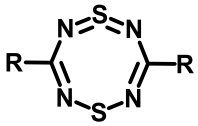

1.6

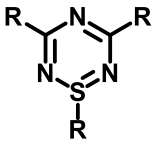

1.7
TTA

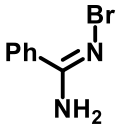

1.8

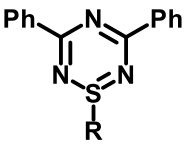

1.9

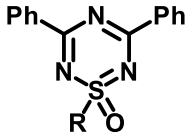

1.10

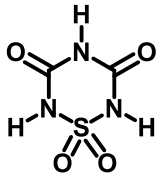

1.11

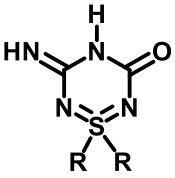

1.12
3.4

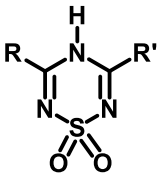

1.13

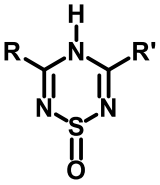

1.14

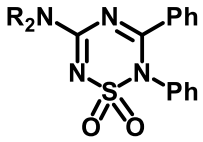

1.15

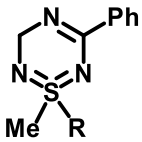

1.16

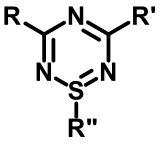

1.17
3.2

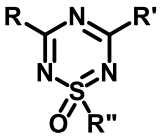

1.18

1.19

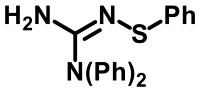

1.20

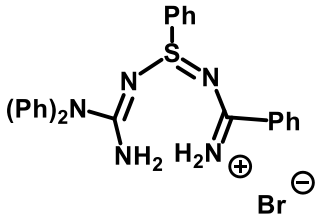

1.21

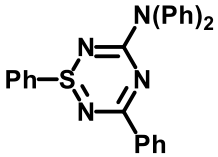

1.22

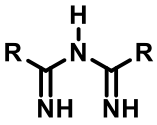

1.23

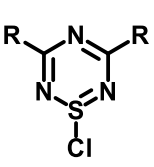

1.24

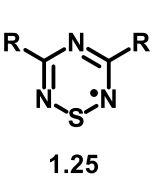

1.25
$TTA^{\bullet}$

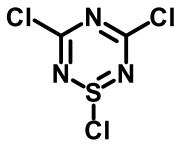

1.26

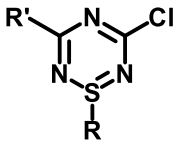

1.27

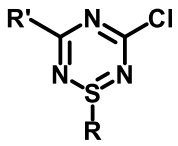

1.28

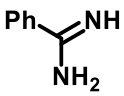

1.29

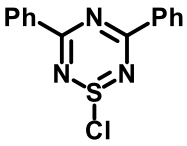

1.30

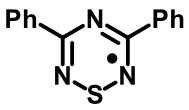

1.31

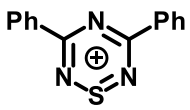

1.32

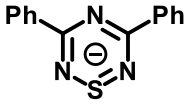

1.33

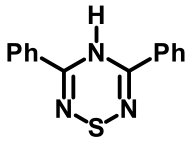

1.34

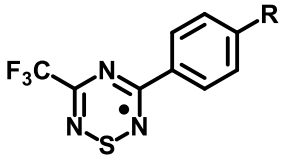

1.35

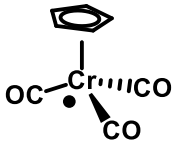

1.36

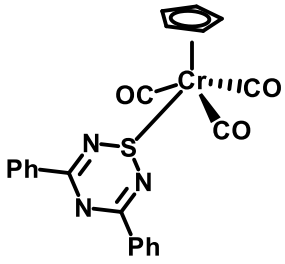

1.37

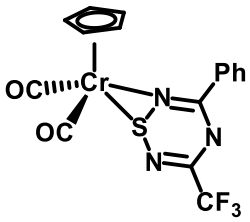

1.38

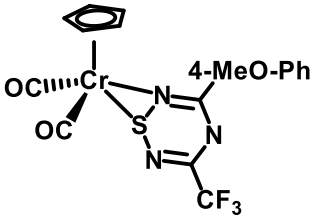

1.39

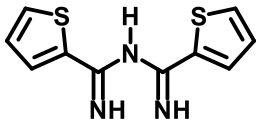

1.40

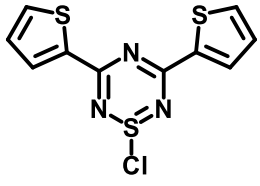

1.41

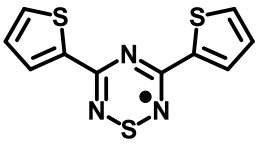

1.42

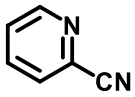

1.43
2.5

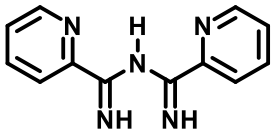

1.44
2.6
5.7

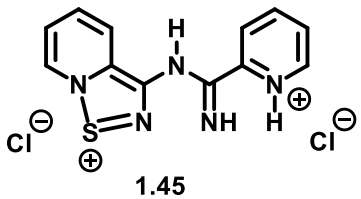

1.45
2.7
3.9

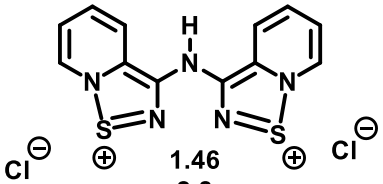

1.46
2.8
3.10

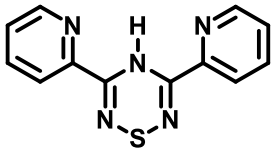

1.47
2.9
3.11
4.1
5.14
Py_2TTAH

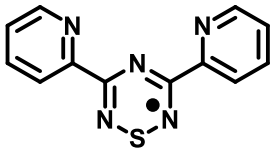

1.48
2.10

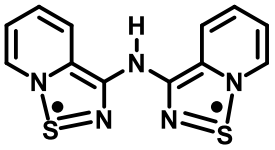

1.49
2.11

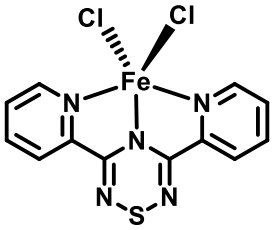

1.50
4.2
[Fe(Py$_2$TTA)Cl$_2$]

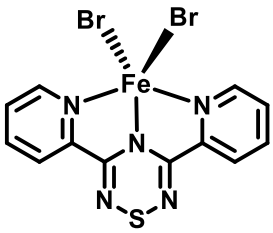

1.51
4.3
[Fe(Py$_2$TTA)Br$_2$]

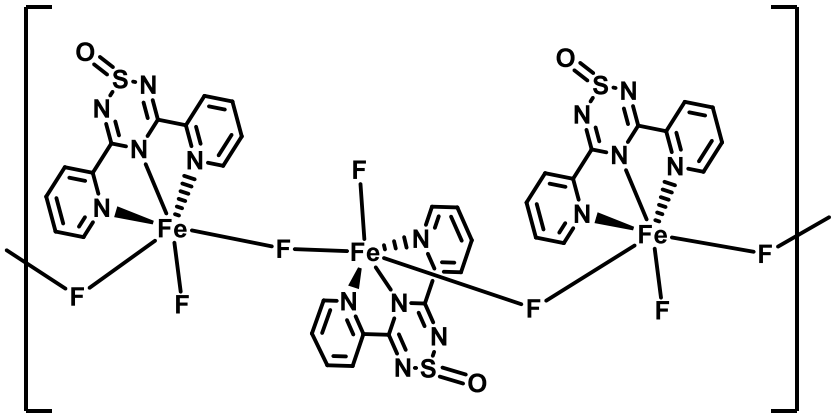

1.52
4.4
[Fe(μ-F)(1-oxo-Py$_2$TTA)F]$_\infty$

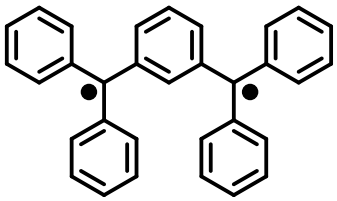

2.1

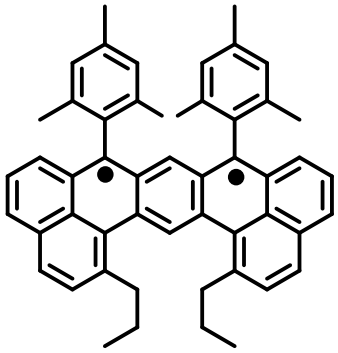

2.2

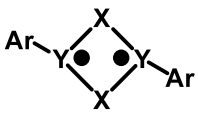

2.3

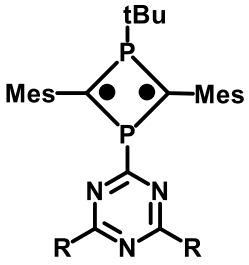

2.4

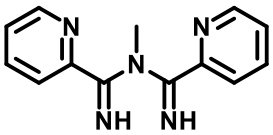

2.12

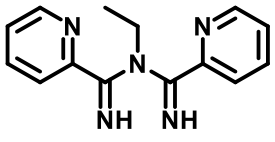

2.13

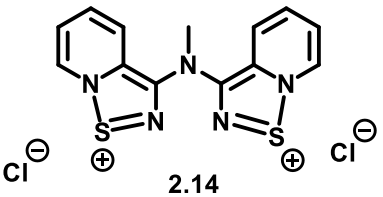

2.14

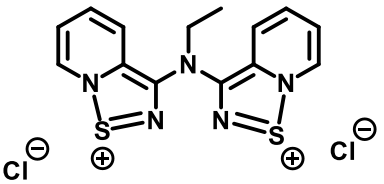

2.15

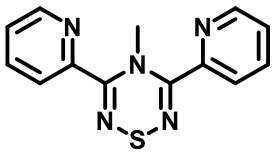

2.16

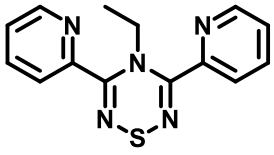

2.17

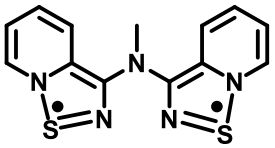

2.18

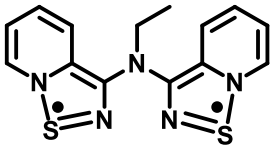

2.19

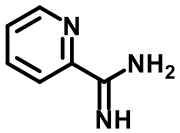

2.20

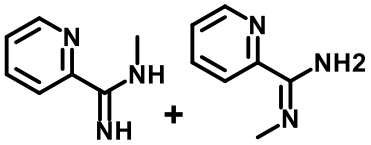

2.21

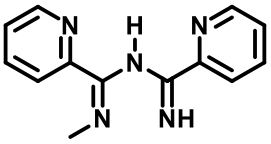

2.22a

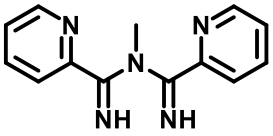

2.22b

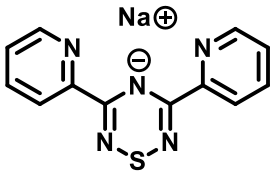

2.23
3.12
4.7
Py_2TTA^-

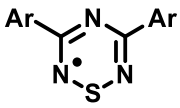

3.1

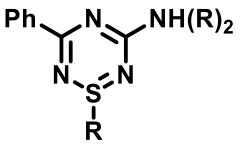

3.3

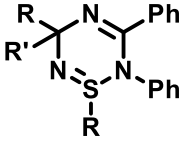

3.5

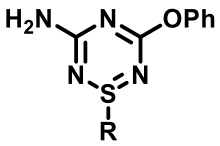

3.6

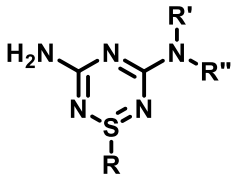

3.7

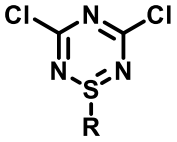

3.8

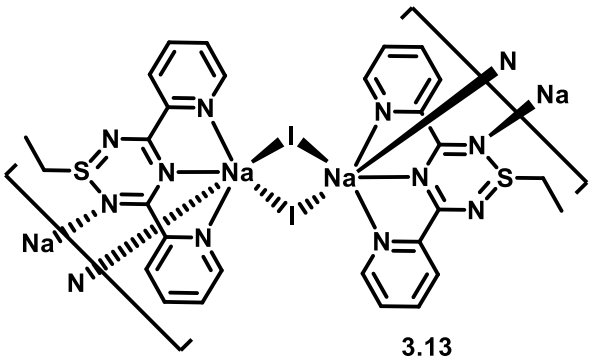

3.13
$[Na(\mu\text{-}I)(S\text{-}Et\text{-}Py_2TTA)]_\infty$

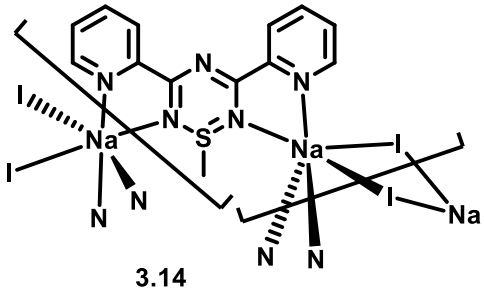

3.14
[Na(μ-I)(*S*-Me-Py_2TTA)] ∞

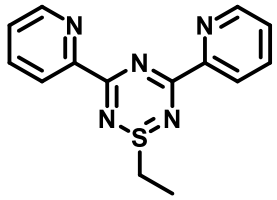

3.15
S-Et-Py_2TTA

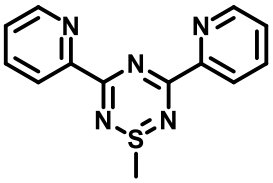

3.16
4.5
S-Me-Py_2TTA

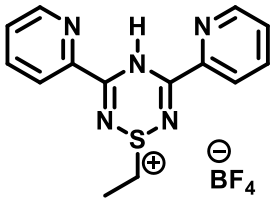

3.17
[*S*-Et-Py_2TTAH][BF_4]

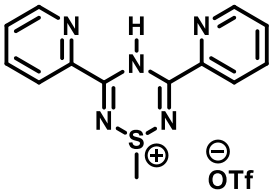

3.18
[*S*-Me-Py_2TTAH][OTf]

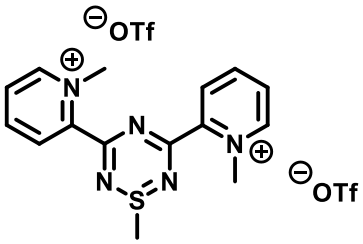

3.19

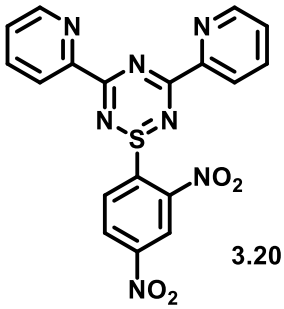

3.20

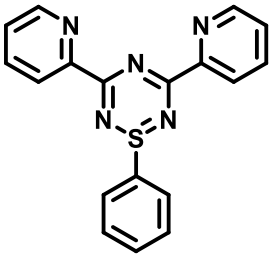

3.21
S-Ph-Py_2TTA

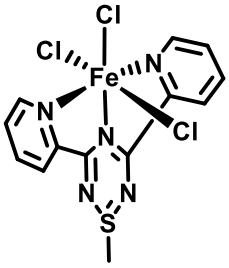

4.6
Fe(*S*-Me-Py_2TTA)Cl_3

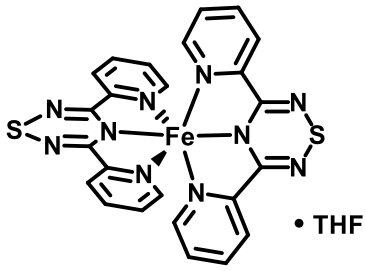

4.8
[Fe(Py_2TTA)$_2$]·THF

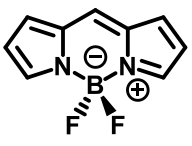

5.1
BODIPY

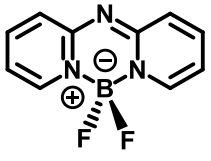

5.2
aza-BODIPY

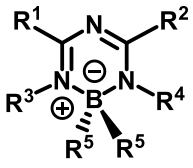

5.3

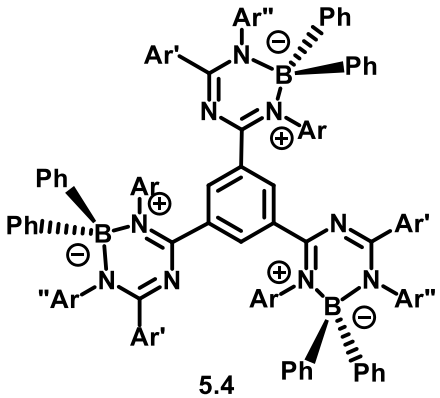

5.4

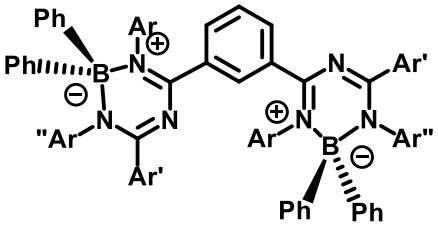

5.5

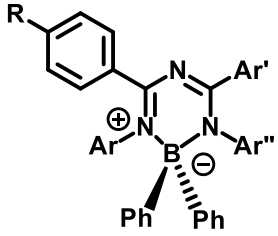

5.6

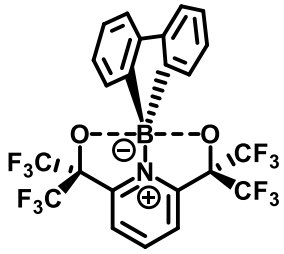

5.8

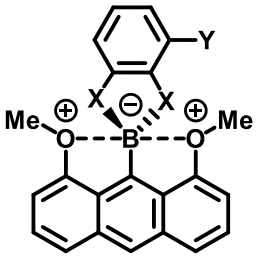

5.9

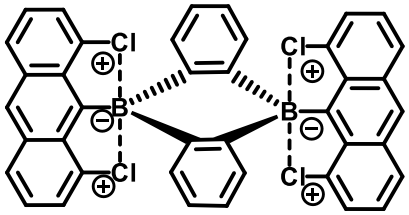

5.10

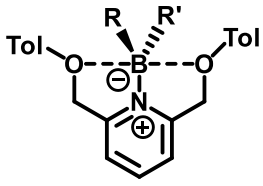

5.11

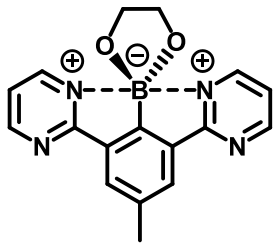

5.12

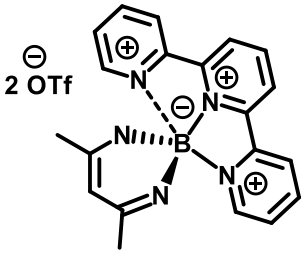

5.13

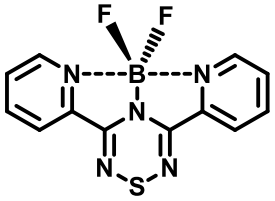

5.15

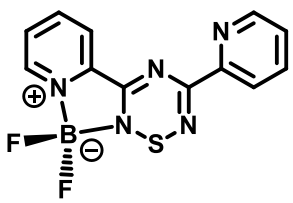

5.16

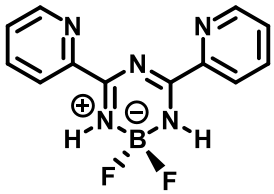

5.17

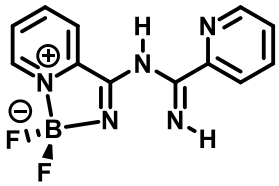

5.18

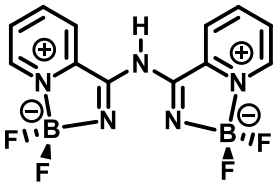

5.19

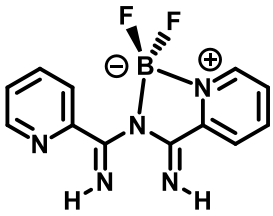

5.20

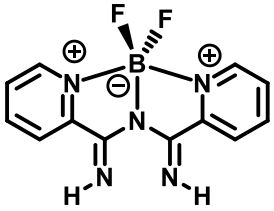

5.21

Contributions

Peer Reviewed Article

Kleisath, E., Yutronkie, N.J., Korobkov, I., Gabidullin, B.M., and Brusso, J.L., "Alkyl-functionalization of 3,5-*bis*(2-pyridyl)-1,2,4,6-thiatriazine", *New Journal of Chemistry*, (2016), **40**, 4472-4479.

Research Presentation

Kleisath, E., Yutronkie, N.J., Korobkov, I., Gabidullin, B.M., and Brusso, J.L., "Alkyl-functionalization of Sulfur and Nitrogen Containing Heterocycles", *Inorganic Discussion Weekend*, Royal Military College, Kingston ON, November 2015.

Conference Poster Presentations

Kleisath, E., Yutronkie, N.J., Korobkov, I., Gabidullin, B.M., and Brusso, J.L., "Alkyl-functionalization of Sulfur and Nitrogen Containing Heterocycles", *Chemistry and Biochemistry Graduate Research Conference*, Concordia University, Montreal QU, November 2015.

Kleisath, E., Yutronkie, N.J., Korobkov, I., and Brusso, J.L., "Progress Towards the Synthesis of a Novel Biradical *Bis*(*N*-Bridgehead-1,2,3-Thiadiazolyl)", *Canadian Chemistry Conference and Exhibition*, Ottawa ON, June 2015.

Kleisath, E., Yutronkie, N.J., Korobkov, I., and Brusso, J.L., "Progress Towards the Synthesis of a Novel Biradical *Bis*(*N*-Bridgehead-1,2,3-Thiadiazolyl)", *Ottawa-Carleton Chemistry Institution Day*, Ottawa ON, June 2015.

Chapter 1 – Introduction

1.1 Molecular Materials Design

Materials chemistry is very prevalent in our daily lives and today's technological society, being used in everything from the solar panels powering communication satellites to the cell phones in our pockets. Materials chemistry is at the forefront of this technology, which uses a variety of applications such as liquid crystalline displays (LCDs) and optoelectronic devices, including organic light emitting diodes (OLEDs),[1] solar cells,[2] and field effect transistors (FETs)[3]. While traditional inorganic devices are silicon-based, their organic counterparts offer a low cost alternative,[4] inherent flexibility,[5] provide opportunities for synthetic design through their tunability,[6] and are typically easier to process compared to their inorganic counterparts.[7] Many organic devices also have the added benefit of biocompatibility, opening up a range of new applications not afforded to their inorganic counterparts.[8] Unfortunately, organic based devices tend to be inferior to inorganic derivatives due to their comparatively lower electron mobilities and stablity.[3]

Among organic molecules, planar π-conjugated materials are attractive for optoelectronic applications, as the necessary charge transport relies on electronic communication between molecules in the active layer. This communication, in turn, is dependent on the extent of orbital overlap between adjacent molecules and the

resulting charge transfer integral. In the solid state, this is influenced by the crystal packing, and thus developing ways to control the solid state structure may lead to improvements in the charge transfer integral.

In the design of organic semiconductors for optoelectronic applications, sulfur and nitrogen containing heterocycles have received much attention as such frameworks have several advantages over their all carbon counterparts. Heteroatoms can add structural control through the enhanced probability of hydrogen bonding, in addition to close contacts between sulfur and nitrogen atoms.[9-11] Furthermore, the larger *p*-orbitals of the sulfur atom can facilitate enhanced intermolecular orbital overlap,[11, 12] which leads to a greater likelihood of intermolecular communication. The inclusion of heteroatoms also adds an element of stability to the resulting molecules, as such atoms generally lower the overall energy of the highest occupied molecular orbital (HOMO).[9, 11, 13-15] The lowering of the HOMO energy (i.e., increasing the ionization potential of the system) is effective at improving the stability, as the higher the ionization potential, the less likely the compound will be oxidized by ambient oxygen.[15]

1.2 Development of S—N Chemistry

Studies focusing on the inclusion of sulfur and nitrogen atoms largely began with the recognition of the conductive properties of polythiazyl, **(SN)$_x$** (**1.1**; Chart 1-1), an inorganic polymer. Interestingly, **(SN)$_x$** was also found to be superconductive at very

low temperatures.[16] This inherent conductivity results from delocalization of electrons in the π-system. More specifically, there are three electrons per SN subunit, which leads to filling of the π-bonding and half-filling the π-antibonding molecular orbitals. Overlap between the nitrogen and sulfur orbitals allows for conduction along the polymer chain, and the presence of weak interactions between chains prevents electron localization.[16] The recognition of conductive properties in **(SN)**$_x$ initiated a great deal of research into heterocycles in search of other electronically active compounds, such as the examples shown in Chart 1-1.[11, 17-24] Of particular importance to this thesis is **1.7**, the 1,2,4,6-thiatriazine (**TTA**) framework, which consists of a six-membered ring containing nitrogen, sulfur, and carbon that can exist as an aromatic, anti-aromatic or unsaturated framework. The **TTA** system is an attractive moiety for materials applications, as it possesses an N—S—N fragment, which can promote intermolecular communication through heteroatom interactions. Furthermore, the **TTA** ring is stable in several redox states, with cationic, anionic and neutral radical (seven π electron) states accessible.[19, 25] In addition, **TTA** has been shown to be an effective ligand for metal coordination.[26-30]

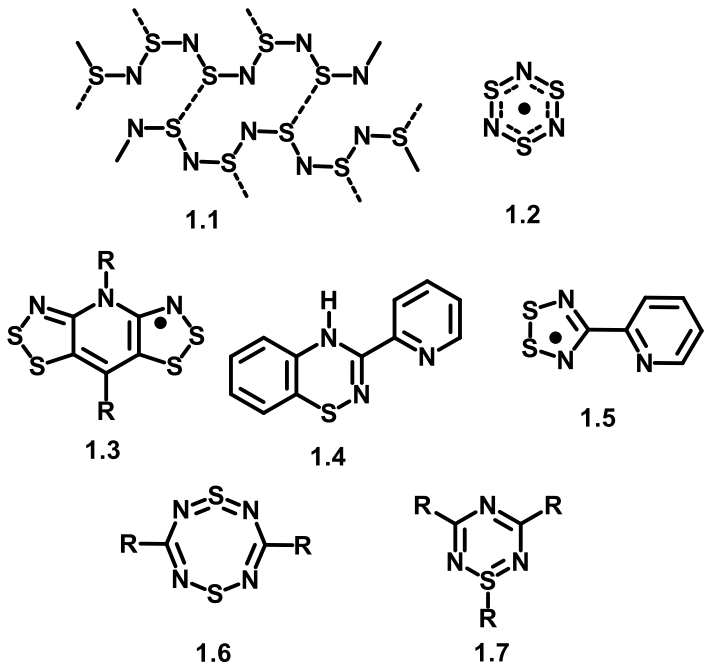

Chart 1-1. Examples of sulfur and nitrogen containing compounds including the **(SN)**$_x$ polymer (**1.1**) and select heterocyclic systems.

1.3 Closed Shell Thiatriazines: Synthesis and Development

In 1954, Goerdeler and Loevenich first reported the synthesis of the **TTA** framework (**1.9** and **1.10**; Scheme 1-1), prepared *via* the reaction between *N*-bromo-benzenecarboxamidine and alkylated sulfides.[31] Over the next few decades, a number of unsaturated and aromatic **TTA** derivatives were described (**1.11**-**1.18**, Chart 1-2).[32-39] In the case of the aromatic examples, functionalization with a wide variety of R groups (e.g., alkyl chains, cyclic substituents, halides, amino groups) has been demonstrated,[40-58] with the majority of these studies focused on the development of **TTA** compounds, some of which have been used in herbicidal and pesticidal applications.[59-63] For almost three decades, the synthetic procedure was relatively unchanged, starting from

substituted sulfides (e.g., **1.19**) and building a linear S—N framework using nitrogen containing moieties such as amidines. The thiatriazine was subsequently realized through a ring closure reaction with sodium methoxide at the central nitrogen atom of the **TTA** ring. An example of such a synthesis is shown in Scheme 1-2.[41]

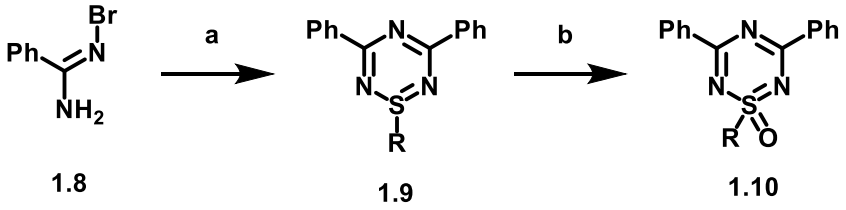

Scheme 1-1. The first reported synthesis of **TTA** rings. Reagents and conditions: (a) MeSR (R=Et, *i*Pro, butyl) (b) $KMnO_4$.

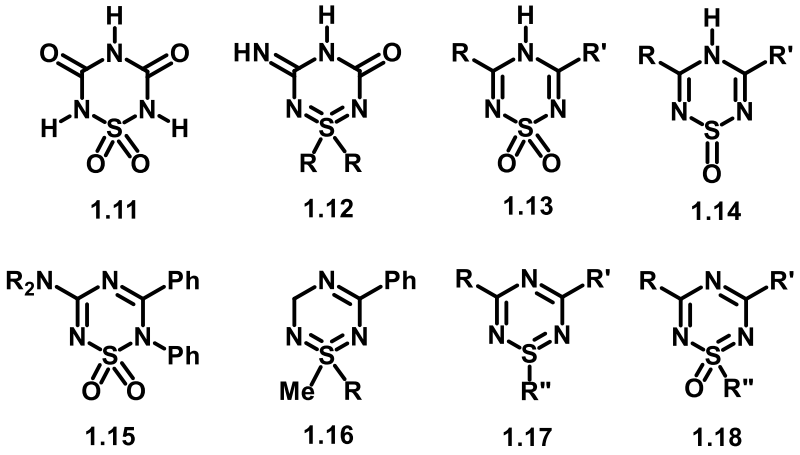

Chart 1-2. Examples of saturated (**1.11**), unsaturated (**1.12**-**1.16**), and aromatic (**1.17** and **1.18**) **TTA** frameworks.

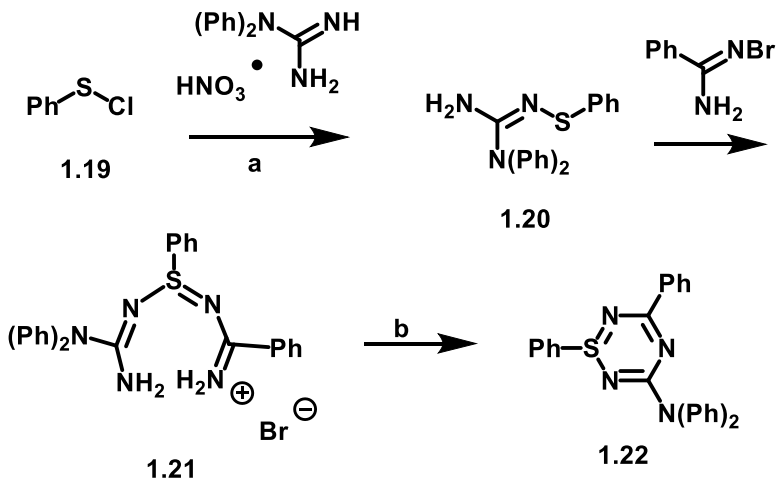

Scheme 1-2. Synthesis of **1.22** (i.e., **1.17** where R = $N(Ph)_2$, R′ = R″ = Ph). This example serves as a representative of the initial synthesis of such compounds. Reagents: (a) 2 NaOMe (b) NaOMe.

In 1980, a new synthetic pathway was developed by Markovskii and coworkers, in which symmetric or asymmetric imidoyl amidines were reacted with sulfur dichloride (SCl_2), forming an aromatic ***S*-chloro-TTA** ring (**1.24**; Scheme 1-3).[53] The use of simpler sulfur-containing molecules provided a more generic pathway for the formation of **TTA** rings. Markovskii *et al.* later went on to describe the reduction of **1.24**, reporting the first persistent **TTA** radical species (**TTA**$^{\cdot}$), identified *in situ* by electron paramagnetic resonance (EPR) spectroscopy.[64]

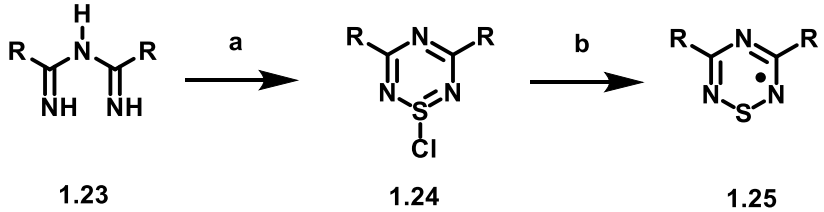

Scheme 1-3. Synthesis of ***S*-chloro-TTA** from imidoyl amidine, and observation of the first **TTA** radical. Reagents: (a) SCl_2 (b) Reducing Agent. R = Ph, CCl_3, CF_3, Cl, $N(Me)_2$.

While the initial synthetic method affords **TTA** derivatives with sulfur substituents, due to the nature of the synthesis (starting with the already substituted sulfide), modification of the sulfur substituent was challenging, as the synthetic conditions needed to be developed and optimized for each new sulfide starting material.[39, 54-57, 65] Alternately, the route developed by Markovskii *et al.* enables a more facile method for attaining sulfur functionalized **TTA**. This method was employed by Stoller in 2000 when he developed a route to substitute the sulfur atom of the **TTA** post-ring formation *via* the replacement of chloride ions in 1,3,5-trichloro-1,2,4,6-thiatriazine (**1.26**; Scheme 1-4).[58]

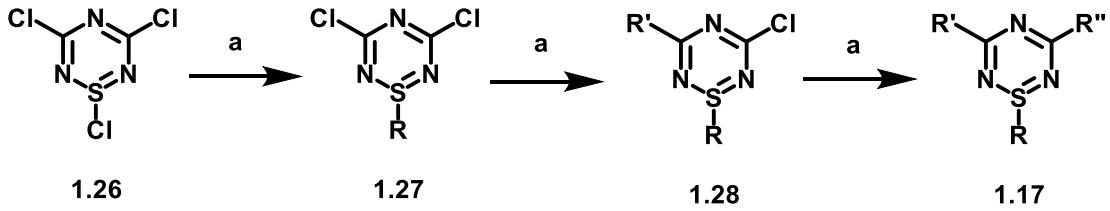

1.26 **1.27** **1.28** **1.17**

Scheme 1-4. Alkylation of ***S*-chloro-TTA** compounds post **TTA** ring formation. Reagents: (a) various nucleophiles.

1.4 Thiatriazines: From a Materials Point of View

To this point, the majority of previous studies had considered the **TTA** framework from a synthetic standpoint, with the only applications as pesticides and herbicides. Following the observation of a radical species by Markovskii *et al.*, Oakley and coworkers began to investigate the potential of **TTA** in materials chemistry applications.[66] Their initial work focused on 3,5-*bis*-phenyl-1,2,4,6-thiatriazinyl (**1.31**),

which was accessed *via* reduction of *S*-chloro-3,5-diphenyl-TTA (**1.30**) with triphenyl antimony (Scheme 1-5).[67] In the EPR spectrum (Figure 1-1), the lack of hyperfine coupling between the unpaired electron and the hydrogen atoms of the phenyl rings suggests that the lone spin centre is localized within the **TTA** framework.[68] Furthermore, the equivalent coupling constants for the three nitrogen atoms indicates that the unpaired electron is delocalized throughout the six-membered **TTA** ring.[68] In the solid state, single crystal X-ray diffraction (XRD) revealed dimerization of the radicals, forming the lower energy co-facial π dimer with a S-S bond between the two **TTA** rings (Figure 1-2).[68]

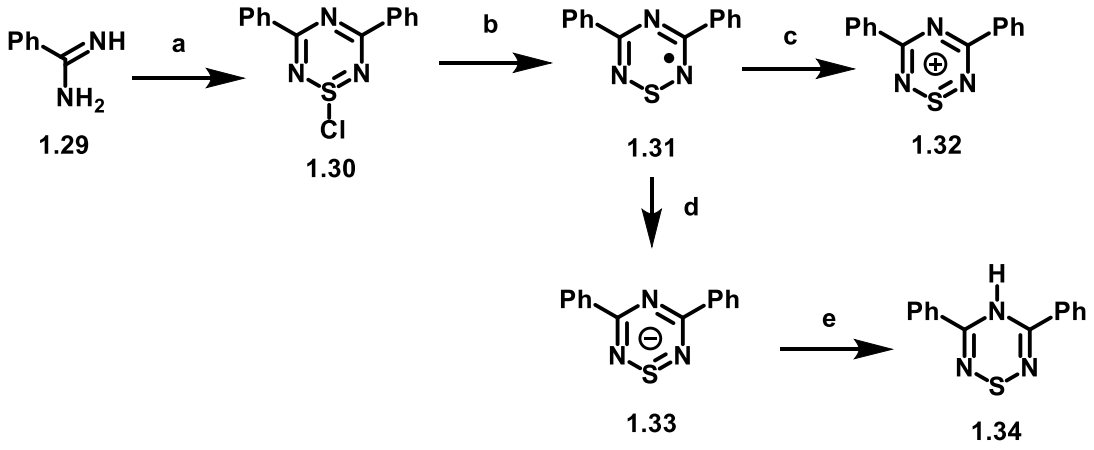

Scheme 1-5. Synthesis of **1.31**. Reagents and Conditions: (a) $S_3N_3Cl_3$, MeCN, reflux, (b) $SbPh_3$, DCM, (c) $[NO][BF_4]$ or $[NO][PF_6]$, MeCN, reflux, (d) Na metal, $NH_{3\,(l)}$, (e) $NH_4{\cdot}Cl$.

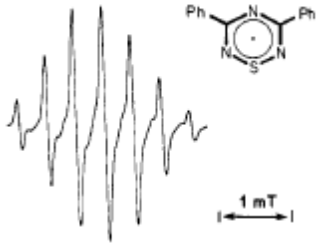

Figure 1-1. EPR Spectrum of **1.31** in DCM (a_N = 0.397 mT).[68]

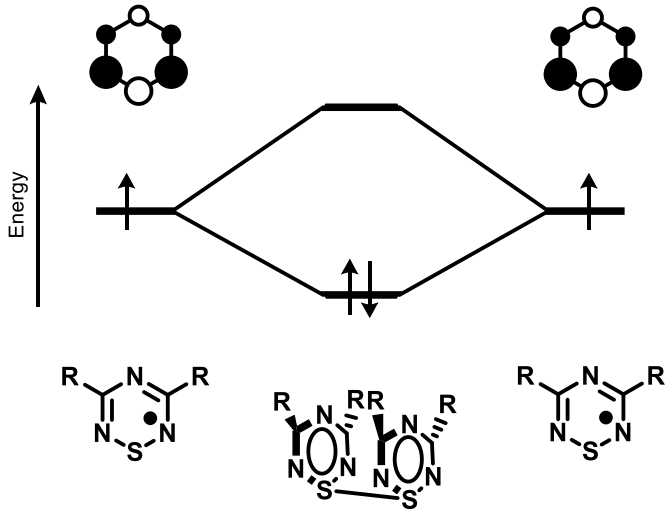

Figure 1-2. Qualitative MO diagram of the singly occupied molecular orbitals of a general **TTA** radical (left and right), illustrating the interaction of these radical centres to form the lower energy dimerized **(TTA)**$_2$ (centre). (Modified from reference [66])

In addition to the neutral radical **1.31**, Oakley and coworkers also reported cationic (**1.32**) and anionic (**1.33**) derivatives of the **TTA** framework. While the cation could be studied as synthesized *via* addition of a nitrosyl cation to the radical system, due to isolation difficulties of the anion, it was necessary to study the anionic form from the protonated **TTA** derivative (**1.34**). As such, **1.34** was obtained by reacting the radical dimer with sodium metal in liquid ammonia, followed by the addition of ammonium chloride.[69] XRD analysis revealed that these systems were structurally stable under different redox states, with only small structural differences. This therefore suggests

that conductivity may be achievable in similar **TTA** species, if dimerization can be prevented.[69] In addition to the phenyl derivative, Oakley also reported several other symmetrically substituted **TTA** derivatives.[68, 70]

Following Oakley's work in the mid 80's, it was nearly two decades before the next **TTA** radical was reported. Boeré and Roemmele carried out characterization of previously reported **TTA** radicals symmetrically substituted at the 3- and 5- positions (**1.25**; Chart 1-3).[53, 68, 70, 71] The EPR spectra of these compounds were reported, and found to be in agreement with the predicted EPR spectra.[72] In subsequent work, Boeré and Roemmele developed asymmetrically substituted **TTA** systems, with a CF_3 group at the 3-position and an aryl group at the 5-position of the **TTA** ring (**1.34**, Chart 1-3).[73] These radicals were all found to dimerize through S-S bonds in the solid state.

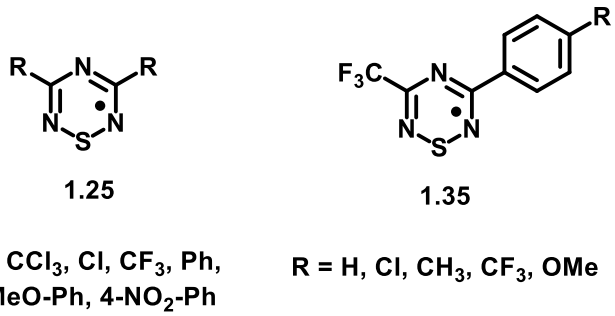

Chart 1-3. Symmetric and asymmetrically substituted **TTA** radicals (**1.25** and **1.35**, respectively) studied by Boeré and coworkers.

1.5 Metal Coordination with Thiatriazines

Following work with **TTA** radicals, Boeré and coworkers reported the first examples of metal coordination to **TTA** using a chromium cyclopentadienyl (cp) precursor, $[CpCr(CO)_3]_2$. Interestingly, depending on the **TTA** derivative employed in the reaction, different coordination environments were obtained, as shown in Scheme 1-6. More specifically, using the 3,5-diphenyl radical **1.31**, the chromium complex **1.37** was generated through the formation of a bond between the chromium centre and sulfur atom, with the cp ligand in the exo orientation (i.e., pointing away from the **TTA** ring). In this complex, the five-coordinate geometry around the chromium ion is completed by three carbonyl groups.[26] Here, the **TTA** ligand was determined to be an intermediate between the neutral radical and *mono*-reduced anionic forms, as established through bond length comparisons with previously reported **TTA** compounds.

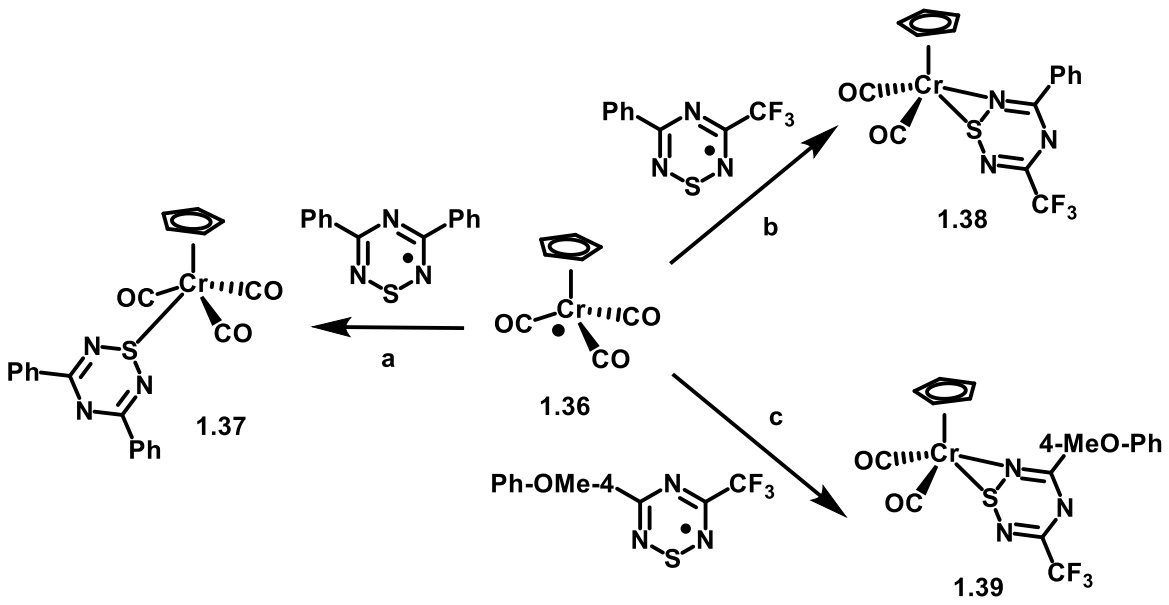

Scheme 1-6. Coordination of **TTA** radicals with $[CpCr(CO)_3]_2$ (**1.36**). Reaction Conditions: (a) toluene, RT, (b) toluene, -29°C. (c) toluene, RT.

Alternatively, coordinating asymmetrically substituted **TTA** radicals 3-trifluoromethyl-5-phenyl-TTA and 3-trifluoromethyl-5-(*p*-methoxyphenyl)-TTA as ligands with $[CpCr(CO)_3]_2$ led to complexation differing that of the symmetrically substituted complex (i.e., **1.38** and **1.39** vs. **1.37**).[27] In this case, the chromium ion coordinates in a side-on fashion to the sulfur and nitrogen atom para to the CF_3 group in an η^2 style. The cp ligand orients itself away from the **TTA** ring in the exo conformation, and two carbonyl groups remain bound to the metal centre. Here, the asymmetric coordination of the **TTA** ligand was attributed to a higher electron density on that side of the ring, as measured by EPR spectroscopy of the radical starting material. Upon comparison of bond lengths and angles of **1.37**, **1.38** and **1.39** with similar heterocycles, Boeré and coworkers concluded that in **1.38** and **1.39**, the **TTA**

ligand donates three electrons to the metal centre, resulting in a bond order of 1.5. For comparison, **1.37** donates one electron, leading to an overall bond order of 1. The increased bond order of the η^2 complexes affords a stronger metal-ligand bond and a more oxidized ligand state (greater anionic character) when compared to **1.37**.[26, 27]

1.6 Thiatriazine Derivatives with Pendant Heterocycles

While metal coordination of **TTA** through the sulfur atom has been shown, the formation of a chelating pocket was sought in order to facilitate multidentate metal coordination. To that end, the addition of heterocyclic substituents such as pyridyl or pyrimidyl rings at the 3- and 5- positions is desirable. Such substitution would create a framework analogous to the terpyridine (terpy) ligand, which is highly studied for a variety of different applications (e.g., catalysis, molecular magnetism, biomedical applications, etc).[19, 74-76] Therefore, the design of a redox active coordination environment analogous to terpy is attractive, as it is anticipated that this could facilitate tunable spin bearing ligands in metal coordination. Such ligands may lead to a variety of applications including catalysis, as well as molecular magnetism.[28] Furthermore, metal coordination with terpy-like pockets in TTA ligands would leave the N—S—N fragment of the molecule open for enhanced intermolecular interactions, which may lead to better electronic communication between adjacent molecules.

To that end, Brusso and coworkers have reported **TTA** derivatives functionalized with heteroaromatic substituents, namely thiophene and pyridine.[25] The symmetrically substituted 3,5-*bis*-(thienyl)-1,2,4,6-thiatriazyl radical (**1.42**, Scheme 1-7) was recently synthesized *via* generation of the ***S*-chloro-TTA** intermediate (**1.41**) and subsequent reduction with triphenylantimony.[25] EPR studies exhibited the expected seven line pattern, indicative of the unpaired electron coupling with three equivalent nitrogen atoms (Figure 1-3). In the solid state, this compound formed cofacial π dimers, with the interacting sulfur atoms exhibiting the shortest close contact.[25]

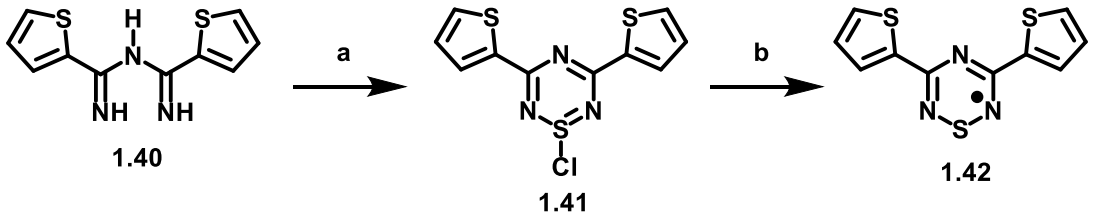

Scheme 1-7. Synthesis of **1.42**. Reagents and conditions: (a) S_2Cl_2, MeCN, reflux. (b) Ph_3Sb, MeCN, RT.

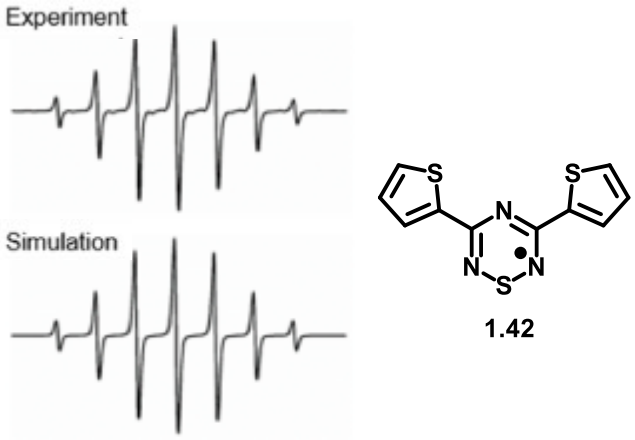

Figure 1-3. Experimental and simulated EPR spectrum of **1.42** in DCM (a_N = 0.386 mT [4-position] and 0.392 mT [2- and 6-position]).[25]

In regards to the pyridyl substituted **TTA** derivative, 3,5-*bis*-(2-pyridyl)-1,2,4,6-thiatriazyl radical (**1.48**; Scheme 1-8), the synthetic pathway exhibited several significant differences from previously reported **TTA** radicals. Most notably, the synthetic pathway to the radical was shown to proceed through the protonated derivative 3,5-*bis*(2-pyridyl)-4-hydro-1,2,4,6-thiatriazine (**Py_2TTAH**, **1.46**), as opposed to the precedented *S*-chloro intermediate (Scheme 1-8).[19] This difference is attributed to the presence of the pyridyl nitrogen atoms, which were found to be non-innocent during the reaction between the *N*-2-pyridylimidoyl-2-pyridylamidine (**1.44**) and S_2Cl_2. Instead of creating the expected ***S*-chloro-TTA** intermediate, the reaction proceeded through one of two *N*-bridgehead thiadiazolium salts, depending on the reaction temperature.[19] At room temperature, an asymmetrical *mono*-*N*-bridgehead-1,2,5-thiadiazolium dication (**1.45**) was obtained, while under reflux, a symmetrical *bis*-*N*-bridgehead-1,2,5-thiadiazolium dication (**1.46**) was isolated.[19] Compound **1.46** was seen as a candidate for the synthesis of a biradical upon a two electron reduction (i.e., **1.49**). Alternatively, ring opening may occur upon treatment with a reducing agent, as observed by Rawson for the similar compound 3-(pyridyl)-[1,2,5]thiadiazolo[2,3-*a*]-1-pyridinium.[77] Upon treatment of **1.46** with triphenylantimony, instead of forming a biradical, a six-membered thiatriazine ring was generated (i.e., **Py_2TTAH**, **1.47**).[19] Interestingly, the same compound could also be prepared through thermolysis of **1.45**. As well, it was found that **Py_2TTAH** and the thiadiazolium dications **1.45** and **1.46** are interconvertible.

The addition of acid lead to the regeneration of **1.45**, whereas **1.46** was accessible *via* treatment of **Py$_2$TTAH** with S_2Cl_2 at room temperature.

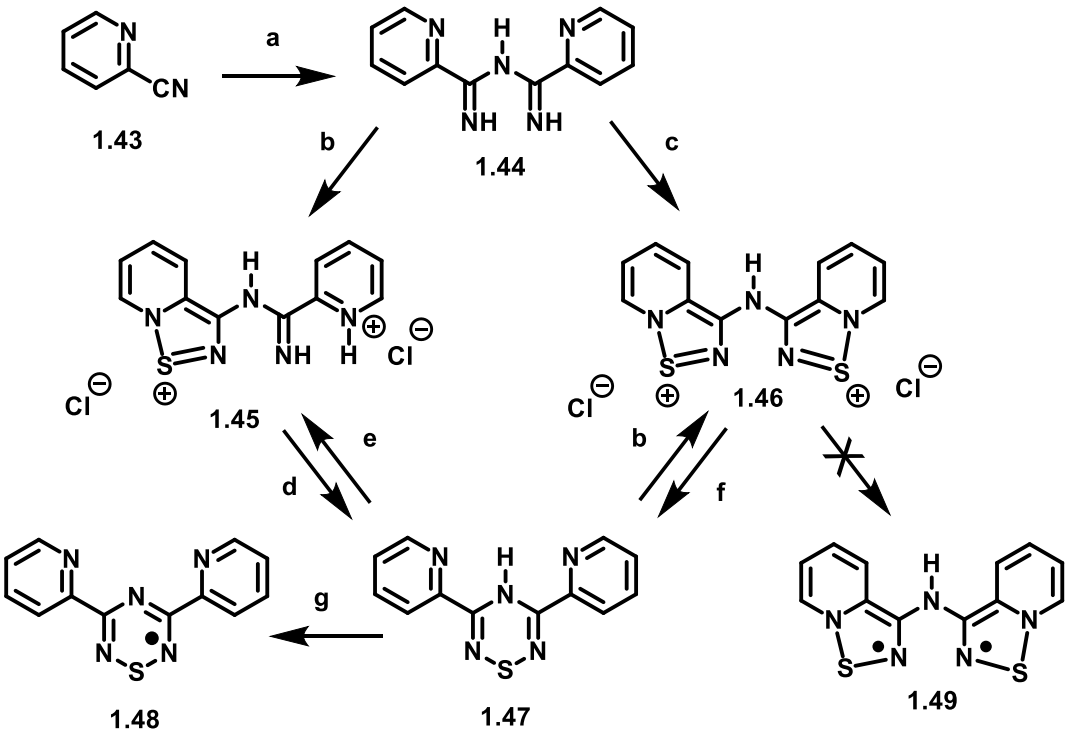

Scheme 1-8. Synthesis of the 3,5-*bis*-(2-pyridyl)-1,2,4,6-thiatriazyl radical **1.48**. Reagents and conditions: (a) NH_3, MeCN (b) S_2Cl_2, MeCN, RT (c) S_2Cl_2, MeCN, reflux (d) PhCl, reflux (e) H^+ (f) Ph_3Sb, MeCN, RT (g) NCS, DMAP, MeCN, RT.

The radical **1.48** was realized through oxidation of **Py$_2$TTAH** using *N*-chlorosuccidimide in the presence of an auxiliary base (e.g., 4-dimethylaminopyridine)[25] and characterized by EPR spectroscopy and X-ray crystallography. The EPR spectrum (Figure 1-4) showed a seven line pattern with additional hyperfine coupling attributed to the decreased electron density in the N—S—N portion of the ring resulting from the electron withdrawing pyridyl substituents. This causes the nitrogen atoms of the **TTA** ring to interact with the unpaired spin unequally, having coupling constants of 0.438

mT (4-position) and 0.377 mT (2- and 6-position).[19] In the solid state, the radical exists as a cofacial π dimer, similar to the thienyl derivative.[25]

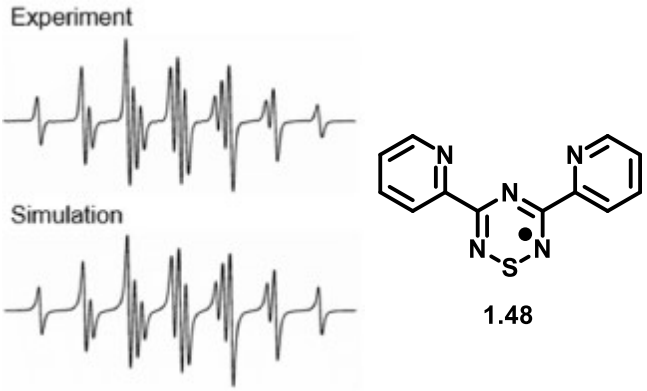

Figure 1-4. Experimental and simulated EPR spectrum of **1.48** in toluene (a_N = 0.438 mT [4-position] and 0.377 mT [2- and 6-position]).[25]

Isolation of **1.48** bodes well for metal coordination, as the terpy-like chelating pocket should enable complexation with a variety of metals. To that end, the use of **Py$_2$TTA** as a ligand has been explored in complexes with both transition metals and lanthanides.[28-30] In the case of the transition metal derivatives, a family of iron halide complexes has been reported (Scheme 1-9).[28, 29] In reactions between **Py$_2$TTAH** and $FeCl_3$ or $FeBr_3$, similar compounds were obtained (**1.50** and **1.51**). These complexes were discrete molecules with a five-coordinate iron centre consisting of the tridentate **Py$_2$TTA** ligand and two halide ligands completing the coordination sphere. For simplicity, the chloride derivative (**1.50**) will be discussed here. In **1.50**, the crystal structure suggests that the ligand contained bond lengths consistent with the anionic form (i.e., discrete single and double bonds in the **TTA** ring). This was further

supported by Mössbauer and magnetic susceptibility studies, in which the parameters were consistent with an Fe(III) complex.[28]

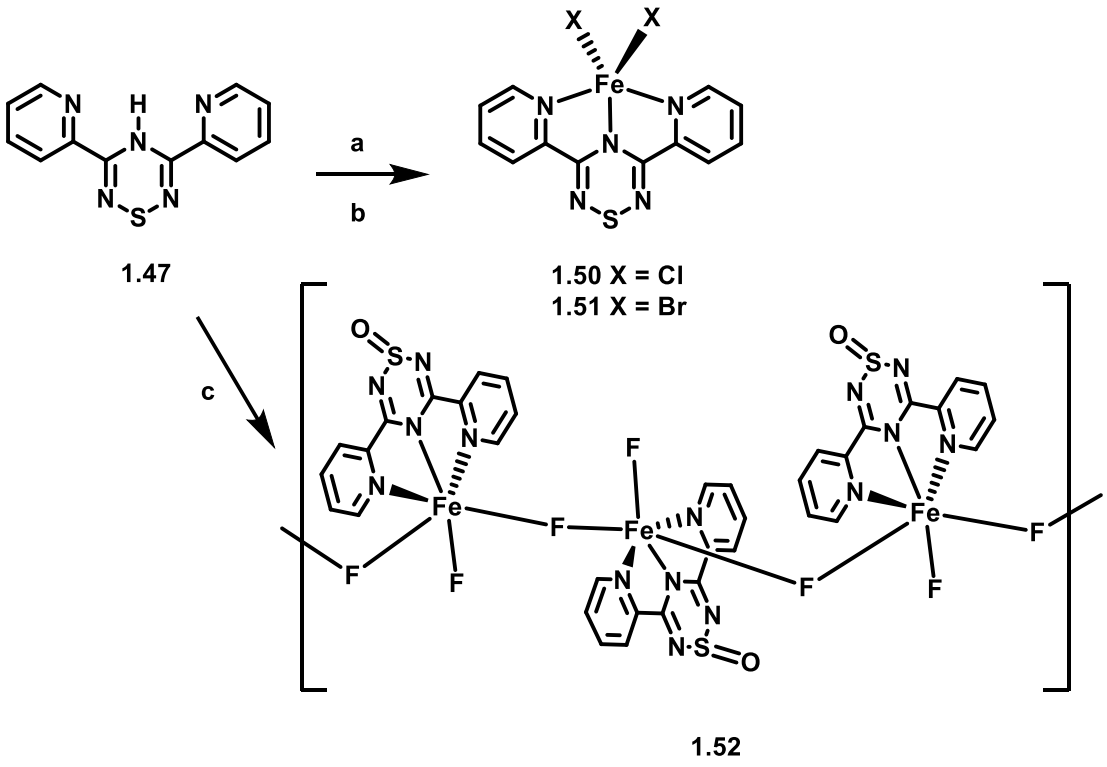

Scheme 1-9. Synthesis of iron halide complexes with **Py$_2$TTAH**. Reagents and conditions: (a) $FeCl_3$, DMF/MeOH (b) $FeBr_3$, MeCN/$CHCl_3$ (c) FeF_3, DMF/MeOH/Et_2O.[28, 29]

While the chloro and bromo derivatives resulted in complexes with similar five-coordinate geometries, upon treatment of **Py$_2$TTAH** with FeF_3, a six-coordinate 1D coordination polymer containing μ-bridging fluoride ions was isolated. This difference in structure (mononuclear vs. polymeric) was attributed to the small size and large electronegativity of the fluoride ions. In **1.52**, a six-coordinate Fe(III) geometry is observed, with a tridentate oxidized **Py$_2$TTA** ligand, as well as three fluoride anions – two of which are μ-bridging. In addition to the difference in coordination geometry and

the polymeric structure, the fluoride derivative also demonstrated that the sulfur atom in the **TTA** ligand is susceptible to metal assisted oxidation.[28, 29]

1.7 Functionalization of Heterocyclic Thiatriazines

The development of **Py_2TTAH** is of particular importance to this thesis, as it provides a stable **TTA** containing starting material for further studies. While previous **TTA** compounds considered for molecular materials applications were air sensitive, **Py_2TTAH** provides an alternative starting material which is stable under a variety of conditions (e.g., air, moisture, basic, thermal, aqueous). To that end, functionalization of **Py_2TTAH** and its synthetic precursors have been studied from a materials chemistry point of view, demonstrating their potential for facile functionalization, and thus influencing and fine tuning the chemical and materials properties. This thesis describes post functionalization of **Py_2TTAH** and its precursor compounds *via* alkylation and arylation of the sulfur atom, as well as through coordination with iron and boron moieties.

In Chapter 2, work towards generating a stable derivative of 1.46 (*bis*-*N*-bridgehead-1,2,5-thiadiazolium dication), such that a biradical may be realized is presented. Previously, the biradical was inaccessible, attributed to the presence of the central proton in **1.46**. Chapter 2 describes attempts to replace the central proton with an alkyl group, as this was anticipated to enhance the stability of the dication

framework towards reduction. While the biradical remains elusive, the preliminary alkylation studies presented in Chapter 2 led to the development of sulfur functionalized **TTA** derivatives. The synthesis and properties of these derivatives were explored, as detailed in Chapter 3. As well, the repertoire of coordination complexes using the **Py_2TTA** framework has been expanded, with two iron complexes described in Chapter 4. Finally, Chapter 5 presents the coordination of boron difluoride moieties with both *N*-2-pyridylimidoyl-2-pyridylamidine (**1.44**) and **Py_2TTAH** (**1.47**), proposing a boratriazine complex as the most likely product.

1.8 References

1. N. T. Kalyani and S. J. Dhoble, *Renewable & Sustainable Energy Reviews*, 2015, **44**, 319-347.

2. A. Mishra and P. Bauerle, *Angewandte Chemie-International Edition*, 2012, **51**, 2020-2067.

3. C. Wang, H. Dong, W. Hu, Y. Liu and D. Zhu, *Chemical Reviews*, 2012, **112**, 2208-2267.

4. B. Kippelen and J. L. Bredas, *Energy & Environmental Science*, 2009, **2**, 251-261.

5. V. Coropceanu, J. Cornil, D. A. da Silva, Y. Olivier, R. Silbey and J. L. Bredas, *Chemical Reviews*, 2007, **107**, 926-952.

6. Y. Dienes, M. Eggenstein, T. Karpati, T. C. Sutherland, L. Nyulaszi and T. Baumgartner, *Chemistry-a European Journal*, 2008, **14**, 9878-9889.

7. C. D. Dimitrakopoulos and D. J. Mascaro, *Ibm Journal of Research and Development*, 2001, **45**, 11-27.

8. M. Irimia-Vladu, *Chemical Society Reviews*, 2014, **43**, 588-610.

9. T. Kono, D. Kumaki, J. Nishida, S. Tokito and Y. Yamashita, *Chemical Communications*, 2010, **46**, 3265-3267.

10. M. Karikomi, C. Kitamura, S. Tanaka and Y. Yamashita, *Journal of the American Chemical Society*, 1995, **117**, 6791-6792.

11. F. Magnan, I. Korobkov and J. Brusso, *New Journal of Chemistry*, 2015, **39**, 7272-7280.

12. A. Mishra, C. Q. Ma and P. Bauerle, *Chemical Reviews*, 2009, **109**, 1141-1276.

13. S. Steinberger, A. Mishra, E. Reinold, J. Levichkov, C. Uhrich, M. Pfeiffer and P. Bauerle, *Chemical Communications*, 2011, **47**, 1982-1984.

14. R. Z. Tang, F. Zhang, Y. B. Fu, Q. Xu, X. Y. Wang, X. D. Zhuang, D. Q. Wu, A. Giannakopoulos, D. Beljonne and X. L. Feng, *Organic Letters*, 2014, **16**, 4726-4729.

15. G. Lu, H. Usta, C. Risko, L. Wang, A. Facchetti, M. A. Ratner and T. J. Marks, *Journal of the American Chemical Society*, 2008, **130**, 7670-7685.

16. D. Chapman, A. D. Yoffe, A. G. Fitzgerald and R. J. Warn, *Transactions of the Faraday Society*, 1964, **60**, 294-300.

17. R. T. Oakley, *Canadian Journal of Chemistry-Revue Canadienne De Chimie*, 1993, **71**, 1775-1784.

18. S. S. Afjeh, A. A. Leitch, I. Korobkov and J. L. Brusso, *Rsc Advances*, 2013, **3**, 23438-23444.

19. A. A. Leitch, I. Korobkov, A. Assoud and J. L. Brusso, *Chemical Communications*, 2014, **50**, 4934-4936.

20. L. Beer, J. F. Britten, J. L. Brusso, A. W. Cordes, R. C. Haddon, M. E. Itkis, D. S. MacGregor, R. T. Oakley, R. W. Reed and C. M. Robertson, *Journal of the American Chemical Society*, 2003, **125**, 14394-14403.

21. J. Britten, N. G. R. Hearns, K. E. Preuss, J. F. Richardson and S. Bin-Salamon, *Inorganic Chemistry*, 2007, **46**, 3934-3945.

22. N. G. R. Hearns, E. M. Fatila, R. Clerac, M. Jennings and K. E. Preuss, *Inorganic Chemistry*, 2008, **47**, 10330-10341.

23. N. G. R. Hearns, R. Clerac, M. Jennings and K. E. Preuss, *Dalton Transactions*, 2009, 3193-3203.

24. E. R. Clark, J. J. Hayward, B. J. Leontowicz, M. U. Anwar, M. Pilkington and J. M. Rawson, *Dalton Transactions*, 2015, **44**, 2071-2074.

25. N. J. Yutronkie, A. A. Leitch, I. Korobkov and J. L. Brusso, *Crystal Growth & Design*, 2015, **15**, 2524-2532.

26. C. Y. Ang, R. T. Boere, L. Y. Goh, L. L. Koh, S. L. Kuan, G. K. Tan and X. Yu, *Chemical Communications*, 2006, 4735-4737.

27. C. Y. Ang, S. L. Kuan, G. K. Tan, L. Y. Goh, T. L. Roemmele, X. Yu and R. T. Boere, *Canadian Journal of Chemistry*, 2015, **93**, 181-195.

28. K. L. M. Harriman, A. A. Leitch, S. A. Stoian, F. Habib, J. L. Kneebone, S. I. Gorelsky, I. Korobkov, S. Desgreniers, M. L. Neidig, S. Hill, M. Murugesu and J. L. Brusso, *Dalton Transactions*, 2015, **44**, 10516-10523.

29. K. L. M. Harriman, I. A. Kuhne, A. A. Leitch, I. Korobkov, R. Clerac, M. Murugesu and J. L. Brusso, *Inorganic Chemistry*, 2016, 11340-11344.

30. N. J. Yutronkie, I. A. Kuehne, I. Korobkov, J. L. Brusso and M. Murugesu, *Chemical Communications*, 2016, **52**, 677-680.

31. J. Goerdeler and D. Loevenich, *Chemische Berichte-Recueil*, 1954, **87**, 1079-1082.

32. R. Appel and H. Gerber, *Chemische Berichte-Recueil*, 1958, **91**, 1200-1203.

33. R. Appel and G. Vollmer, *Chemische Berichte-Recueil*, 1970, **103**, 2555-2561.

34. H. W. Roesky, *Angewandte Chemie-International Edition*, 1969, **8**, 510.

35. M. Haake, H. Fode and K. Ahrens, *Zeitschrift Fur Naturforschung Section B-a Journal of Chemical Sciences*, 1973, **B 28**, 539-540.

36. G. H. Denny, E. J. Cragoe, C. S. Rooney, J. P. Springer, J. M. Hirshfield and J. A. McCauley, *Journal of Organic Chemistry*, 1980, **45**, 1662-1665.

37. A. Kalman, G. Argay, E. Fischer and M. Teller, *Acta Crystallographica Section B-Structural Science*, 1981, **37**, 164-168.

38. J. D. Michael, B. C. Ross and P. M. Rees, *Tetrahedron Letters*, 1985, **26**, 4149-4152.

39. H. Tashtoush and M. Altalib, *Recueil Des Travaux Chimiques Des Pays-Bas-Journal of the Royal Netherlands Chemical Society*, 1989, **108**, 117-119.

40. J. Goerdeler and B. Wedekind, *Chemische Berichte-Recueil*, 1962, **95**, 147-153.

41. J. Goerdeler and K. Doerk, *Chemische Berichte-Recueil*, 1962, **95**, 154-157.

42. G. Leonhardt, R. Scheibe, W. Schramm, G. Voss, E. Fischer and G. Rembarz, *Zeitschrift Fur Chemie*, 1975, **15**, 193-194.

43. W. Schramm, G. Voss, G. Rembarz and E. Fischer, *Zeitschrift Fur Chemie*, 1974, **14**, 471-472.

44. W. Schramm, G. Voss, M. Michalik, G. Rembarz and E. Fischer, *Zeitschrift Fur Chemie*, 1975, **15**, 19-19.

45. W. Schramm, G. Voss, G. Rembarz and E. Fischer, *Zeitschrift Fur Chemie*, 1975, **15**, 57-58.

46. W. Storek, W. Schramm, G. Voss, G. Rembarz and E. Fischer, *Zeitschrift Fur Chemie*, 1975, **15**, 104-105.

47. P. Jeroschewski, G. Voss and E. Fischer, *Zeitschrift Fur Chemie*, 1977, **17**, 145-145.

48. A. Kalman, G. Argay, E. Fischer, G. Rembarz and G. Voss, *Journal of the Chemical Society-Perkin Transactions 2*, 1977, 1322-1327.

49. M. Michalik, E. Fischer, G. Rembarz, G. Voss and W. Storek, *Journal Fur Praktische Chemie*, 1977, **319**, 739-744.

50. A. Kalman, G. Argay, E. Fischer and G. Rembarz, *Acta Crystallographica Section B-Structural Science*, 1979, **35**, 860-866.

51. E. Fischer, G. Rembarz and M. Teller, *Journal Fur Praktische Chemie*, 1982, **324**, 920-924.

52. S. J. Cousins, B. C. Ross, G. N. Maw and J. D. Michael, *Tetrahedron Letters*, 1985, **26**, 1105-1108.

53. P. P. Kornuta, L. I. Derii and L. N. Markovskii, *Zhurnal Organicheskoi Khimii*, 1980, **16**, 1308-1313.

54. W. Ried and M. A. Jacobi, *Chemische Berichte-Recueil*, 1988, **121**, 383-386.

55. E. Fischer, E. Jaudasprezel, R. Maggiulli, R. Mews, H. Oberhammer, R. Paape and W. D. Stohrer, *Chemische Berichte*, 1991, **124**, 1347-1352.

56. T. V. V. Ramakrishna, A. J. Elias and A. Vij, *Inorganic Chemistry*, 1999, **38**, 3022-3026.

57. M. Haake and W. Jurgler, *Zeitschrift Fur Naturforschung Section B-a Journal of Chemical Sciences*, 1988, **43**, 763-768.

58. A. D. Stoller, *Journal of Heterocyclic Chemistry*, 2000, **37**, 583-595.

59. G. Hamprecht, K. H. Konig and G. Stubenrauch, *Angewandte Chemie-International Edition in English*, 1981, **20**, 151-164.

60. A. Stoller, W. Kunz, H. Zondler, C. Kuethy and J. Wenger, *WO Pat.*, 9808845-A1, 1998.

61. A. Stoller and W. Kunz, *WO Pat.*, 9725319-A, 1997.

62. H. Zondler and A. Stoller, *WO Pat.*, 9725318-A, 1997.

63. L. C. Peng, F. Xiang, E. Roberts, Y. Kawagoe, L. C. Greve, K. Kreuz and D. P. Delmer, *Plant Physiology*, 2001, **126**, 981-992.

64. L. N. Markovskii, P. P. Kornuta, L. S. Kachkovskaya and O. M. Polumbrik, *Sulfur Lett.*, 1983, **1**, 143-145.

65. Y. C. Kong, K. Kim and Y. J. Park, *Tetrahedron*, 2000, **56**, 7153-7161.

66. R. T. Oakley, R. W. Reed, A. W. Cordes, S. L. Craig and J. B. Graham, *Journal of the American Chemical Society*, 1987, **109**, 7745-7749.

67. A. W. Cordes, P. J. Hayes, P. D. Josephy, H. Koenig, R. T. Oakley and W. T. Pennington, *Journal of the Chemical Society-Chemical Communications*, 1984, 1021-1022.

68. P. J. Hayes, R. T. Oakley, A. W. Cordes and W. T. Pennington, *Journal of the American Chemical Society*, 1985, **107**, 1346-1351.

69. R. T. Boere, A. W. Cordes, P. J. Hayes, R. T. Oakley, R. W. Reed and W. T. Pennington, *Inorganic Chemistry*, 1986, **25**, 2445-2450.

70. R. T. Boere, R. T. Oakley, R. W. Reed and N. P. C. Westwood, *Journal of the American Chemical Society*, 1989, **111**, 1180-1185.

71. J. Geevers, J. T. Hackmann and W. P. Trompen, *Journal of the Chemical Society C-Organic*, 1970, 875-878.

72. R. T. Boere and T. L. Roemmele, *Phosphorus Sulfur and Silicon and the Related Elements*, 2004, **179**, 875-882.

73. R. T. Boere, T. L. Roemmele and X. Yu, *Inorganic Chemistry*, 2011, **50**, 5123-5136.

74. E. C. Constable, *Chemical Society Reviews*, 2007, **36**, 246-253.

75. A. Wild, A. Winter, F. Schlutter and U. S. Schubert, *Chemical Society Reviews*, 2011, **40**, 1459-1511.

76. A. Winter, G. R. Newkome and U. S. Schubert, *Chemcatchem*, 2011, **3**, 1384-1406.

77. C. E. Bacon, D. J. Eisler, R. L. Melen and J. M. Rawson, *Chemical Communications*, 2008, 4924-4926.

Chapter 2 – Progress Towards the Formation of *bis*-*N*-bridgehead-1,2,5-thiadiazolyl Biradicals

2.1 Introduction

Molecular biradicals comprise a class of compounds that contain two unpaired electrons. The presence of two spins within the molecular framework can lead to a wide variety of interesting chemical properties, reactivity, and unique electronic structures, making biradicals ideal candidates for materials applications. Conjugated biradicals can be separated into two classes; Kekulé and non-Kekulé.[1] Kekulé biradicals are short-lived open-shell resonance structures of molecules that also exist in a closed shell form. An example of such a molecule is *p*-quinodimethane, where the biradical resonance form is stabilized by aromaticity (Figure 2-1), and the closed shell form also contributes to the overall structure of this molecule.[1]

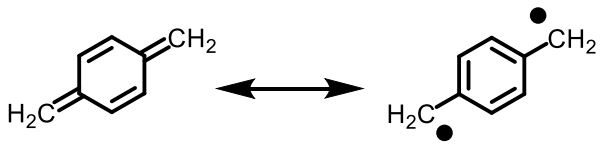

Figure 2-1. Resonance structures of *p*-quinodimethane in the closed shell (left) and biradical (right) states.

Alternately, in non-Kekulé biradicals, each unpaired spin exists in its own spin system, isolated from each other. In other words, a resonance structure without a radical centre does not exist. These unpaired spins are typically aligned in a parallel manor, consistent with Hund's rule, and thus non-Kekulé biradicals typically exhibit

triplet ground states.[2] Such biradicals can be stabilized in several ways, including the addition of bulky side chains, the inclusion of heavier main group atoms, and the addition of electron donating groups, as highlighted by examples in Chart 2-1.[3, 45 6 7-9 10]

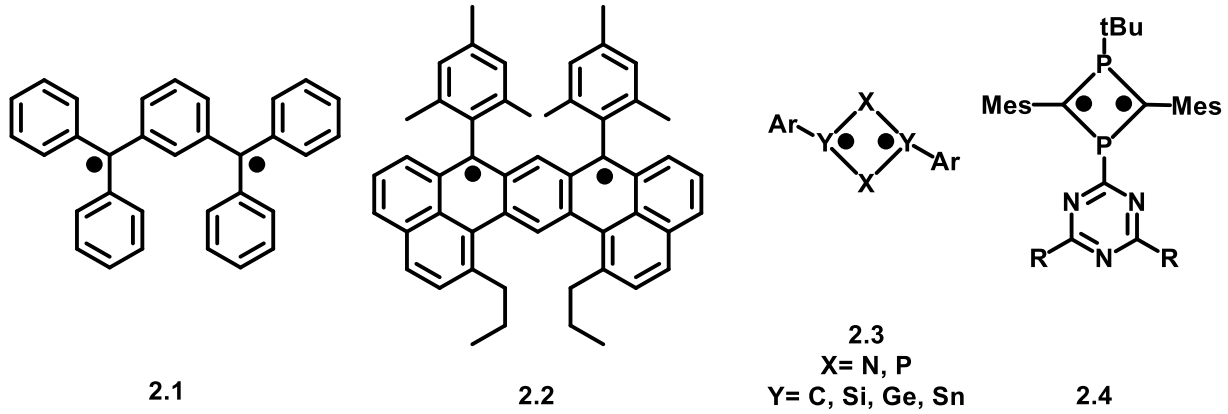

Chart 2-1. Examples of stabilized non-Kekulé biradicals.

2.1.1 Biradical Formation from the *bis*-*N*-bridgehead-1,2,5-thiadiazolium Dication

In addition to being unique and interesting chemically, biradicals are also relevant towards research into materials chemistry applications. As outlined in Chapter 1, previous work in the Brusso lab afforded a *bis*-*N*-bridgehead-1,2,5-thiadiazolium dication (**2.8**) as an intermediate in the synthesis of the 3,5-*bis*(2-pyridyl)-1,2,4,6-thiatriazinyl radical (**2.10**; Scheme 2-1).[11] Formation of a biradical based on the dication framework of **2.8** is quite appealing, as it would represent the first example of an *N*-bridgehead biradical. However, addition of the reducing agent triphenylantimony to **2.8** did not lead to the desired biradical, instead yielding the six-membered TTA ring 3,5-*bis*(2-pyridyl)-4-hydro-1,2,4,6-thiatriazine (**Py_2TTAH**; **2.9**). Here, generation of **2.9**

instead of **2.11** was attributed to the presence of a proton on the central nitrogen of **2.8**, as protons are known to undergo fast rearrangements (proton shifts) during chemical reactions.[12] While the proton remains on the central nitrogen atom of the **TTA** ring of **Py$_2$TTAH**, the yield of this reaction is only 51%,[11] suggesting the possibility of sacrificial starting material, or the possibility of another proton shift, returning the proton to its original location. To test this hypothesis, an analogous framework that replaces the central proton with an alkyl substituent would eliminate the acidic proton on the central nitrogen atom, thus eliminating the potential of proton shifting during the reduction reaction and providing an avenue to realize the biradical.

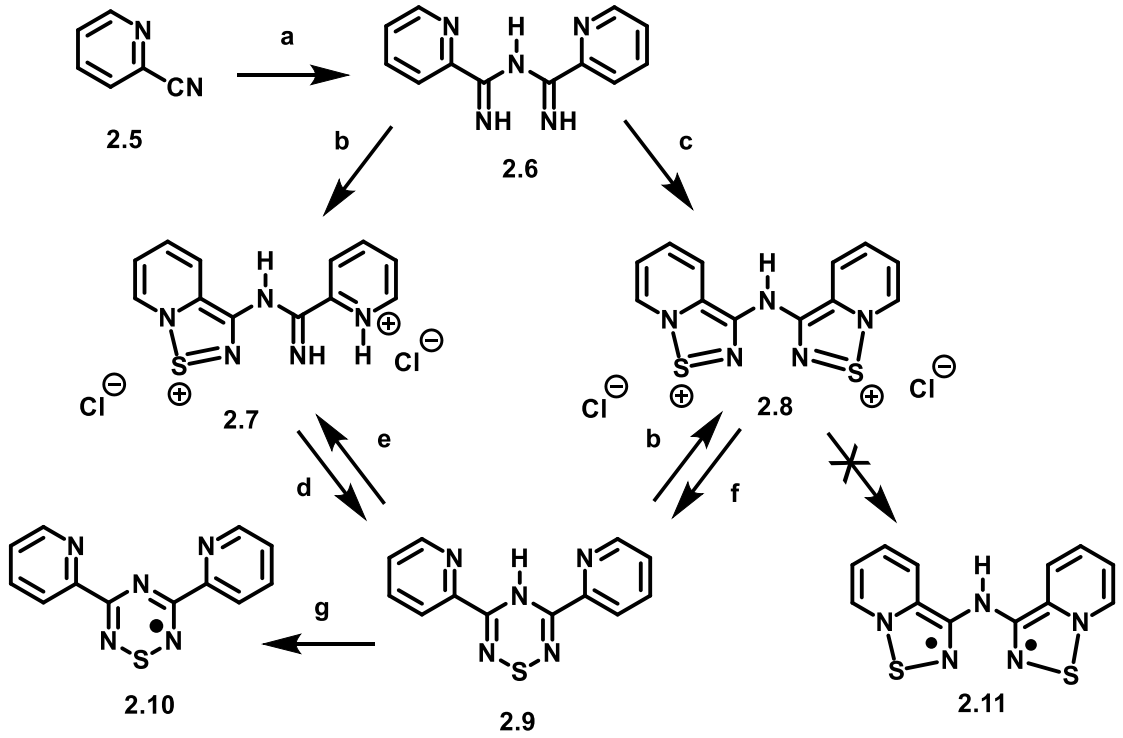

Scheme 2-1. Synthesis of the pyridyl substituted thiatrazinyl radical **2.10**. Reagents and conditions: (a) NH_3, MeCN (b) S_2Cl_2, MeCN, RT (c) S_2Cl_2, MeCN, reflux (d) PhCl, reflux (e) H^+ (f) Ph_3Sb, MeCN, RT (g) NCS, DMAP, MeCN, RT.

2.1.2 Scope of this Chapter

This chapter presents work undertaken to alkylate the *bis*-*N*-bridgehead-1,2,5-thiadiazolium dication, to be used as a precursor in the formation of biradicals. In particular, 3,3′-(methylazanediyl)*bis*([1,2,5]thiadiazolo[2,3-*a*]1-pyridinium) and 3,3′-(ethylazanediyl)*bis*([1,2,5]thiadiazolo[2,3-*a*]1-pyridinium) (**2.14** and **2.15**, respectively; Scheme 2-2) were targeted with the intent to isolate biradicals **2.17** and **2.18**, respectively. As described previously, **2.8** can be prepared from either *N*-2-pyridylimidoyl-*2*-pyridylamidine (**2.6**),[11] or **Py$_2$TTAH** (unpublished results; Scheme 2-1). Therefore, attempts to synthesize **2.14** and **2.15** began with alkylation of **2.6**, **2.8**, and **2.9** (Scheme 2-2). Overall, this chapter documents the steps taken and setbacks encountered while attempting to synthesize a biradical from **2.14** and **2.15**.

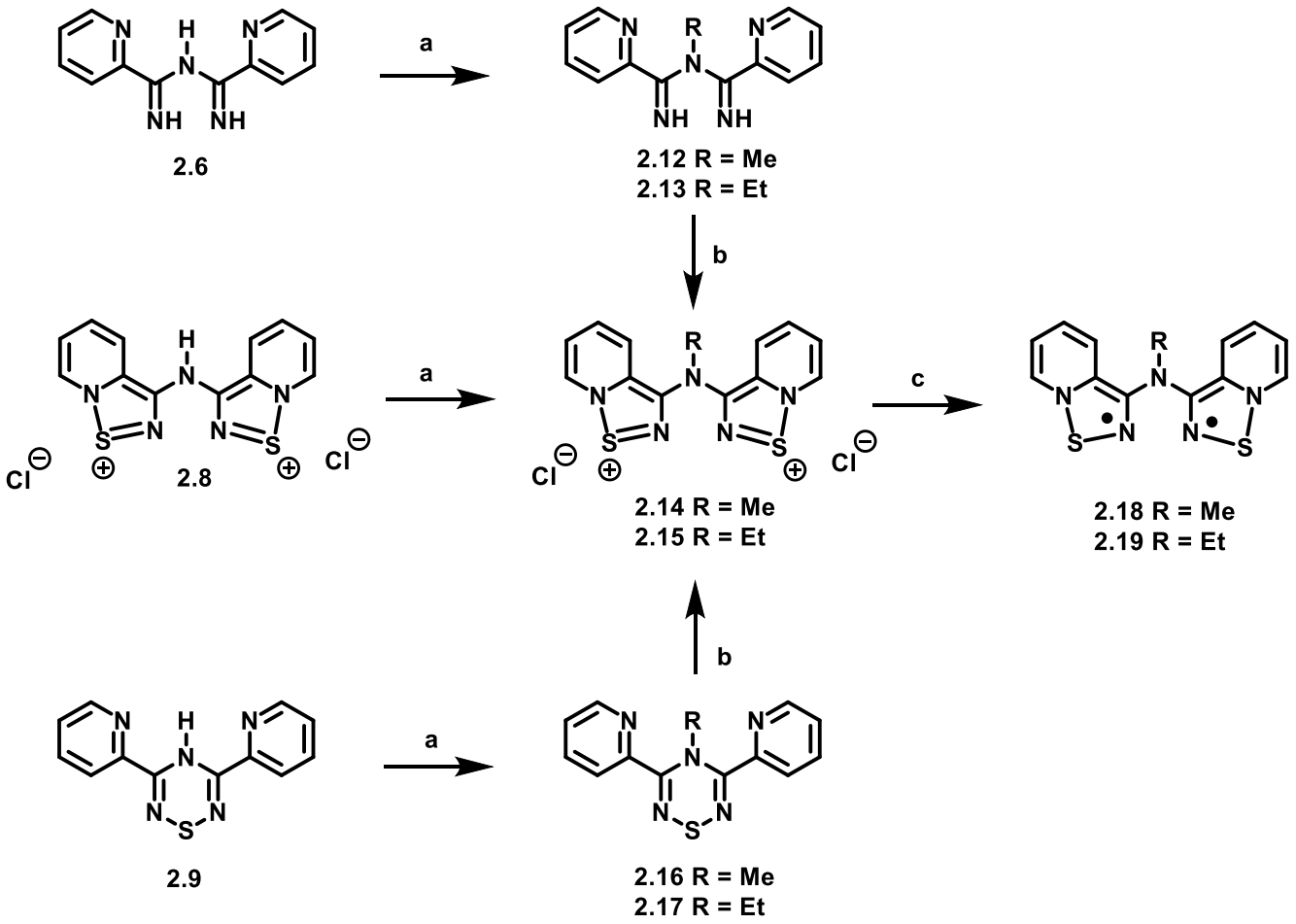

Scheme 2-2. Proposed synthesis of the alkylated dications **2.14** and **2.15** and the alkylated biradicals **2.18** and **2.19**. Proposed reagents: (a) alkylating agent (b) S_2Cl_2 (c) reducing agent.

2.2 Alkylation Reactions

Alkylation of the central nitrogen atom was considered from the three potential starting materials: **2.6**, **2.8**, and **2.9**, as outlined in Scheme 2-2. Of these, alkylation of **2.6** was initially studied, as it is the starting material for the synthesis of both **2.8** and **2.9**.

2.2.1 Alkylation of *N*-2-pyridylimidoyl-2-pyridylamidine

Initial attempts to alkylate **2.6** involved direct deprotonation using sodium hydride (NaH), followed by the addition of methyl or ethyl iodide. These reactions resulted in the formation of a mixture of methylated products, based on ^{1}H NMR analysis (Figure 2.2). Unfortunately, this mixture proved to be inseparable by column chromatography or *via* recrystallization.

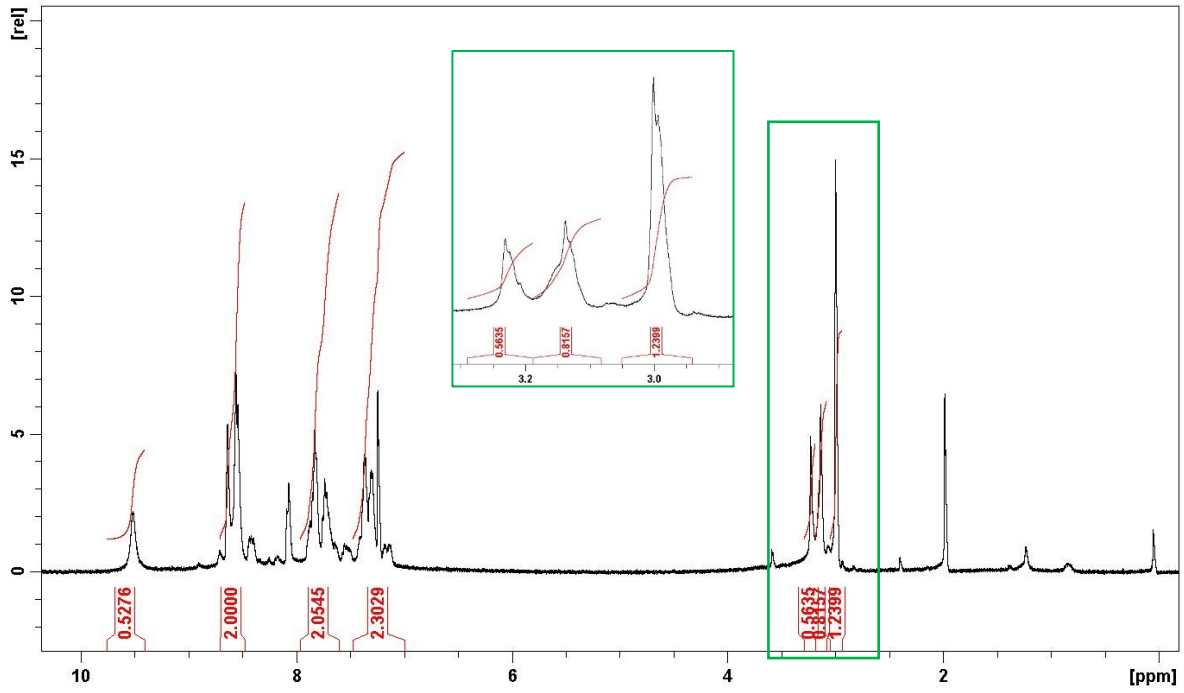

Figure 2-2. ^{1}H NMR spectrum of reaction with **2.6**, NaH, and MeI in $CDCl_3$.

As purification of the product from the aforementioned reaction was unsuccessful, alternate synthetic routes were considered in which alkylation is achieved prior the formation of the imidoyl amidine. Since *N*-2-pyridylimidoyl-2-pyridylamidine (**2.6**) can be prepared *via* the reaction between 2-cyanopyridine (**2.5**) and ammonia gas

in a pressure vessel at 110°C for three days,[11] analogous reactions were carried out in which methylamine solutions (in THF, EtOH, and H_2O) were used in place of the ammonia gas. Unfortunately, these reactions did not afford the desired product (**2.13**). Instead, either only starting materials were observed (THF), or the isolated products did not possess the necessary signal in the aliphatic region for a methyl group upon ^1H NMR analysis (EtOH and H_2O solutions). Based on these results, it was concluded that a concerted one-step synthesis was ineffective under the conditions described.

Another method for preparing imidoyl amidines involves a two-step reaction with solid ammonium chloride ($[NH_4][Cl]$), sodium methoxide, and the desired carbonitrile (i.e., **2.5**; Scheme 2-3).[13] Following this route, the carbonitrile is reacted sequentially with sodium methoxide then $[NH_4][Cl]$. The resulting amine (**2.20**) can then be deprotonated with sodium hydride (NaH) and reacted with a second equivalence of the carbonitrile (**2.5**), forming the imidoyl amidine (**2.6**). Using an adapted version of this synthetic route, **2.5** was reacted with sodium methoxide and then methylamine hydrochloride, instead of ammonium chloride in order to prepare *N*-methyl-2-pyridinecarboximidamide (**2.21**; Scheme 2-3). IR and ^1H NMR analysis revealed the presence of two tautomers. These were taken forward without further purification, as deprotonation should yield the same product. To that end, following treatment of **2.21** with NaH, a second equivalent of **2.5** was added and the reaction was left to stir at room temperature in THF for 16 hours. The resulting slurry was quenched

with H_2O, and then extracted into DCM. The organic layer was collected and the solvent was removed under reduced pressure. Unfortunately, the ^1H NMR of the resulting brown oil indicated that this reaction also yielded a mixture of products (i.e., **2.22a** and **2.22b**), with the major product appearing to be methylated on one of the imine nitrogen atoms (**2.22a**). This conclusion was drawn based on the presence of both asymmetrical and symmetrical pyridyl peaks, with the asymmetrical peaks belonging to the major product. While a minor product did appear to be methylated on the desired central nitrogen, the yield of this species was low, and proved to be inseparable from the major product by chromatography.

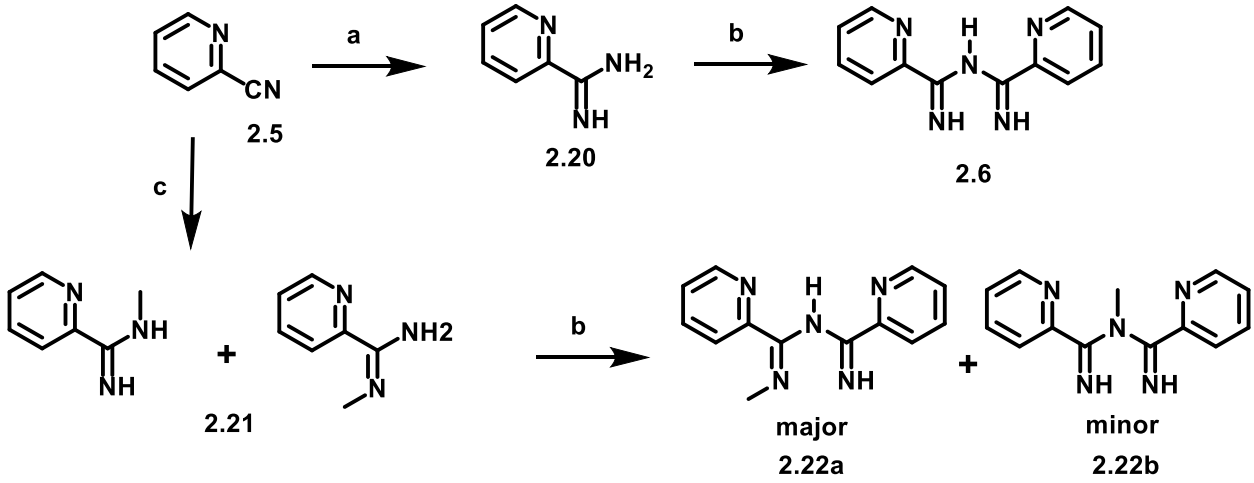

Scheme 2-3. Synthesis of mixture **2.22**. Reagents and conditions: (a) 1. Na, MeOH 2. $[NH_4][Cl]$ (b) 1. NaH 2. CNPy (c) 1. Na, MeOH 2. $[NMeH_3][Cl]$.

2.2.2 Alkylation of the *bis-N*-bridgehead-1,2,5-thiadiazolium dication

Since alkylation of **2.6** proved to be difficult, deprotonation and subsequent alkylation of **2.8** was considered. Addition of NaH to a stirring slurry of **2.8** in THF

resulted in a colour change from pure white to a darker cream coloured slurry, and small bubbles of gas evolved, indicative of hydrogen gas generation. The subsequent addition of alkyl iodides, however, did not promote alkylation, instead reverting the compound back to the protonated starting material upon exposure to atmospheric conditions, as found through IR and ^{1}H NMR spectroscopic analysis. In an analogous reaction, replacing alkyl iodides with a stronger alkylating agent such as methyl triflate resulted in the formation of a very thick, viscous material. When analyzed by IR and ^{1}H NMR spectroscopy, the product only contained signals corresponding to the THF solvent; it was later realized that the methyl triflate was promoting THF polymerization, and thus if the desired alkylation was occurring, it was masked by the resulting polymeric matrix.[14] As simultaneous trials to alkylate **Py$_2$TTAH** were more promising, as described in the next section, alkylation reactions starting from **2.8** were set aside.

2.2.3 Alkylation of 3,5-*bis*-(2-pyridyl)-1,2,4,6-thiatriazine

Starting from **2.9** (**Py$_2$TTAH**), deprotonation is a necessary first step in achieving alkylation due to the presence of a proton on the central nitrogen atom. While previous attempts to deprotonate **Py$_2$TTAH** with bases such as KOH or proton sponge were unsuccessful,[11] deprotonation was achieved upon coordination with iron.[15] Therefore, metal-containing irreversible bases (e.g., NaH) were considered. Upon addition of NaH

to a solution of **Py_2TTAH** in THF, the initial dark purple solution turned a bright emerald green with fine yellow solids and bubbles of H_2 gas formed. The subsequent addition of methyl iodide (MeI) to the reaction mixture afforded an orangey-yellow precipitate, which was isolated by filtration after 16 hours of stirring at RT. The ^{1}H NMR spectrum of this solid (Figure 2-3) contained four aromatic peaks with integrations, chemical shifts and coupling patterns consistent with two symmetrical pyridyl substituents, which differed from the starting material. In addition, a signal at 2.86 ppm that integrated to three protons was present, suggesting heteroatomic alkylation of the product, consistent with the formation of *N*-methyl-3,5-*bis*-(2-pyridyl)-1,2,4,6-thiatriazine (**2.16**, Scheme 2-4).

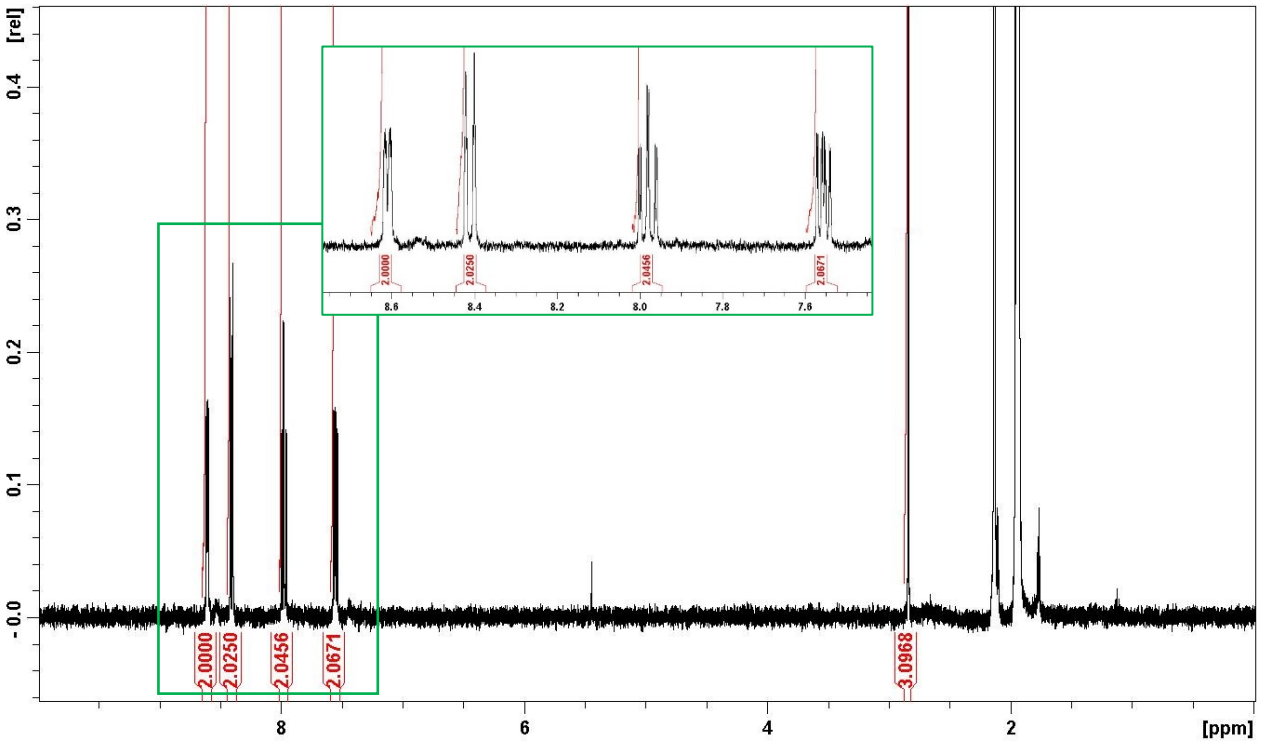

Figure 2-3. ^{1}H NMR spectrum of **2.16** in MeCN-d_3.

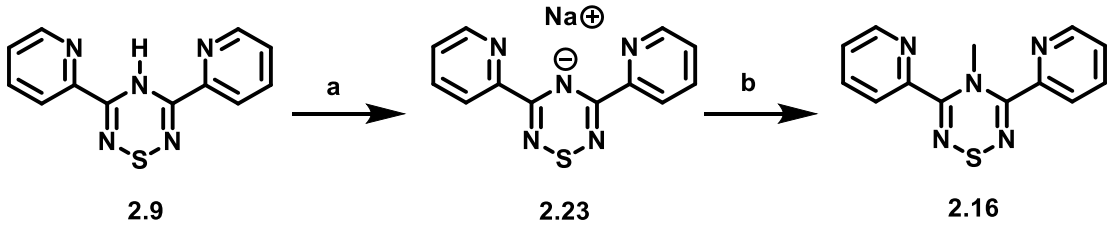

Scheme 2-4. Synthesis of *N*-Methyl-3,5-*bis*-(2-pyridyl)-1,2,4,6-thiatriazine (**2.16**). Reagents and conditions: (a) NaH, THF (b) MeI, THF.

2.3 Attempts to Prepare the Alkylated Dication 2.14

Encouraged by the successful alkylation of **Py$_2$TTAH**, experiments were carried out to convert **2.16** to the dication framework **2.14**. Initial attempts involved treatment of **2.16** with S_2Cl_2 in MeCN. Approximately three minutes after the addition of S_2Cl_2, the clear yellow solution turned into a cloudy yellow slurry before becoming an opaque peach coloured slurry. The reaction was then stirred for four hours at room temperature, after which a small amount of air-sensitive pink-beige coloured solid was isolated by filtration. Purification and characterization of this product proved challenging due to its insolubility in common organic solvents, although this would be expected if the product was a dichloride salt, as they tend to display very limited solubility. In order to enhance solubility and enable characterization, a metathesis reaction was performed using trimethylsilyl triflate (TMS OTf). While the resulting fine beige powder was partially soluble in MeCN-d_6, the ^{1}H NMR spectrum exhibited signals that were inconsistent with what would be expected for **2.14**.

A variety of reaction conditions were used to synthesize **2.14** from **2.16**, including various solvents (i.e., dichloroethane (DCE), MeCN/DCE mixtures, chlorobenzene), reaction temperatures (i.e., RT, reflux), and reaction times. In all cases, only a small amount of solid was obtained and, upon IR analysis, they were found to contain starting materials and other unidentifiable compounds that showed no similarities to **2.8**. When metathesis reactions were attempted to characterize these products, dark viscous products were obtained that were unidentifiable *via* ^{1}H NMR spectroscopy.

2.4 Analagous Reactions Using Ethyl Iodide

In order to determine if steric bulk was preventing alkylation, reactions with ethyl idodide (EtI) were considered in order to make *N*-ethyl-3,5-*bis*-(2-pyridyl)-1,2,4,6-thiatriazine (**2.17**; Scheme 2-2). While an ethyl substituent is larger overall than a methyl group, the steric bulk directly beside the central nitrogen is decreased from a $-CH_3$ to a $-CH_2$ group. As such, the ethyl derivative was prepared following a similar synthetic procedure to that of **2.16** (i.e., deprotonating Py_2TTAH and reacting with EtI). The resulting product was obtained as an orange-yellow powder, which was found to be very similar to the methyl derivative upon analysis by IR, ^{1}H NMR (Figure 2-4) and ^{13}C NMR (Figure 2-5) spectroscopy. Chapter 3 (section 3.2) contains more details regarding the spectroscopic analysis.

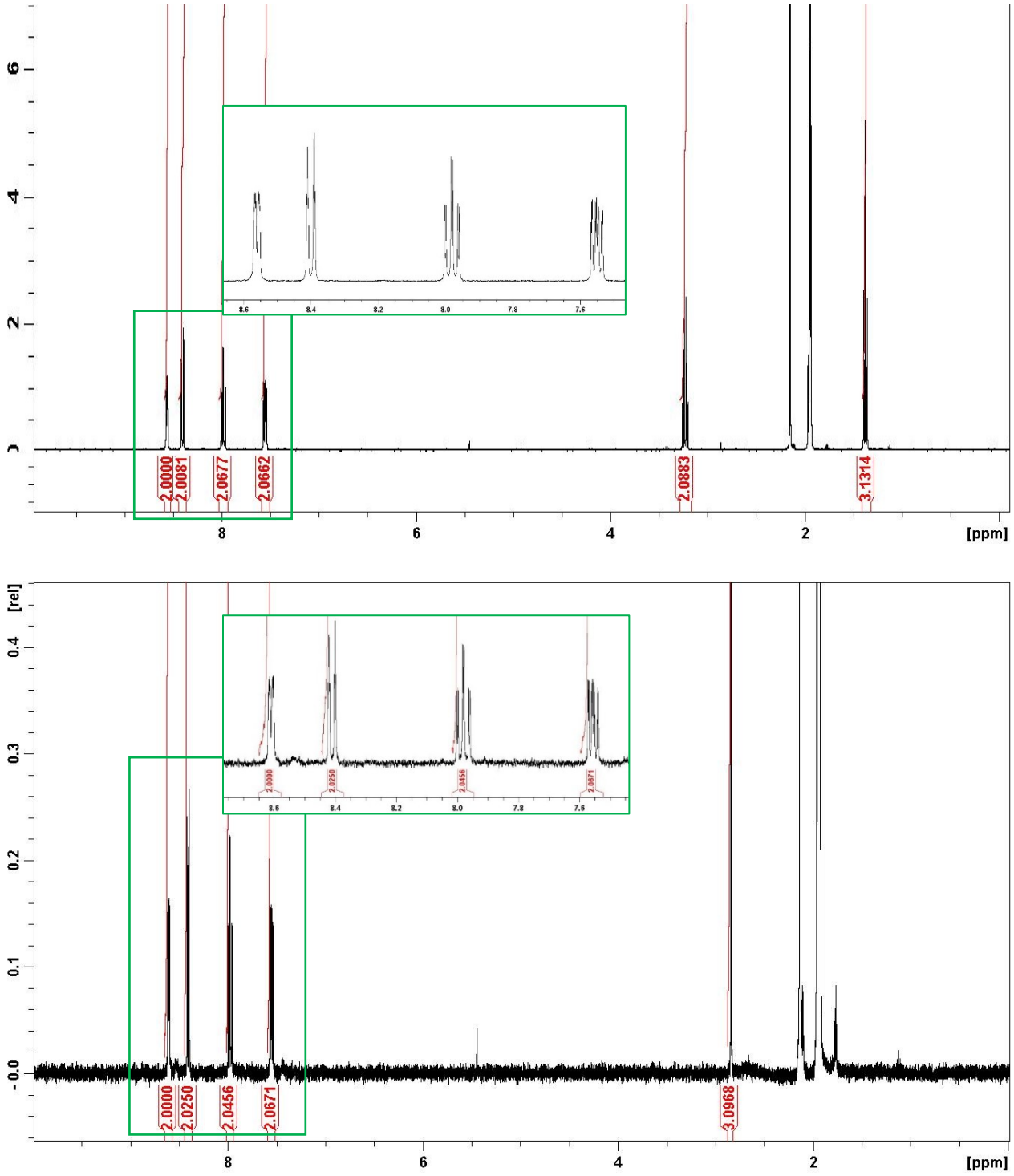

Figure 2-4. ^{1}H NMR spectra of **2.17** (top) and **2.16** (bottom) in MeCN-d_3.

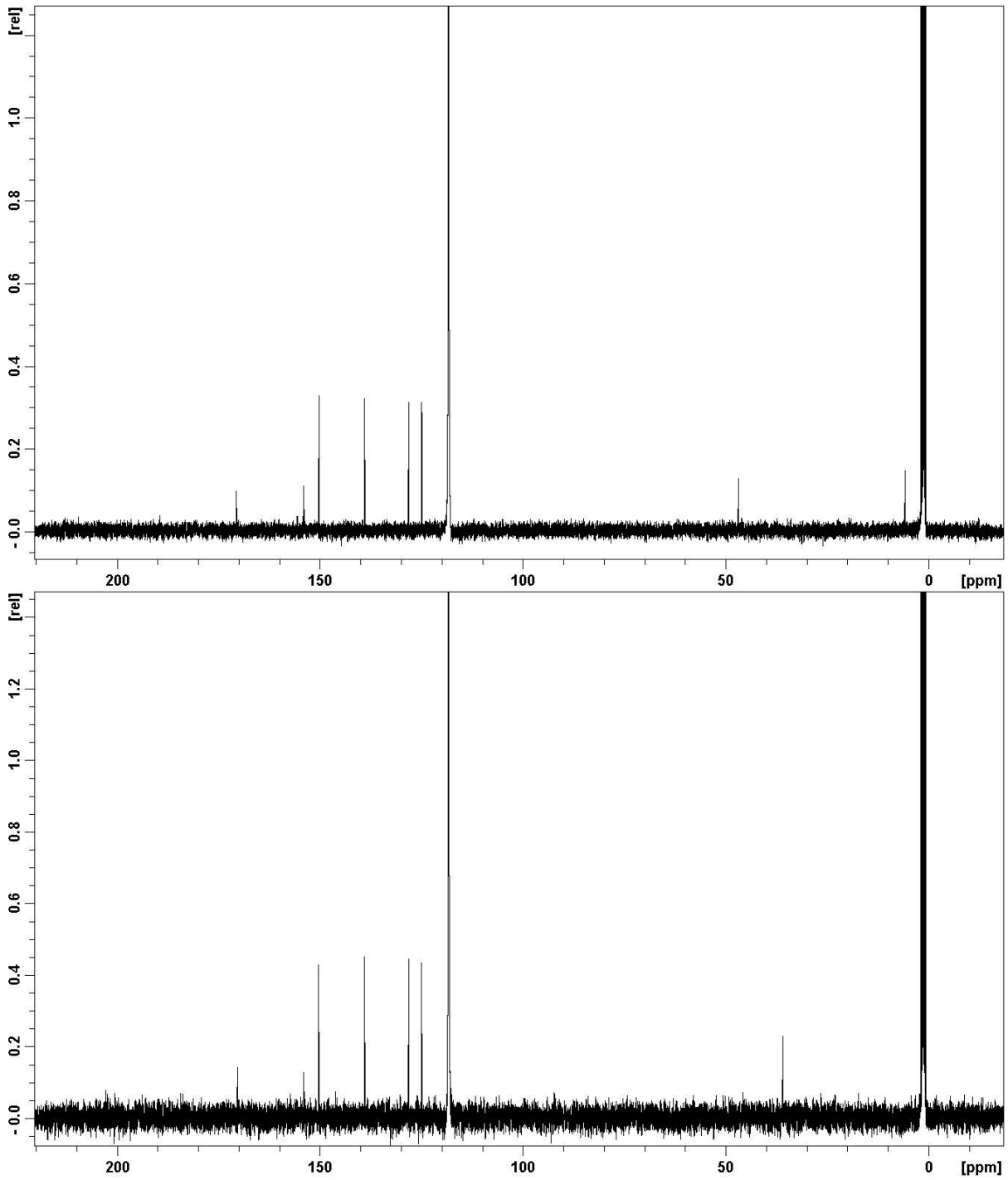

Figure 2-5. ^{13}C NMR spectra of **2.17** (top) and **2.16** (bottom) in MeCN-d_3.

Reactions to synthesize the ethylated dication framework (**2.15**), however, were plagued with the same challenges and shortcomings as the methyl derivative, resulting

in very low yields, as well as dark, viscous products following metathesis with TMS triflate. Furthermore, in a couple of trials, instead of achieving the alkylated dication (**2.15**) the major product was actually identified to be **2.8** (the protonated dication), as verified by both IR and ^{1}H NMR spectroscopy.

As the synthesis of **2.14** and **2.15** was not proceeding as expected based on the known reactivity of **Py$_2$TTAH** with S_2Cl_2, the purity and identity of these compounds were reconsidered. X-ray quality yellow block-like crystals of the ethyl derivative were eventually achieved *via* vapour diffusion of Et_2O into a saturated DCM solution. X-ray analysis revealed ethylation occurred on the sulfur atom of the TTA ring as opposed to the central nitrogen, forming *S*-ethyl-3,5-*bis*-(2-pyridyl)-1,2,4,6-thiatriazine. As well, the *S*-ethylated **TTA** derivative formed a one dimensional coordination polymer through interactions with sodium and μ-bridging iodide ions (Figure 2-6). Given that the ^{1}H and ^{13}C NMR and IR analyses of the methyl and ethyl derivatives were consistent with each other, it is reasonable to conclude that methylation also occurs on the sulfur atom, forming a similar coordination complex. A more detailed description and analysis of these compounds can be found in Chapter 3.

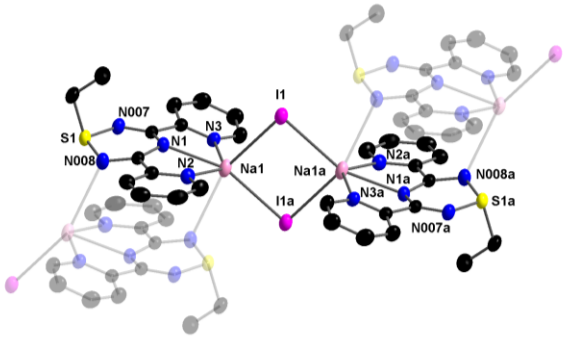

Figure 2-6. Asymmetric unit of the obtained ethyl coordination polymer using 50% thermal ellipsoids. Hydrogen atoms omitted for clarity.

2.5 Conclusions

In conclusion, several starting materials were considered in an endeavour to synthesize 3,3′-(methylazanediyl)*bis*([1,2,5]thiadiazolo[2,3-*a*]1-pyridinium) (**2.14**) and the ethyl analog (**2.15**), with the intent to isolate **2.18** and **2.19**. While the biradicals remain elusive, a synthetic pathway for sulfur functionalization post-TTA ring formation was established. This discovery has potential in a number of interesting applications including the use of *S*-functionalized TTA products as ligands in metal coordination or as a building block in polymers and networks, and is described in more detail in Chapters 3 and 4.

2.6 Future Work

While a biradical was not realized, future work towards an alkylated framework (i.e., **2.14** or **2.15**) should involve deprotonation and alkylation of **2.8**. Although reactions reported here were unsuccessful, alkylation may be achieved using MeOTf in solvents other than THF, in order to prevent polymerization of the solvent. Although

the formation of a zwitterionic species during the deprotonation of a dication may seem unlikely, small gas bubbles were seen to evolve upon the addition of NaH to **2.8** in THF, indicative of the formation of hydrogen gas; therefore, this pathway may still hold some potential.

In addition to varying the solvent, different alkylating agents should also be considered. While the work here indicates primary alkyl chains are unsuccessful at alkylating **2.8**, secondary alkyl substituents (e.g., isopropyl iodide) may be more likely to promote alkylation. The mechanism of alkylation with primary electrophiles (i.e., MeI) follows an S_N2 type reaction, preventing a primary carbocation intermediate. Due to the nature of the transition state of this reaction, the nucleophile must be relatively unhindered. The nucleophile **2.8**, however, is fairly bulky, and thus it is more likely to undergo an S_N1 type reaction. The use of isopropyl iodide should increase the stability of a carbocation intermediate, making an S_N1 mechanism more feasible with **2.8**. Once an alkylated dication is achieved, then work examining the reduction potential should be performed in order to effectively reduce the alkylated dication to the biradical.

2.7 Experimental Details

2.7.1 General Procedures

The reagents sodium hydride (60% dispersion in mineral oil, Alfa Aesar), methyl iodide (Alfa Aesar), ethyl iodide (Sigma-Aldrich), methyl trifluorosulfonate (methyl

triflate, Synquest Labs Inc.), triethyloxonium tetrafluoroborate (Sigma-Aldrich), 2-cyanopyridine (Alfa Aesar) and trimethylsilyl trifluorosulfonate (TMS triflate, TCI America) were obtained commercially and used as received. THF and MeCN were dried by passing them through activated alumina on a J.C. Meyer solvent purification system and stored over 4Å Molecular sieves. DCE was dried over 4Å Molecular sieves. All other solvents were reagent grade. 3,5-*bis*(2-pyridyl)-4-hydro-1,2,4,6-thiatriazine (**Py_2TTAH**), *N*-2-pyridylimidoyl-2-pyridylamidine (**2.6**) and *bis*-*N*-bridgehead-1,2,5-thiadiazolium dication (**2.8**) were prepared as described in literature.[11] All reactions were performed under an atmosphere of dry nitrogen unless otherwise stated. ^{1}H NMR and ^{13}C NMR spectra were run in MeCN-d_3 or $CDCl_3$ solutions at room temperature on Bruker Avance 400 MHz or Bruker Avance 300 MHz spectrometers. IR spectra of solid samples were recorded on an Agilent Technologies Cary 630 FT-IR spectrometer. Synthetic procedures for the methyl and ethyl coordination polymers are detailed in Chapter 3 (Section 3.12.4).

2.7.2 Crystal Growth

Yellow blocks of the ethyl coordination polymer suitable for X-ray analysis were recrystallized *via* vapour diffusion of Et_2O into a saturated solution of DCM. Crystallographic details and descriptions of XRD analysis can be found in the Appendix.

2.8 References

1. A. Shimizu, M. Nakano, Y. Hirao and T. Kubo, *Journal of Physical Organic Chemistry*, 2011, **24**, 876-882.

2. W. T. Borden, H. Iwamura and J. A. Berson, *Accounts of Chemical Research*, 1994, **27**, 109-116.

3. R. A. Moss and M. S. Platz, *Reactive Intermediate Chemistry*, John Wiley & Sons, 2004.

4. G. Kothe, K. H. Denkel and W. Summerma, *Angewandte Chemie-International Edition*, 1970, **9**, 906-907.

5. Y. Li, K. W. Huang, Z. Sun, R. D. Webster, Z. B. Zeng, W. D. Zeng, C. Y. Chi, K. Furukawa and J. S. Wu, *Chemical Science*, 2014, **5**, 1908-1914.

6. E. Niecke, A. Fuchs, F. Baumeister, M. Nieger and W. W. Schoeller, *Angewandte Chemie-International Edition in English*, 1995, **34**, 555-557.

7. C. M. Cui, M. Brynda, M. M. Olmstead and P. P. Power, *Journal of the American Chemical Society*, 2004, **126**, 6510-6511.

8. H. Cox, P. B. Hitchcock, M. F. Lappert and L. J. M. Pierssens, *Angewandte Chemie-International Edition*, 2004, **43**, 4500-4504.

9. K. Takeuchi, M. Ichinohe and A. Sekiguchi, *Journal of the American Chemical Society*, 2011, **133**, 12478-12481.

10. S. Ito, Y. Ueta, T. T. T. Ngo, M. Kobayashi, D. Hashizume, J. Nishida, Y. Yamashita and K. Mikami, *Journal of the American Chemical Society*, 2013, **135**, 17610-17616.

11. A. A. Leitch, I. Korobkov, A. Assoud and J. L. Brusso, *Chemical Communications*, 2014, **50**, 4934-4936.

12. M. Jones Jr and S. A. Fleming, *Organic Chemistry*, Norton, Fourth ed., 2010.

13. N. J. Yutronkie, A. A. Leitch, I. Korobkov and J. L. Brusso, *Crystal Growth & Design*, 2015, **15**, 2524-2532.

14. J. S. Hrkach and K. Matyjaszewski, *Macromolecules*, 1990, **23**, 4042-4046.

15. K. L. M. Harriman, A. A. Leitch, S. A. Stoian, F. Habib, J. L. Kneebone, S. I. Gorelsky, I. Korobkov, S. Desgreniers, M. L. Neidig, S. Hill, M. Murugesu and J. L. Brusso, *Dalton Transactions*, 2015, **44**, 10516-10523.

16. R. M. Silverstein, F. X. Webster and D. J. Kiemle, *Spectrometric Identification of Organic Compounds*, Wiley, Seventh ed., 2005.

Chapter 3 – Sulfur Functionalization of 3,5-*bis*(2-pyridyl)-1,2,4,6-thiatriazine *via* Alkylation and Arylation

Authorship Disclosure: A version of this work was published in the *New Journal of Chemistry* as "Alkyl-functionalization of 3,5-*bis*(2-pyridyl)-1,2,4,6-thiatriazine" **Kleisath, E.**, Yutronkie, N.J., Korobkov, I., Gabidullin, B.M., and Brusso, J.L. *New Journal of Chemistry*, (2016), **40**, 4472-4479.

3.1 Introduction

In recent years, the design and development of sulfur and nitrogen based heterocycles has received much attention due, in large part, to their suitability in a variety of applications.[1-6] In that regard, 1,2,4,6-thiatriazines (**TTA**s) represent an important class of S–N heterocycles that have been explored as building blocks in the development of molecular conductors,[7-9] as well as their use as spin bearing ligands in coordination complexes.[10-13] In contrast, the functionalization of **TTA** compounds post ring formation has yet to be explored in depth. The generation of a flexible and general route that enables modification of the exocyclic substituents holds significant potential in the design of novel heterocyclic compounds that can be targeted for a variety of applications, such as liquid crystalline mesogens, ionic liquids or electroactive substrates, in addition to their implementation as biologically active materials, namely in herbicidal applications.[14-17] Inclusion of heterocycles at the 3- and 5-positions of the **TTA** ring that contain nitrogen, or sulfur facilitates the development of chelating ligands. This, in combination with substituents attached to the sulfur atom, can lead to novel systems in which multimetallic coordination complexes, polymers and extended

networks can be envisioned. While thiatriazines functionalized at the 3- and 5-position of the **TTA** ring are well known,[10-12] only recently have heteroaromatic substituted **TTA** derivatives been reported (i.e., **3.1** where Ar = thienyl, pyridyl; Chart 3-1).[18] To that end, **3.1** (Ar = pyridyl) is an ideal candidate to explore, as the heteroaromatic substituents are expected to promote coordination through the chelating effect, rendering the N—S—N portion of the heterocyclic ring available for modification.

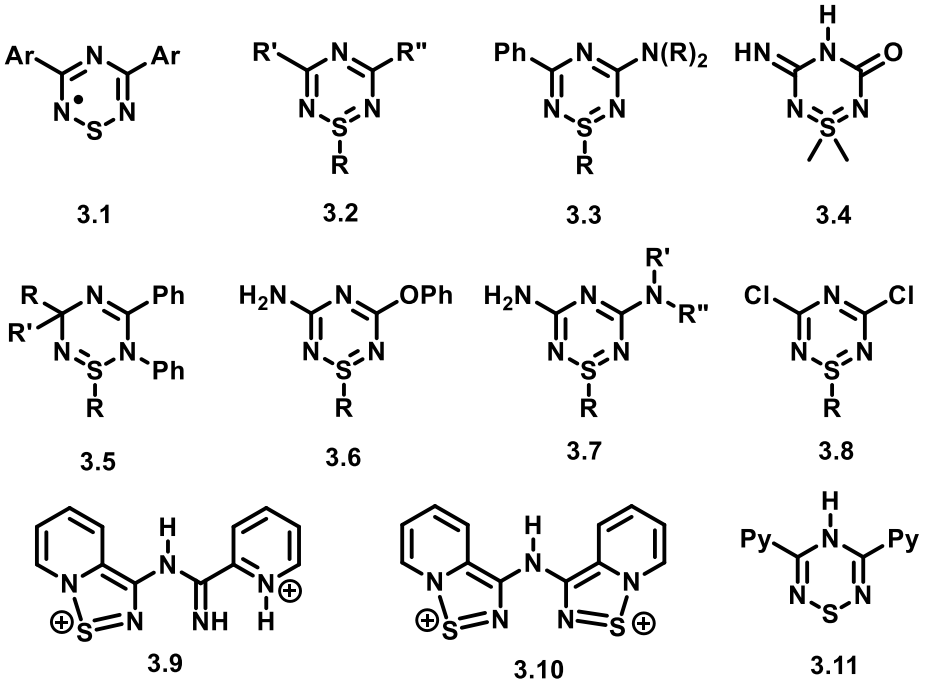

Chart 3-1. Examples of sulfur functionalized **TTA** rings (**3.1**-**3.8**), as well as intermediates (**3.9**-**3.11**) in the synthesis of the pyridyl substituted thiatriazinyl radical (**3.1**, Ar = Py).

With respect to *S*-functionalization of **TTA** rings, examples **3.2**-**3.8** have been reported. For the most part, the synthetic methods used require alkylation or arylation of the sulfur atom prior to **TTA** ring formation.[19-24] The one exception to this is **3.8**,

where alkylation occurs *via* nucleophilic addition to 1,3,5-trichloro-1,2,4,6-thiatriazine in an S_N2 fashion.[25] Although shown to be effective, the latter route requires the generation of an air sensitive *S*-chloro-1,2,4,6-thiatriazine. In the case of **3.1** (Ar = pyridyl), its synthesis involves the intermediacy of *mono*- and *bis*-*N*-bridgehead-1,2,5-thiadiazolium salts **3.9** and **3.10**, instead of the preparation of an *S*-chloro-1,2,4,6-thiatriazine.[26] This unique behaviour is attributed to the proclivity of the pyridyl moieties to form *N*-bridgehead-heterocycles, which enables the isolation of 3,5-*bis*(2-pyridyl)-4-hydro-1,2,4,6-thiatriazine (**Py_2TTAH**; **3.11**), a surprisingly robust compound with a high tolerance towards aqueous, basic, and thermal conditions. Since the N—S—N portion of the **TTA** ring in **Py_2TTAH** is devoid of substituents, its potential towards functionalization was explored.

3.1.1 Scope of this Chapter

This chapter describes post-functionalization of the sulfur atom in pyridyl substituted **TTA** rings with both alkylation and arylation. Using different alkylating agents, neutral *S*-alkylated derivatives were obtained through both anionic and cationic reaction pathways. All of the *S*-alkylated species were isolated and characterized. In addition to alkyl groups, the susceptibility of sulfur to arylation was studied, and found to be most successful with the use of hypervalent iodine reagents. Overall, this work demonstrates an alternative and versatile synthetic route for sulfur functionalization

post **TTA** ring formation, through alkylation, which can be achieved *via* cationic or anionic pathways, and arylation, which can be achieved through the use of diaryl iodonium salts.

3.2 Alkylation of 3,5-*bis*(2-pyridyl)-4-hydro-1,2,4,6-thiatriazine *via* Alkyl Iodides

As outlined in Chapter 2, alkylation attempts began with deprotonation of **Py_2TTAH**, followed by the addition of an alkyl iodide. In this method, upon the treatment of **Py_2TTAH** with sodium hydride (NaH) in tetrahydrofuran (THF), hydrogen gas evolved and the initial purple solution turned bright emerald green, indicative of deprotonation. Subsequent treatment of the deprotonated species (**Py_2TTA^-**; **3.12**; Scheme 3-1) with alkyl iodides (EtI and MeI) afforded a brown solution from which air-stable yellow-orange precipitates formed. The ethyl and methyl derivatives were both identified upon single crystal X-ray diffraction (*vide infra*) as the coordination polymers **3.13** and **3.14** (Scheme 3-1), respectively. Although X-ray analysis indicated **3.13** and **3.14** exist as coordination polymers in the solid state, it should be noted that these compounds most likely exist as discrete monomers or dimeric units in solution.

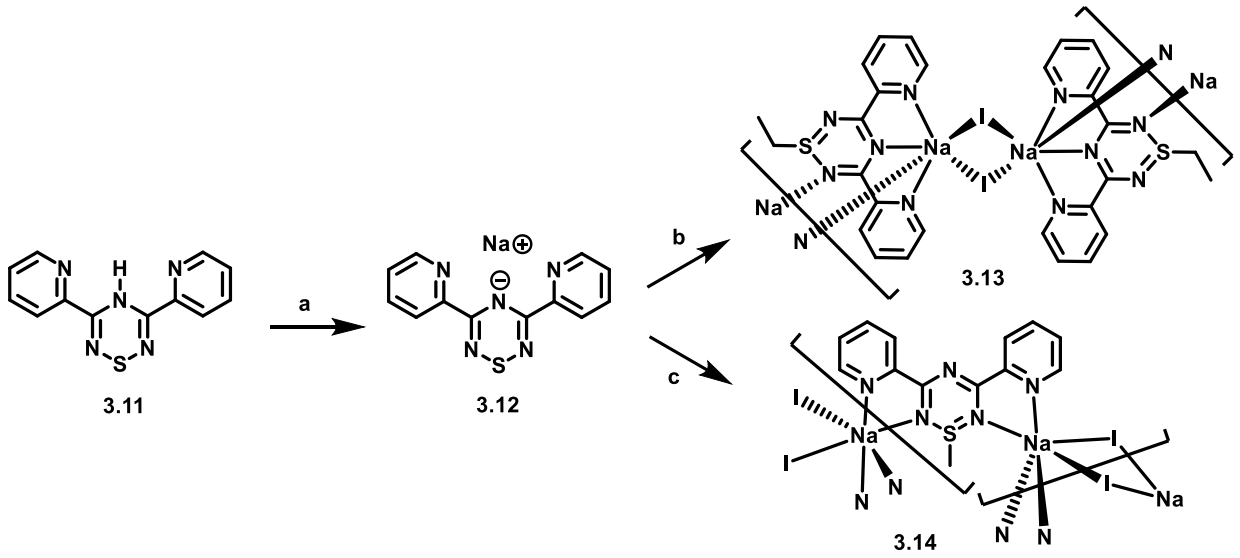

Scheme 3-1. Synthesis of **3.13** and **3.14**. Reagents and Conditions: (a) NaH; THF (b) EtI; THF (c) MeI; THF.

Comparison of the IR, ^{1}H NMR and ^{13}C NMR spectra of **3.13** and **3.14** revealed many similarities. For example, the fingerprint regions in the IR spectra share many of the same peaks, albeit with slightly shifted frequencies. While **3.13** has more activity below 800 cm^{-1}, this is to be expected since C—H rocking bands in alkanes appear in this region and **3.13** has a greater quantity compared to **3.14**. The ^{1}H NMR spectra of **3.13** and **3.14** show identical pyridyl signals (8.6, 8.4, 8.0, and 7.6 ppm; Figure 3-1). In addition, the methyl and methylene peaks of **3.14** and **3.13**, respectively, are similarly deshielded, with the methyl group displaying a small upfield shift of 0.37 ppm. This shift is consistent with shifts expected between methyl and methylene peaks in an otherwise equivalent chemical environment.[16] Likewise, the ^{13}C NMR spectra of the methyl and ethyl derivatives are almost identical, with the only difference being a small upfield shift of the methyl signal in **3.14** compared to the methylene of **3.13** (Figure 3-2).

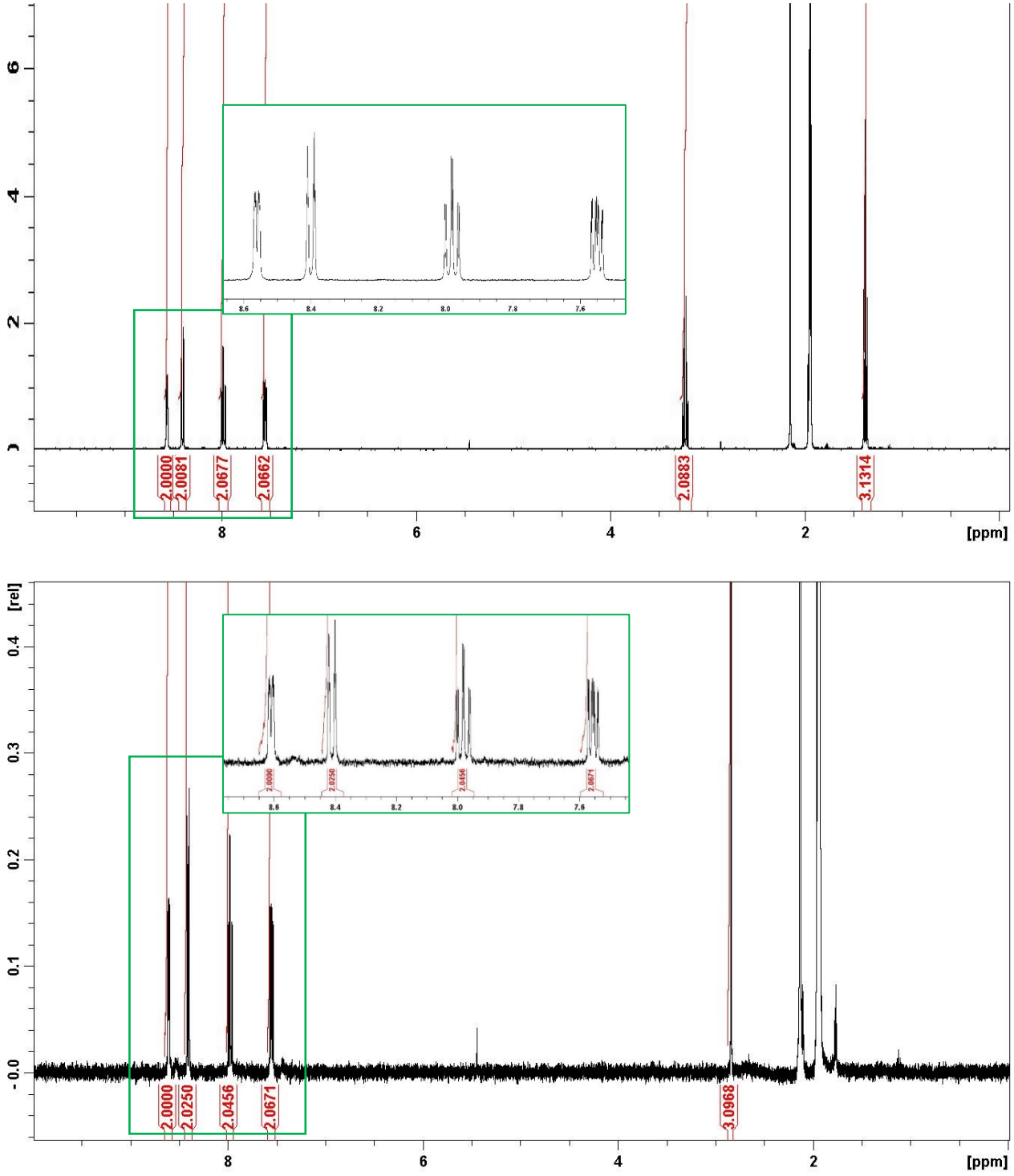

Figure 3-1. ^{1}H NMR spectra of **3.13** (top) and **3.14** (bottom) in MeCN-d_3.

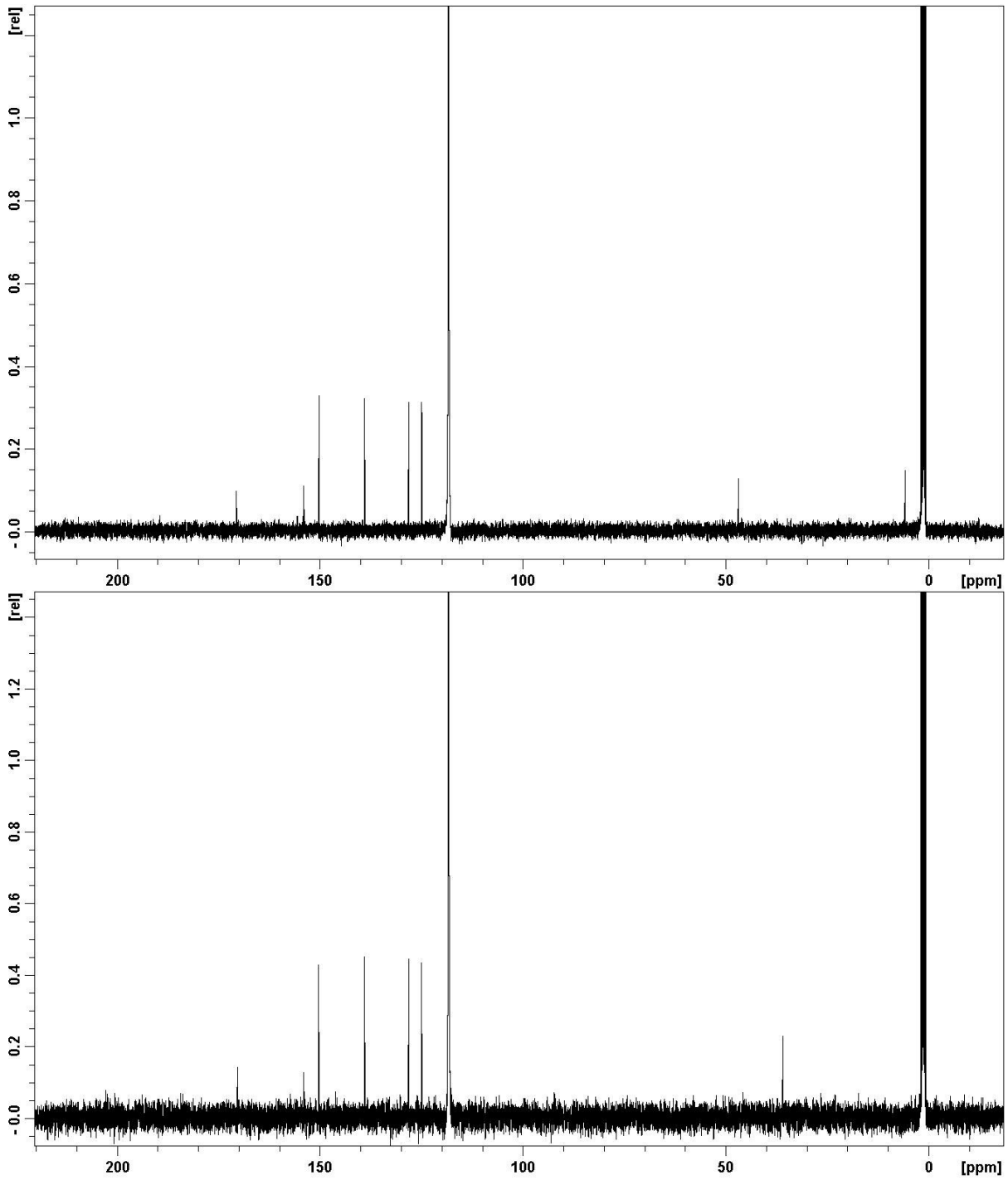

Figure 3-2. ^{13}C NMR spectra of **3.13** (top) and **3.14** (bottom) in MeCN-d_3.

3.2.1 Crystallographic Analysis of the Ethyl Coordination Polymer 3.13

The product obtained from the reaction between **3.12** and EtI was crystallized through vapour diffusion of diethyl ether (Et_2O) into a saturated dichloromethane (DCM) solution, and afforded yellow block-like crystals suitable for single crystal X-ray analysis, confirming the identity of **3.13** as **[Na(*μ*-I)(*S*-Et-Py$_2$TTA)]$_\infty$**, (**3.13**).

Crystals of **[Na(*μ*-I)(*S*-Et-Py$_2$TTA)]$_\infty$** belong to the triclinic space group $P\bar{1}$ and consist of dimeric units that are connected through a weak bond between the sodium and a nitrogen atom on a neighbouring **TTA** ligand, leading to a 1-D coordination polymer (See Figure 3-3). Full crystallographic details can be found in Table A-1 in the Appendix. The metal ion adopts a distorted six coordinate geometry with the sodium centre bound to the pincer-type ***S*-Et-Py$_2$TTA** ligand through three nitrogen atoms (N1, N2 and N3). Two additional iodide ions (I1 and I1a) are μ-bridging to the next sodium centre in the dimer, resulting in a diamond-like arrangement between the sodium and iodide ions in the plane perpendicular to the tridentate ***S*-Et-Py$_2$TTA** ligand. A weak Na—N bond from the N—S—N portion of a neighbouring **TTA** ring occupies the remaining coordination site, thus forming a 1D chain. The Na—N bond lengths (2.445(2)-2.483(1) Å), as well as charge balance, suggests that the ***S*-Et-Py$_2$TTA** ligand is neutral. This, coupled with the relatively uniform C—N bond lengths in the **TTA** ring (Table 3-1), is indicative of aromatic character in the central ligand ring.

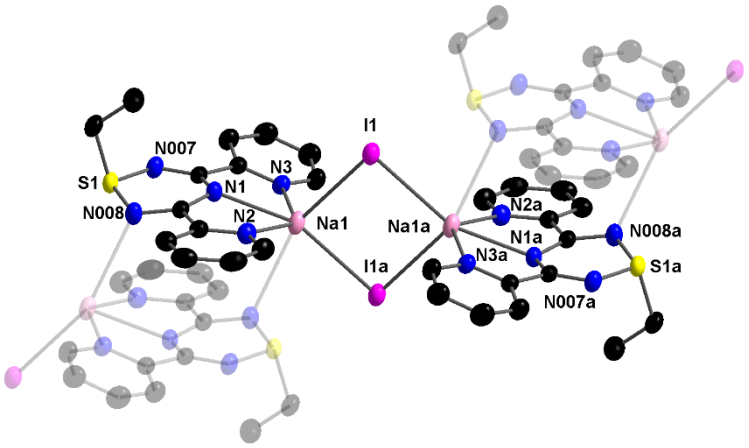

Figure 3-3. Asymmetric unit of **[Na(*μ*-I)(S-Et-Py$_2$TTA)]$_\infty$** using 50% thermal ellipsoids. Hydrogen atoms are omitted for clarity.

Table 3-1. Bond length comparisons of the central **TTA** ring for compounds **3.13**, **3.15**, **3.17**, and **3.19** (*vide infra*), as well as other previously reported **TTA** derivatives for comparison [3,5-*bis*(*N*-hydro-2-pyrinium)-*S*-bromo-1,2,4,6-thiatriazine][Br][Br$_3$],[27] 3,5-*bis*(pyridyl)-4-hydro-*S*-oxo-1,2,4,6-thiatriazine[27] and **Py$_2$TTAH** (**3.11**).[26] Bond numbers are in reference to the numbers shown in the schematic, and all lengths are reported in Angstroms (Å).

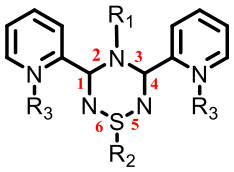	**Bond 1 length**	**Bond 2 length**	**Bond 3 length**	**Bond 4 length**	**Bond 5 length**	**Bond 6 length**	
3.13	1.317(3)	1.341(2)	1.355(2)	1.312(3)	1.669(1)	1.652(2)	
3.15	1.333(3)	1.339(3)	1.350(4)	1.316(3)	1.664(2)	1.654(2)	
3.19	1.306(2)	1.357(2)	1.336(2)	1.320(2)	1.673(1)	1.670(2)	**Aromatic**
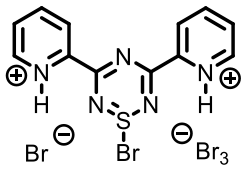	1.340(5)	1.338(5)	1.345(6)	1.318(5)	1.622(4)	1.603(4)	
3.17	1.287(4)	1.356(3)	1.361(4)	1.286(4)	1.663(2)	1.673(2)	
3.11	1.279(2)	1.396(2)	1.391(2)	1.278(2)	1.693(2)	1.692(2)	
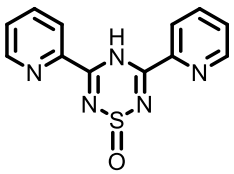	1.285(4)	1.373(4)	1.367(4)	1.283(4)	1.686(3)	1.681(3)	**Non-aromatic**

From the bond lengths in Table 3-1, the aromaticity, or lack thereof for the various **TTA** derivatives can be determined. This can be achieved by considering the bonds within the **TTA** ring of each molecule; in aromatic systems, the C—N bond lengths should be relatively equivalent. Conversely, non-aromatic derivatives should possess C—N bonds that vary in length corresponding to discrete single and double bonds, due to localization of the π-electrons. Bonds 1-4 represent the C—N bonds within the **TTA** ring while bonds 5 and 6 represent the S—N bonds. In **3.13** for example, the C—N bond lengths are all within 0.1 Å of each other, and the two S—N bonds are approximately equal. This therefore suggests that the π-electrons are delocalized about the **TTA** ring. Comparatively, in compound **3.17**, the C—N bond lengths in the **TTA** ring consist of discrete single and double bonds based on the alternating bond lengths, and is therefore indicative of non-aromatic character.

Looking at the crystal packing of compound **3.13**, a number of close ligand-ligand interactions are observed within the polymeric chains of **[Na(*μ*-I)(*S*-Et-Py$_2$TTA)]$_\infty$**, whereas only two close π-π interactions exist between the ***S*-Et-Py$_2$TTA** ligands on neighbouring polymers (Figure 3-4). This is likely due to the *S*-Et group, which limits inter-chain interactions. These two unique C—C′ contacts between the pyridyl rings on neighbouring polymers leads to an ordered array along the *a* axis of the 1D chains, which are themselves aligned along the *b* axis.

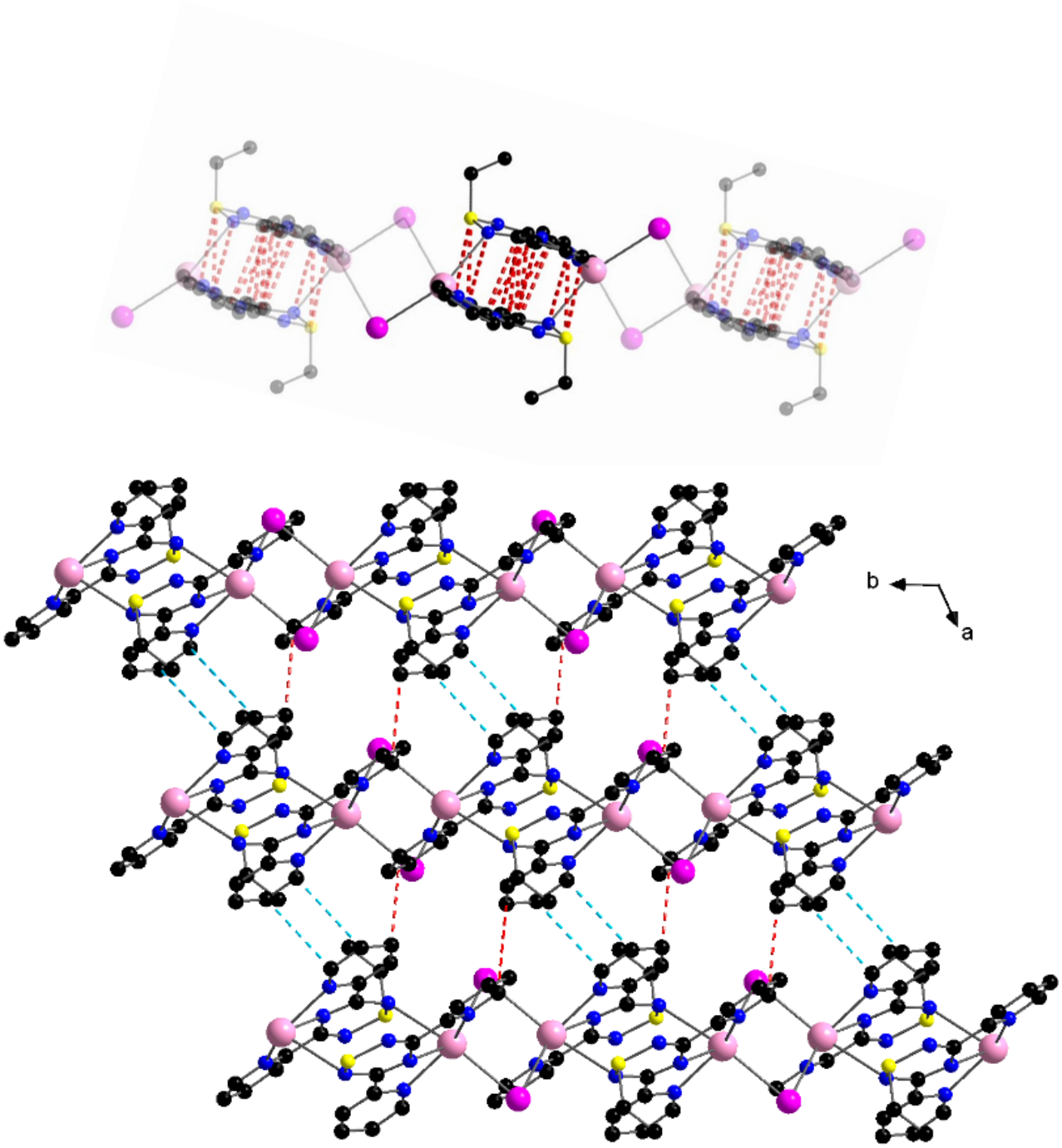

Figure 3-4. **[Na(*μ*-I)(*S*-Me-Py$_2$TTA)]$_\infty$** close ligand-ligand contacts (top) and inter-chain polymer contacts as viewed from the side (bottom). Intermolecular C—C′ contacts are highlighted with blue (3.486(3) Å) and red (3.449(3) Å) dashed lines. Hydrogen atoms omitted for clarity.

3.2.2 Crystallographic Analysis of the Methyl Coordination Polymer 3.14

Reactions were also carried out with MeI, mimicking the synthetic route used with EtI. To that end, a yellow precipitate formed upon treatment of **3.12** with MeI (Scheme 3-1, above). Recrystallization *via* vapour diffusion of Et_2O into a saturated solution of acetonitrile (MeCN) afforded pure material as very small yellow plate-like crystals. While X-ray analysis of these crystals proved challenging due to the small size, a crystal structure belonging to the *Pbca* orthorhombic space group was obtained (Figure 3-5), enabling identification of this product as the coordination polymer **[Na(*μ*-I)(*S*-Me-Py$_2$TTA)]$_\infty$** (**3.14**). Crystallographic details are summarized in the Appendix.

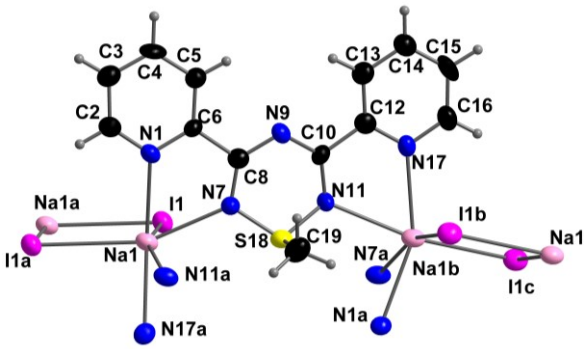

Figure 3-5. Coordination environment of **[Na(*μ*-I)(*S*-Me-Py$_2$TTA)]$_\infty$** using 50% thermal ellipsoids. Note that each hanging nitrogen is part of an adjacent ***S*-Me-Py$_2$TTA** moiety, and each hanging sodium atom is coordinated to two additional ***S*-Me-Py$_2$TTA** building blocks.

Similar to the ethyl derivative, crystals of **[Na(*μ*-I)(*S*-Me-Py$_2$TTA)]$_\infty$** also consist of a coordination polymer in which sodium-iodide ionic bridges exist between *S*-alkylated **Py$_2$TTA** rings, where two *μ*-bridging iodide ions form a diamond-like configuration. However, unlike **3.13**, the sodium ion in **3.14** sits in the bidentate

chelating pocket formed by one of the pyridyl nitrogen atoms and a nitrogen atom from the N—S—N fragment of the **TTA** ring. Two separate ***S*-Me-Py$_2$TTA** ligands are coordinated to a single sodium atom in this fashion, thus creating a six-coordinate geometry. Overall, this coordination environment results in a 2-dimensional (2D) polymeric network in the *bc* crystallographic plane (Figure 3-6). The ***S*-Me-Py$_2$TTA** ligands are oriented perpendicular to the plane of the complete polymeric network (i.e., perpendicular to the *bc* plane), and the sulfur atom alternates pointing in the positive and negative directions of the *a* axis. This rotation creates a zig-zag like pattern, with the pyridyl substituents pointing both above and below of the central plane of the polymeric network layer, as shown in Figure 3-6 (bottom). The sodium iodide ionic bridges, as well as the N—S—N portion of each **TTA** ring, are located in the central plane, sandwiched between the pyridyl rings in the polymeric network.

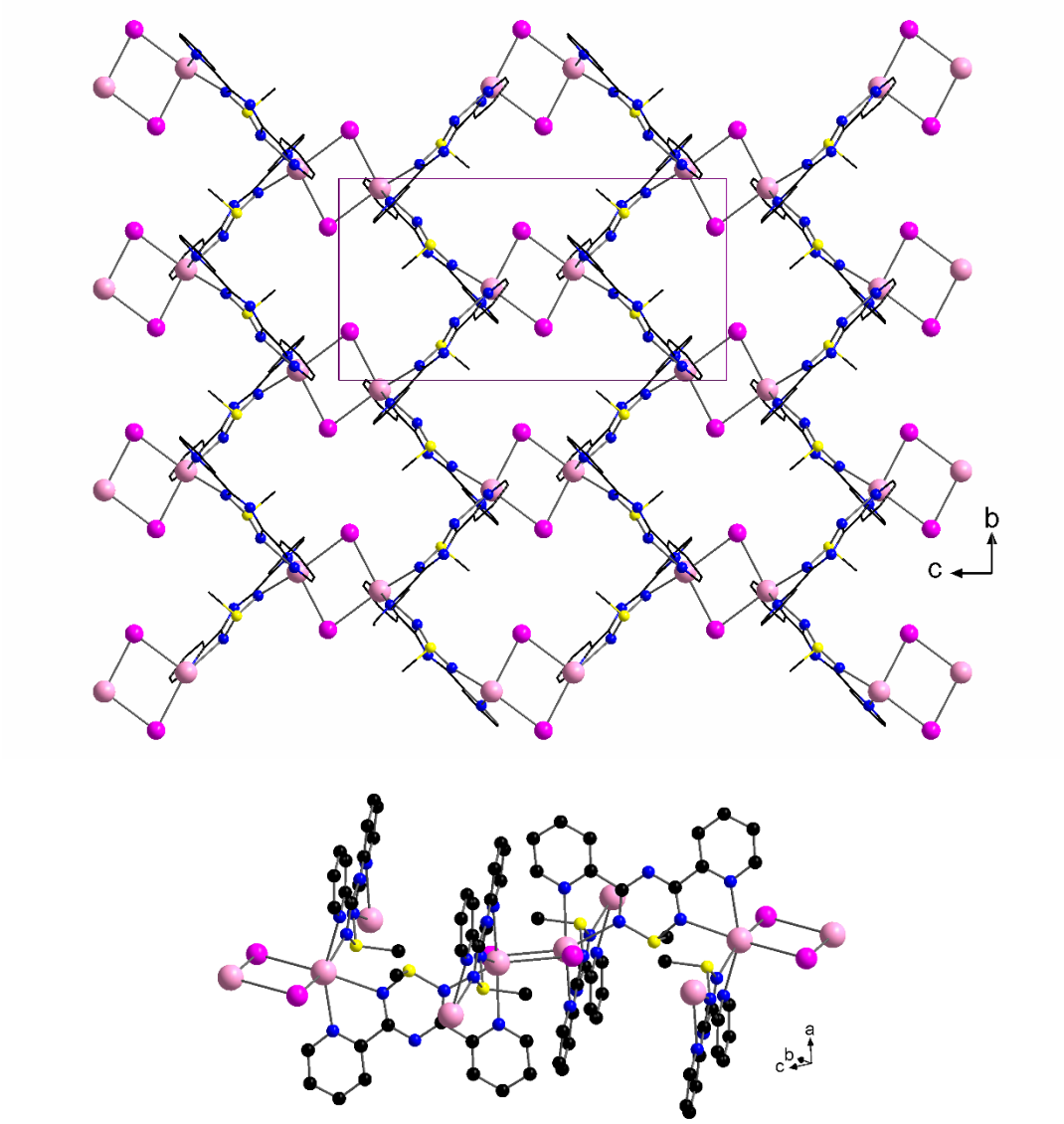

Figure 3-6. Two views of **[Na(*μ*-I)(*S*-Me-Py$_2$TTA)]$_\infty$** showing the polymeric packing motif. Top: looking down the *a* axis onto the 2D plane. The polymeric structure is continued from the sodium ions at the edges along both the *b* and *c* axes. For clarity, hydrogen atoms are removed and carbon atoms are shown as a wire frame. Bottom: Edge-view of the 2D polymeric sheet, showing the alternating ***S*-Me-Py$_2$TTA** ligand directions. The ligand frameworks shown on edge alternate coming into and out of the page. The network extends out from hanging sodium ions shown. Hydrogen atoms are removed for clarity.

3.3 Isolation and Characterization of Neutral *S*-Alkylated Py$_2$TTA

Dissolution of the coordination polymers **3.13** and **3.14** into water followed by extraction with DCM afforded the neutral *S*-alkylated products 3,5-*bis*(2-pyridyl)-*S*-

ethyl-1,2,4,6-thiatriazine (***S*-Et-Py$_2$TTA**; **3.15**) and 3,5-*bis*(2-pyridyl)-*S*-methyl-1,2,4,6-thiatriazine (***S*-Me-Py$_2$TTA**; **3.16**), respectively (Scheme 3-2). Recrystallization of the ethyl derivative with hexanes afforded lustrous yellow needles of ***S*-Et-Py$_2$TTA** suitable for structural analysis, the results of which are shown in Figure 3-7; full crystallographic data is presented in the Appendix. In **3.15**, the six membered **TTA** ring adopts a shallow boat-like conformation with the S1 and N3 atoms deviated from the mean plane of the remaining four atoms by 0.402(7) Å and 0.074(2) Å, respectively. The relatively uniform C—N bond lengths in the **TTA** ring (see Table 3-1, *vide supra*) is indicative of aromatic character, which is consistent with the expected six π-electron system. The molecular framework of ***S*-Et-Py$_2$TTA** is twisted with torsion angles of 12.798(7)° and 6.400(1)° between the pyridyl rings and the central **TTA** (Figure 3-8), with the C6 atom of the exocyclic ethyl substituent linked pseudo-axially.

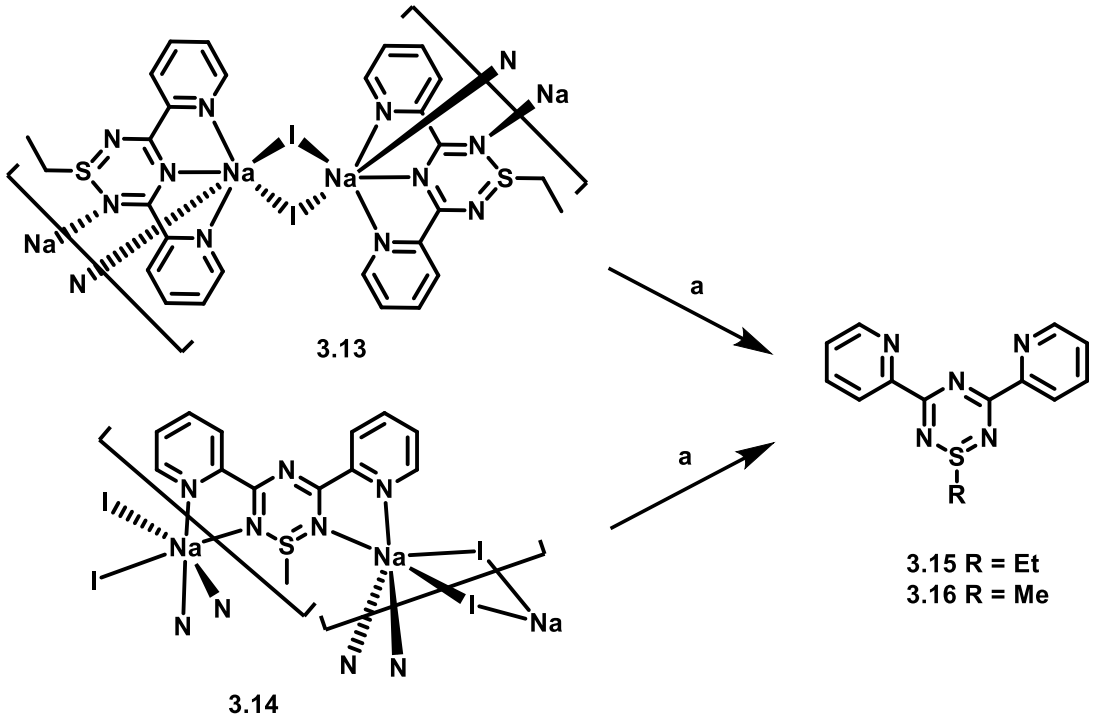

Scheme 3-2. Synthesis of 3,5-*bis*(2-pyridyl)-*S*-ethyl-1,2,4,6-thiatriazine (**3.15**) and 3,5-*bis*(2-pyridyl)-*S*-methyl-1,2,4,6-thiatriazine (**3.16**). Reagents and conditions: (a) DCM/H_2O.

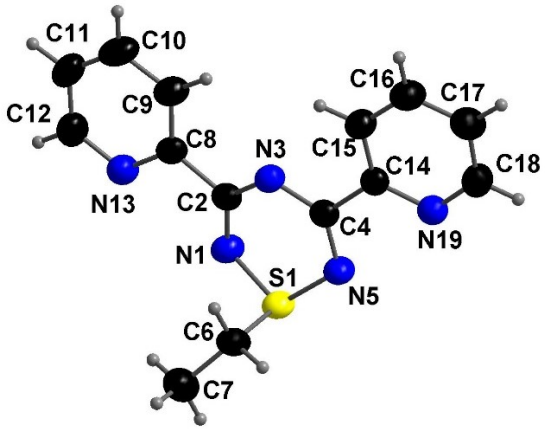

Figure 3-7. Asymmetric unit cell of ***S*-Et-Py$_2$TTA** using 50% thermal ellipsoids for non-hydrogen atoms.

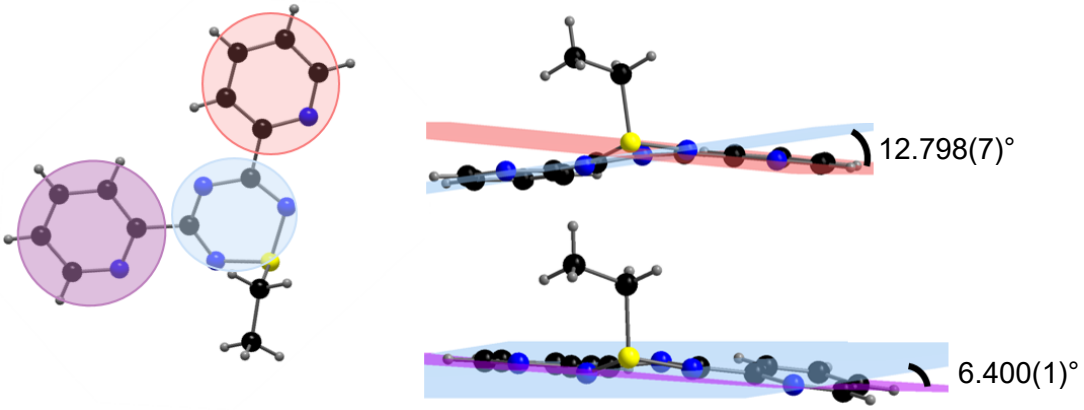

Figure 3-8. Calculated twist angles between planes of the thiatriazine and pyridyl rings of **S-Et-Py$_2$TTA**. The central plane was calculated without the S and N3 atoms, as this ring adopts a shallow boat-like arrangement.

Yellow needles of the neutral methyl species (**3.16**) were obtained from recrystallization in a THF/hexanes mixture; however, crystals suitable for X-ray analysis remain elusive. Nonetheless, comparison of the IR, ^{1}H NMR and ^{13}C NMR spectra with those of the ethyl derivative (***S*-Et-Py$_2$TTA**) (Figure 3-9 ^{1}H NMR and Figure 3-10 ^{13}C NMR) support the identification of **3.16** as ***S*-Me-Py$_2$TTA**.

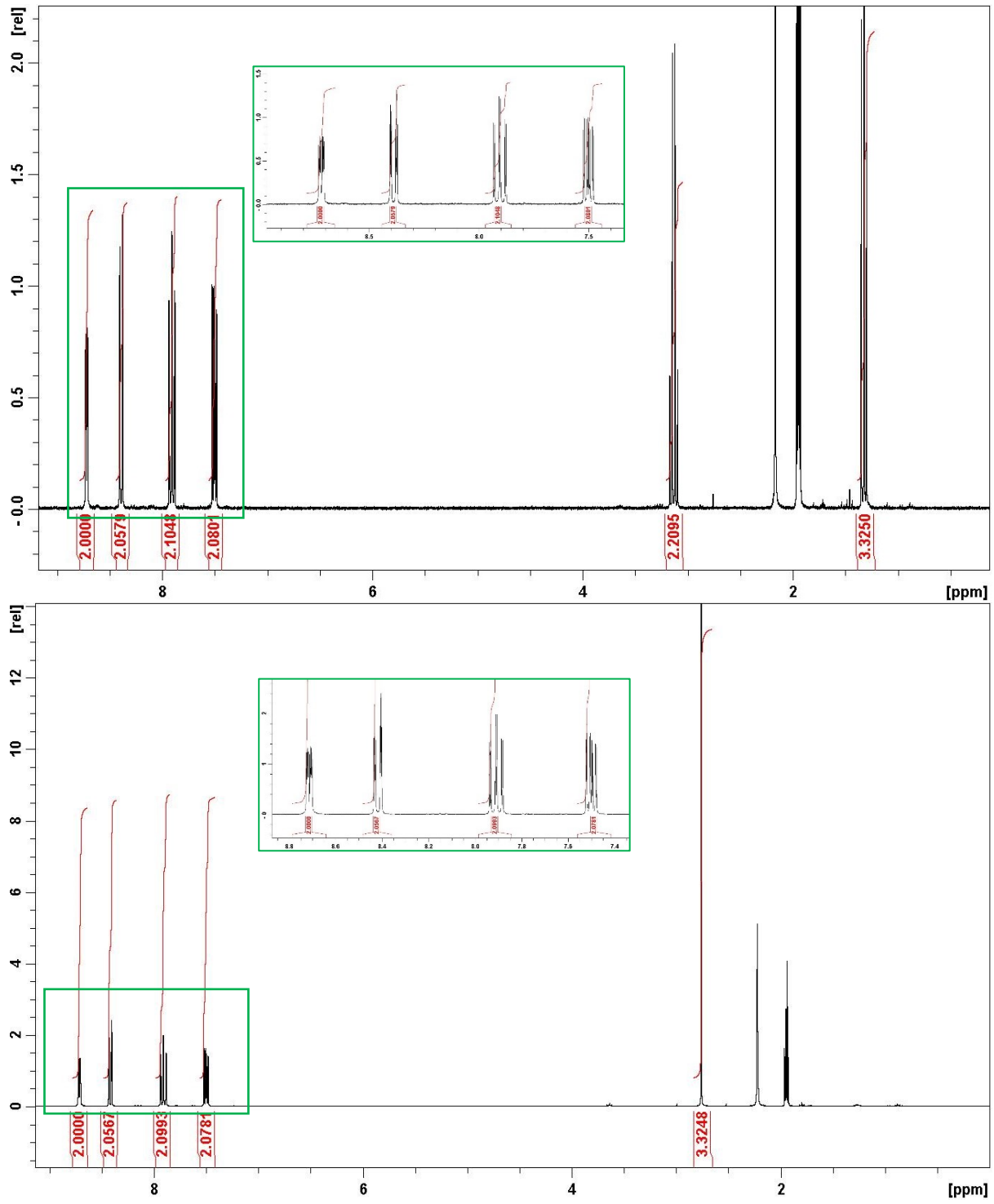

Figure 3-9. ^{1}H NMR spectra of ***S*-Et-Py$_2$TTA** (top) and ***S*-Me-Py$_2$TTA** (bottom) in MeCN-d$_3$.

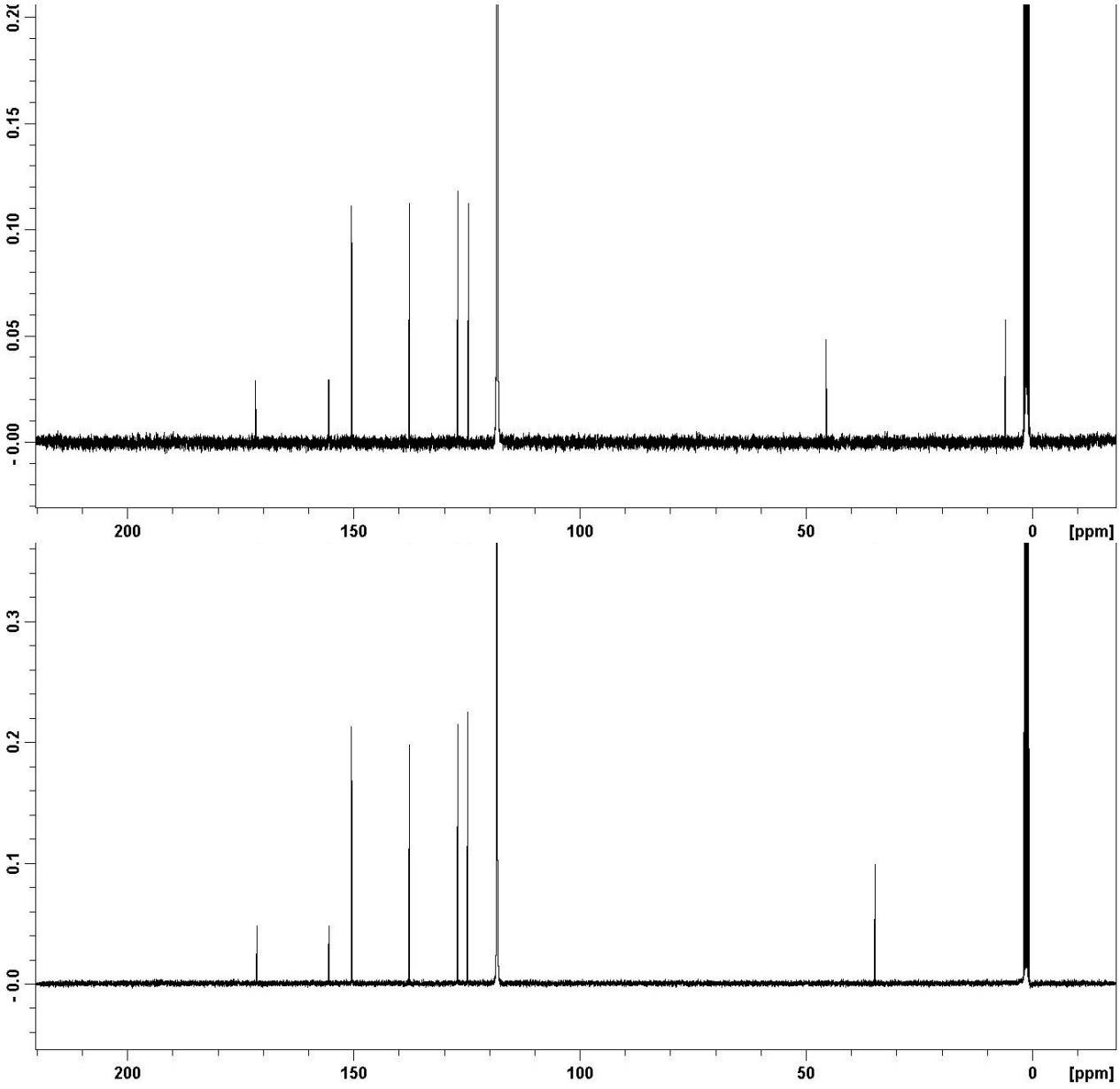

Figure 3-10. ^{13}C NMR spectra of ***S*-Et-Py$_2$TTA** (top) and ***S*-Me-Py$_2$TTA** (bottom) in MeCN-d$_3$.

3.4 Alkylation *via* Triethyloxonium Tetrafluoroborate

In addition to alkyl halides, reactions were also carried out using [Et$_3$O][BF$_4$] under similar conditions. To that end, following deprotonation of **Py$_2$TTAH** with NaH in THF, the addition of [Et$_3$O][BF$_4$] turned the reaction mixture into a think, insoluble

sticky residue. Upon searching the literature, it was clear this was not a feasible synthetic route as $[Et_3O][BF_4]$ (and MeOTf) are initiators for the polymerization of THF.[28, 29]

In order to avoid polymerization, the solvent was changed to DCM, as it was known to be stable towards strong alkylating agents. Unfortunately, deprotonation of **Py_2TTAH** with NaH was not achievable due to its insolubility in DCM. Nevertheless, the addition of $[Et_3O][BF_4]$ to **Py_2TTAH** afforded a mixture of purple needles and yellow block-like crystals upon slow evaporation of the reaction mixture. The purple needles, which were confirmed to be unreacted starting material, could easily be removed due to the solubility of **Py_2TTAH** in a variety of organic solvents. The resulting yellow block-like crystals were suitable for X-ray analysis (Figure 3-11), confirming the structural identity of **[*S*-Et-Py_2TTAH][BF_4]** (**3.17**; Scheme 3-3). Crystallographic data can be found in the Appendix.

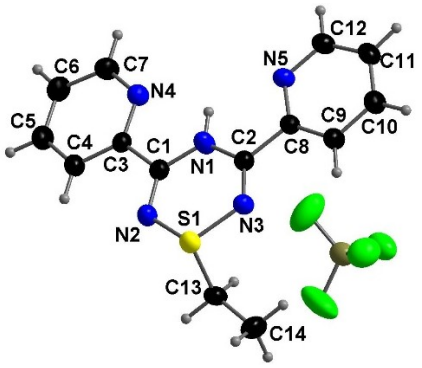

Figure 3-11. Asymmetric unit of **[*S*-Et-Py_2TTAH][BF_4]** with 50% thermal ellipsoids for non-hydrogen atoms.

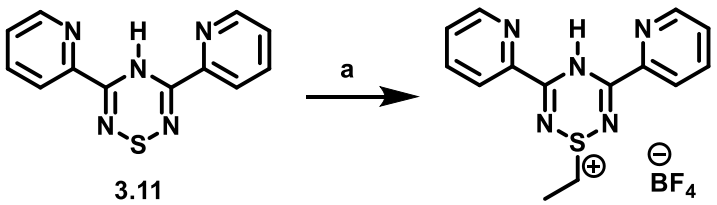

Scheme 3-3. Synthesis of **[*S*-Et-Py$_2$TTAH][BF$_4$]**. Reagents and conditions: (a) [Et$_3$O][BF$_4$]·DCM; DCM.

Crystals of **[*S*-Et-Py$_2$TTAH][BF$_4$]** belong to the orthorhombic space group $P2_12_12_1$. Considering the **TTA** framework in **3.17**, the differences observed in the C—N bond lengths suggest discrete single and double bonds, indicative of anti-aromatic character (Table 3-1 above). This, coupled with the N—H signal observed in the IR and ^{1}H NMR spectra, as well as the presence of BF_4^- anions in the asymmetric unit, confirms **3.17** is an ionic species. In the solid-state, the crystal structure of **[*S*-Et-Py$_2$TTAH][BF$_4$]** consists of alternating **[*S*-Et-Py$_2$TTAH]$^+$** cations separated by BF_4^- anions, which form a herringbone arrays along the *a* axis, as shown in Figure 3-12. Interestingly, numerous close C—C′ and C—N′ contacts exist between the **[*S*-Et-Py$_2$TTAH]$^+$** cations, all of which are due to intermolecular interactions between the pyridyl rings on adjacent molecules. The lack of intermolecular interactions associated with the central **TTA** ring is likely due to the presence of BF_4^- anions, as well as the bulky *S*-ethyl substituent, which prohibits close contacts between the **TTA** ring and neighbouring molecules.

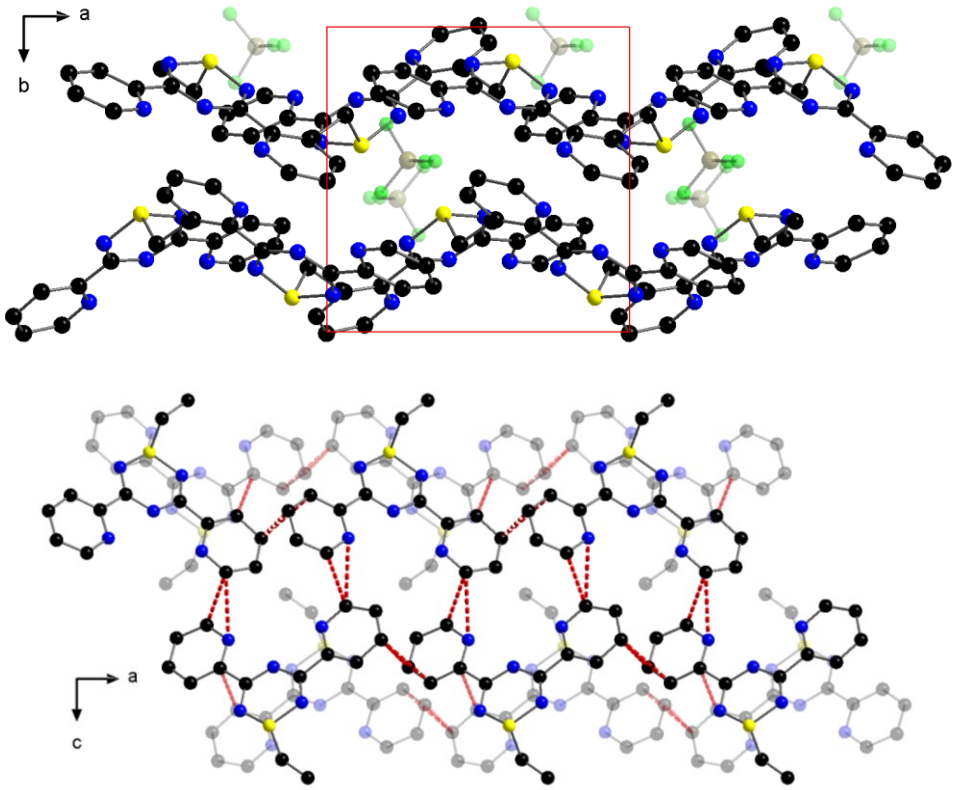

Figure 3-12. Two views of the crystal structure of **3.17** showing the herringbone arrays along the *a* axis (top; anions faded for clarity), and close contacts between adjacent pyridyl groups, highlighted with red dashed lines (bottom; anions removed for clarity). Hydrogen atoms omitted for clarity.

3.5 Methyl Triflate Alkylation

Following a similar route as the $[Et_3O][BF_4]$ alkylation, the reaction of **Py_2TTAH** with MeOTf in DCM affords **[*S*-Me-Py_2TTAH][OTf]** as an iridescent white powder in 90% yield (**3.18**, Scheme 3-4). Comparison of the IR, ^{1}H NMR and ^{13}C NMR spectra **of [*S*-Me-Py_2TTAH][OTf]** with **[*S*-Et-Py_2TTAH][BF_4]** reveal several similarities with the most significant differences attributed to the anion stretching frequencies in the IR spectra. Similar to the differences between the methyl and ethyl coordination polymers (Section 3.2), there was also an increase in the number of stretches below 800 cm^{-1} in

[*S*-Et-Py$_2$TTAH][BF$_4$] compared with **[*S*-Me-Py$_2$TTAH][OTf]** attributed to the C—H rocking bands, which are more numerous in the ethyl derivative. In the ^{1}H NMR spectra, signals corresponding to the N—H and pyridyl protons overlap when comparing **3.17** and **3.18**, while the methyl peak for the **[*S*-Me-Py$_2$TTAH]$^+$** cation and the methylene peak of the **[*S*-Et-Py$_2$TTAH]$^+$** cation are in close proximity (Figure 3-13). This is consistent with what is expected between methylene and methyl protons in an otherwise similar environment. Comparison of the ^{13}C NMR spectra also revealed many parallels, with overlapping pyridyl signals and deshielded *S*-alkyl peaks (Figure 3-14). Considering the deshielded *S*-alkyl peaks, an upfield shift of 9 ppm for the methyl carbon of **[*S*-Me-Py$_2$TTAH][OTf]** can be observed in comparison to the methylene of **[*S*-Et-Py$_2$TTAH][BF$_4$]**.

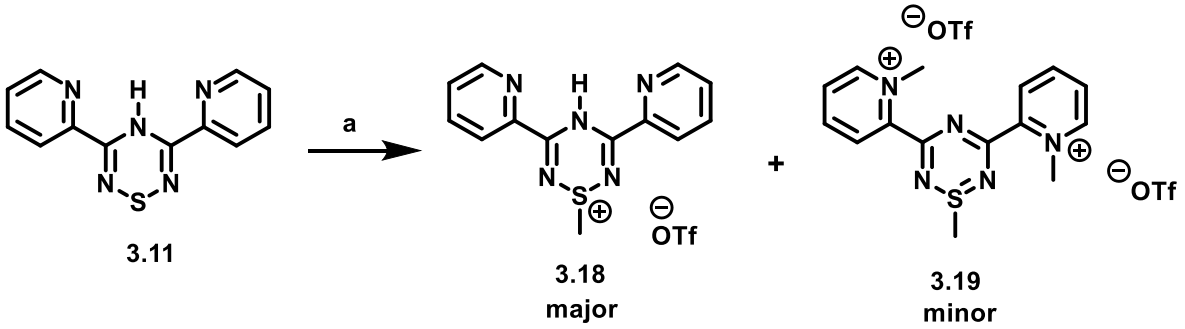

Scheme 3-4. Synthesis of **[*S*-Me-Py$_2$TTAH][OTf]** and 3,5-*bis*(*N*-methyl-2-pyridinium)-*S*-methyl-1,2,4,6-thiatriazine dication (*vide infra*). Reagents and conditions: (a) MeOTf; DCM.

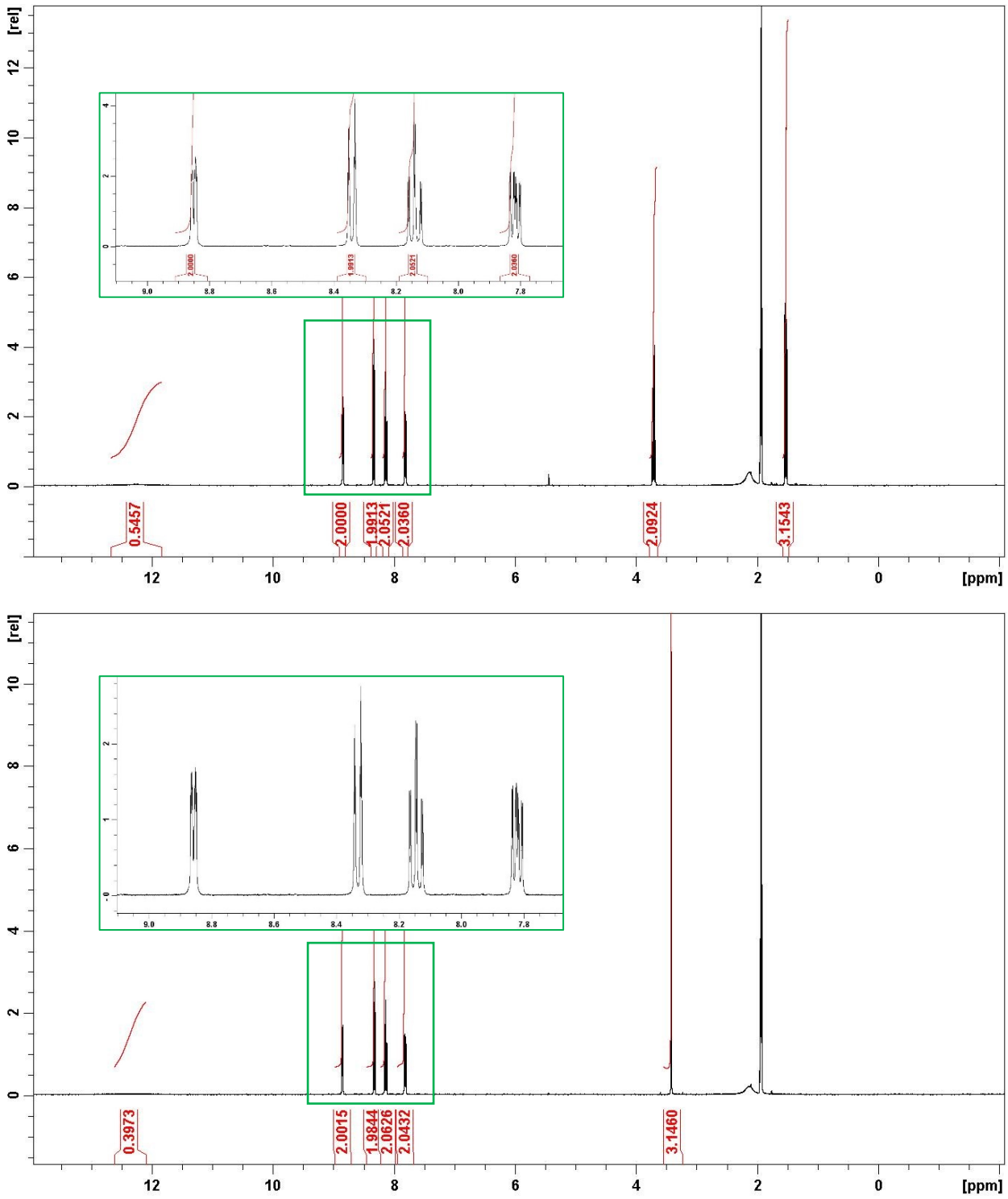

Figure 3-13. ^{1}H NMR spectra of **[*S*-Et-Py$_2$TTAH][BF$_4$]** (top) and **[*S*-Me-Py$_2$TTAH][OTf]** (bottom) in MeCN-d$_3$.

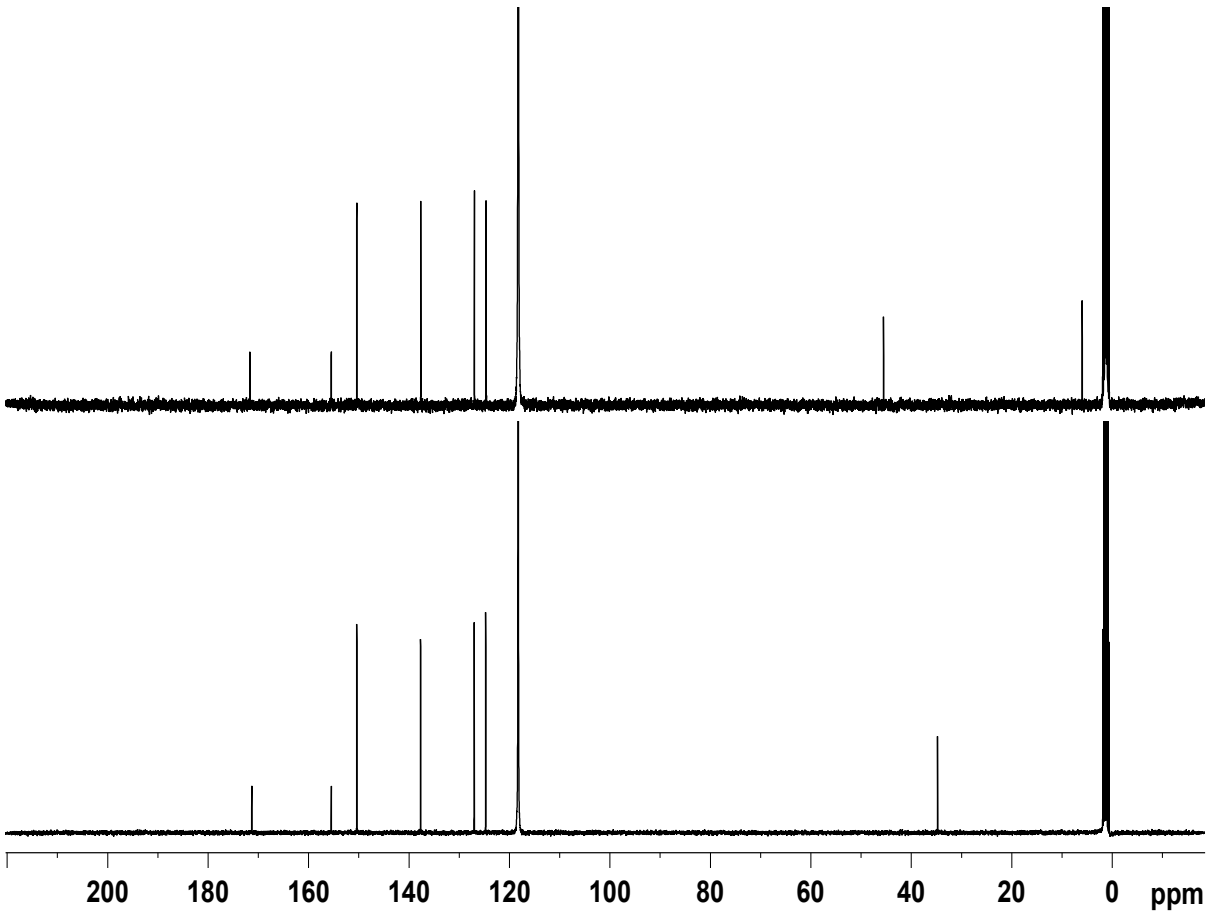

Figure 3-14. ^{13}C NMR spectra of **[*S*-Et-Py$_2$TTAH][BF$_4$]** (top) and **[*S*-Me-Py$_2$TTAH][OTf]** (bottom) in MeCN-d$_3$.

Interestingly, upon inspection of the mother liquor removed from the reaction between **Py$_2$TTAH** and MeOTf, a minor side product crystallized (Scheme 3-4 above), which afforded different IR and ^{1}H NMR spectra compared to **[*S*-Me-Py$_2$TTAH][OTf]** (Figure 3-15). In addition to shifts in the pyridyl peaks, the ^{1}H NMR spectrum revealed two unique methyl singlets, which integrate in a 1:2 ratio, consistent with the preparation of the 3,5-*bis*(*N*-methyl-2-pyridinium)-*S*-methyl-1,2,4,6-thiatriazine dication (**3.19**).

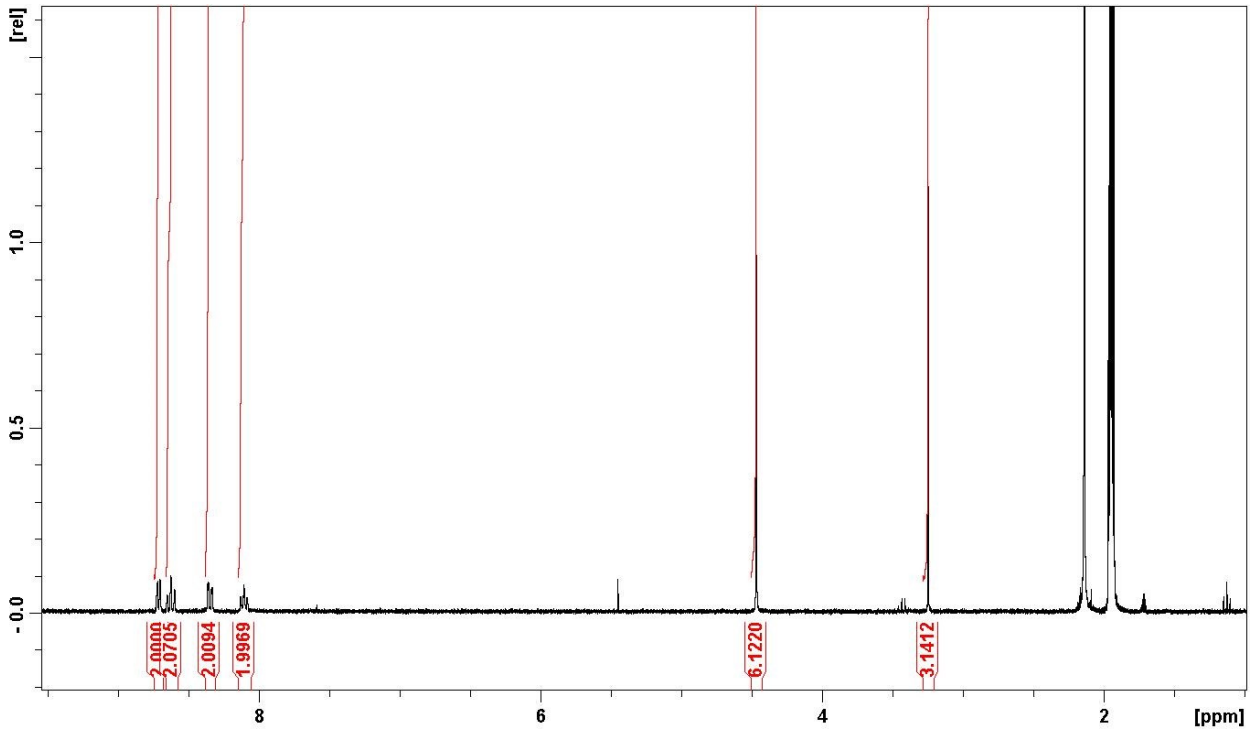

Figure 3-15. ^{1}H NMR spectrum of **3.19** in MeCN-d$_3$.

In order to confirm the identity, the yellow block-like crystals were studied *via* single crystal X-ray analysis (details provided in the Appendix). Crystals of **3.19**, which belong to the triclinic space group $P\bar{1}$, confirmed methylation occurred on both pyridyl substituents in addition to the sulfur atom in the **TTA** ring (Figure 3-16). The presence of two triflate anions in the asymmetric unit simply serves to balance the charge induced by the methylated pyridinium substituents. This, coupled with the uniformity of the C—N bond lengths in the TTA framework (Table 3-1 above), is indicative of a neutral, aromatic **TTA** moiety. Similar to ***S*-Et-Py$_2$TTA**, the six membered **TTA** ring also adopts a shallow boat-like conformation with the S1 and N3 atoms displaced from the mean plane of the remaining four atoms by 0.409(1) Å and 0.120(1) Å, respectively. As well, the pyridyl rings are twisted with respect to the **TTA** ring with torsion angles of

17.088(6)° and 49.473(6)° (Figure 3-17). These twist angles are larger than the angles observed in ***S*-Et-Py$_2$TTA**, which can likely be attributed to the increase in steric bulk from the methyl pyridinium rings of **3.19**. Nonetheless, numerous C—C′, C—N′, C—S′ and N—N′ contacts exist between adjacent molecules, leading to an array of alternating dications connected by close contacts along the *c* axis, which are separated along the *a* and *b* axes by triflate anions (Figure 3-18).

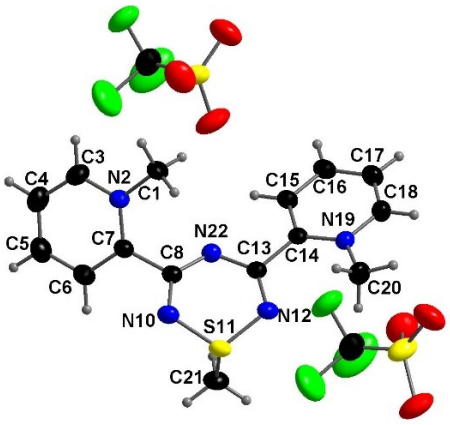

Figure 3-16. Asymmetric unit of **3.19** with 50% thermal ellipsoids for non-hydrogen atoms.

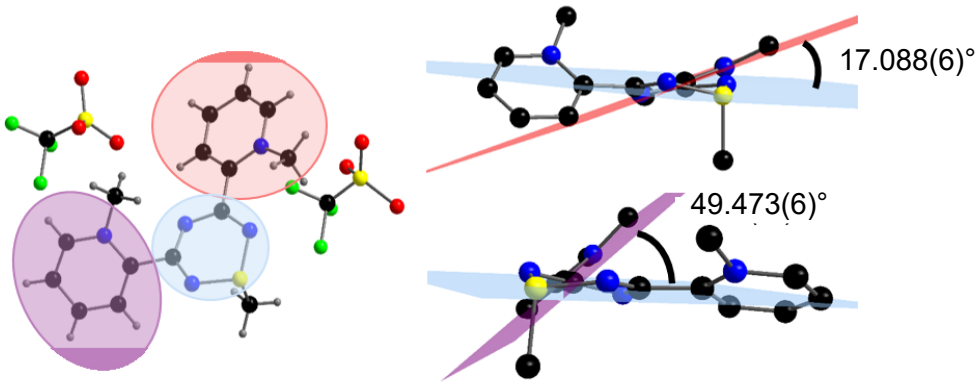

Figure 3-17. Calculated twist angles between planes of the thiatriazine and pyridyl rings of **3.19**. The central plane was calculated without the S11 and N22 atoms, as this ring adopts a shallow boat-like arrangement. Hydrogen atoms and triflate ions removed for clarity (right).

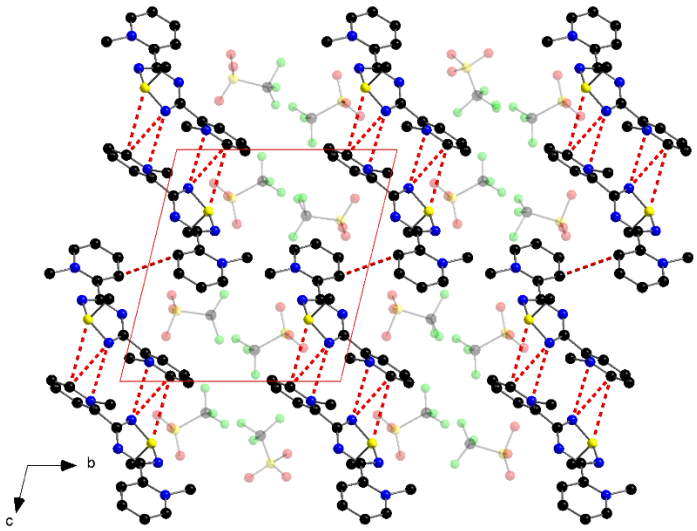

Figure 3-18. Packing of **3.19** with close contacts shown as dashed red lines. Hydrogen atoms omitted and triflate anions faded for clarity.

3.6 Neutral *S*-Alkylated Species *via* Cationic Salts

The neutral compounds ***S*-Et-Py$_2$TTA** (**3.15**) and ***S*-Me-Py$_2$TTA** (**3.16**), could also be isolated *via* deprotonation of **[*S*-Et-Py$_2$TTAH][BF$_4$]** and **[*S*-Me-Py$_2$TTAH][OTf]**, respectively, with NaH (Scheme 3-5). Characterization of both the methyl and ethyl derivatives were identical to the corresponding neutral products obtained from their coordination polymer analogues. This demonstrates that neutral *S*-alkylated **TTA** can be prepared through either cationic (*via* [Et$_3$O][BF$_4$] or MeOTf) or anionic (*via* coordination polymer) intermediates. While both routes are effective at generating the neutral *S*-alkylated **TTA**, the anionic route is superior in terms of enhanced yields (<10 vs. >80%) and purity of the crude material. Furthermore, the reaction with alkyl iodides is more cost effective and less time consuming (>48h vs. 20h).

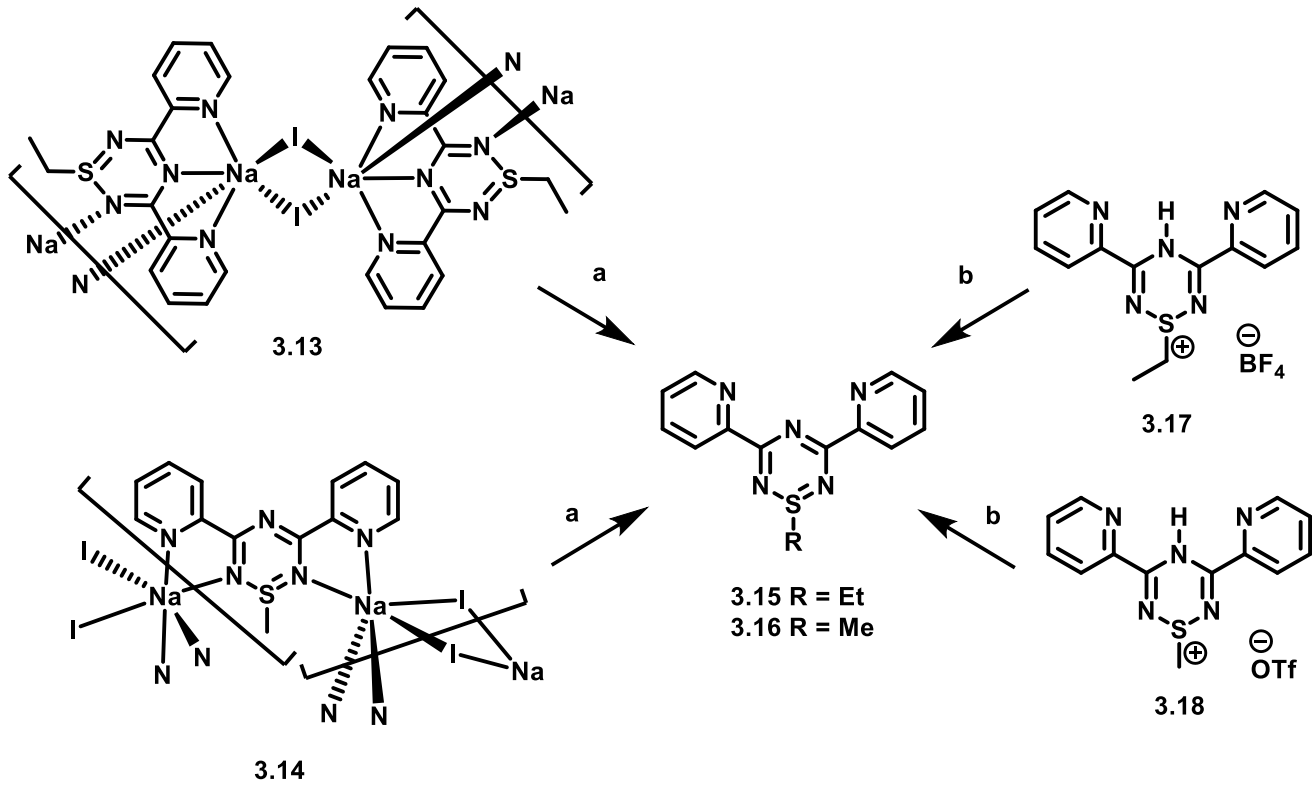

Scheme 3-5. Synthesis of ***S*-Et-Py$_2$TTA** and ***S*-Me-Py$_2$TTA** *via* polymeric and cationic intermediates. Reagents and conditions: (a) DCM/H_2O, (b) NaH; THF.

3.7 UV-vis Spectroscopy

To probe the effect of *S*-alkylation on the electronic structure, UV-vis-NIR spectroscopic studies were carried out on MeCN solutions of **3.13**-**3.19** in the range of 200-1200 nm; the results of which are presented in Figure 3-19. Interestingly, the cationic and coordination polymer intermediates (which likely dissociate in solution), as well as the neutral species exhibit similar UV-vis spectra comprised of two main regions; intense bands absorbing at 200-300 nm, and weaker broad band centred around 390 nm. For comparative purposes, **Py$_2$TTAH** was also investigated and, although the

absorption profile is similar, it is red shifted by ~100 nm. Perhaps unsurprisingly, the absorption profiles of the *S*-methylated compounds (both intermediates and the neutral species) are superimposable on their respective ethyl analogues. Considering the UV-vis spectra of **3.13** and **3.14** compared to the alkylated salts **3.17** and **3.18**, the main distinction in the absorption profiles lies in the relative intensities of the three absorption bands in the 200-300 nm range. In the case of **3.19**, only two intense absorption bands exist in the 200-300 nm region. While the neutral products (**3.15** and **3.16**) show only two major peaks in the 200-300 range, there is the suggestion of a third peak around 200 nm, which cannot be measured accurately due to the solvent cutoff.

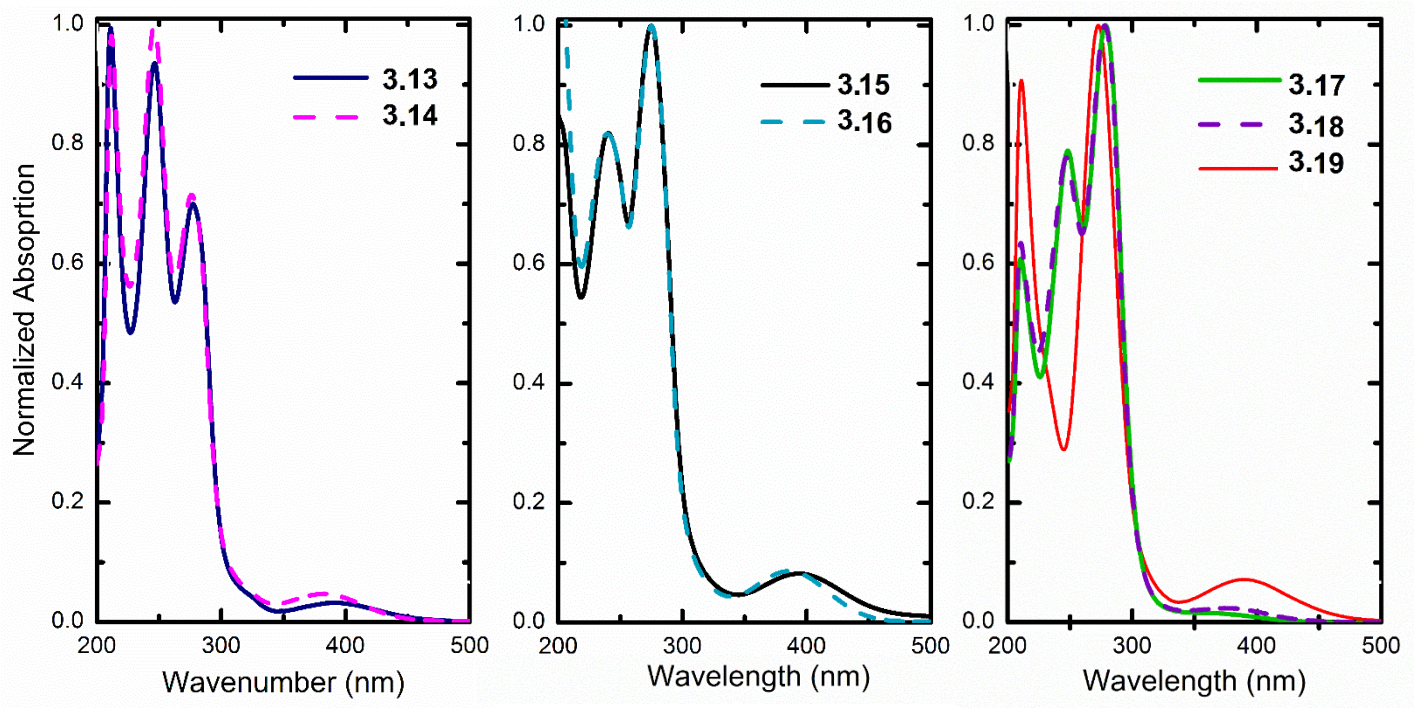

Figure 3-19. Experimental absorption spectra measured on MeCN solutions of (left) polymeric **TTA** intermediates* **3.13** (blue solid line) and **3.14** (pink dashed line), neutral *S*-alkylated species (centre) **3.15** (black solid line) and **3.16** (light blue dashed line) and cationic **TTA** intermediates (right) **3.17** (green solid line), **3.18** (purple dashed line) and **3.19** (red solid line). *It should be noted that in solution, the polymeric intermediates are likely dissociated.

3.8 Rationalization of *S*-Alkylation using Theoretical and Spectroscopic Studies

The apparent regioselective alkylation observed here, that is, preferential *S*-alkylation, may be rationalized in terms of the orbital coefficients of the frontier molecular orbitals of the deprotonated species (i.e., **Py_2TTA^-**). DFT calculations using the B3LYP/6-311+G(2d,p) level of theory were performed on **Py_2TTAH**, **Py_2TTA^-**, ***S*-Me-Py_2TTA**, and ***S*-Et-Py_2TTA**; geometry optimized molecular orbitals and orbital energetics are provided in Table 3-2. Perhaps unsurprisingly, the molecular orbitals calculated for **Py_2TTAH** and **Py_2TTA^-** are very similar to each other; the difference between the two structures simply being the presence of a proton on the central nitrogen atom, thus the electronic structure of the two molecules is expected to be alike. The HOMO of both **Py_2TTAH** and **Py_2TTA^-** consist of two nodal planes bisecting the **TTA** ring through the S—N bonds and the C—N bonds opposite them. While there is electron density throughout the **TTA** ring, the greatest electron density is at the sulfur atom, as can be seen in the side view of the HOMO of **Py_2TTA^-** (Figure 3-20). This may explain the regioselectivity, as electrophilic addition tends to occur preferentially at the site whose frontier orbital has the largest coefficient. Comparing the neutral species, **Py_2TTAH**, **3.15** and **3.16**, while slight variations in the relative energy levels are observed, the symmetry of the molecular orbitals of these compounds is similar. The high energies of the anionic derivative, **Py_2TTA^-**, are consistent with the greater reactivity of this compound.

Table 3-2. Frontier molecular orbitals and corresponding energies (in eV) for **3.15**, **3.16**, **Py$_2$TTA$^-$** and **3.11**. Energies were calculated at the B3LYP/6-311+G(2d,p) level of theory, and orbital probability diagrams were generated using GaussView 5.0 software.[30]

	***S*-Et-Py$_2$TTA**	***S*-Me-Py$_2$TTA**	**Py$_2$TTA$^-$**	**Py$_2$TTAH**
LUMO	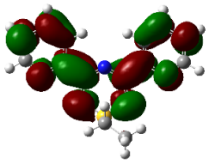 -2.27324	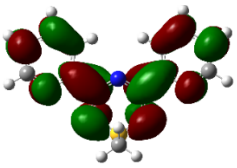 -2.53801	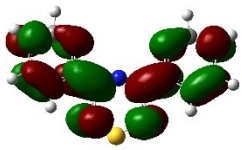 1.58996	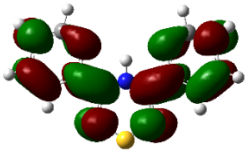 -2.26861
HOMO	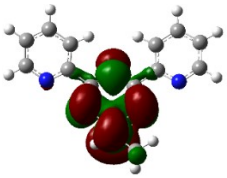 -6.22216	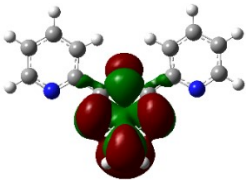 -6.60013	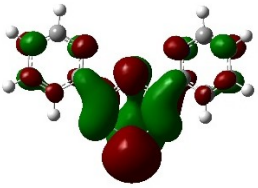 -0.6079	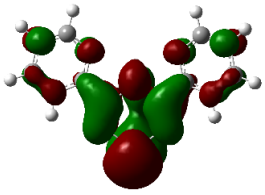 -5.28364

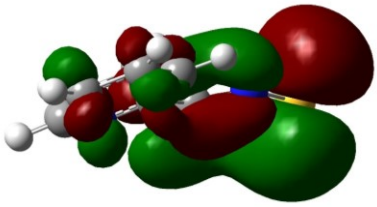

Figure 3-20. HOMO of **Py$_2$TTA$^-$** viewed from the side, showing the large electron density residing on the sulfur atom (right most atom).

The photophysical properties of **3.15** and **3.16** were investigated and, although these compounds do not fluoresce, they absorb strongly in the UV-vis region of the electromagnetic spectrum (see section 3.7). To probe the optical transitions, TD DFT calculations were performed on optimized geometries of **3.15** and **3.16**; the results of which are presented in Figure 3-21 and the twenty vertical excitation energies calculated for each compound are listed in Table 3-3. Overall, the predicted absorption profiles are in reasonable agreement with those experimentally obtained – i.e., the

calculated maximum absorption wavelengths and relative intensities match the experimental behaviour well. The highest wavelength absorption, which is associated with the HOMO to LUMO transition, has relatively low oscillator strength (f =0.0276 for **3.15**; f = 0.0273 for **3.16**). The band with the largest oscillator strength (f = 0.2499 and 0.2303 for **3.15** and **3.16**, respectively) corresponds to excitations arising from contributions of several transitions (see Tables 3-4 and 3-5). Furthermore, the oscillator strength predicted by computational methods correlates well with the measured molar extinction coefficients (see Table 3-6).

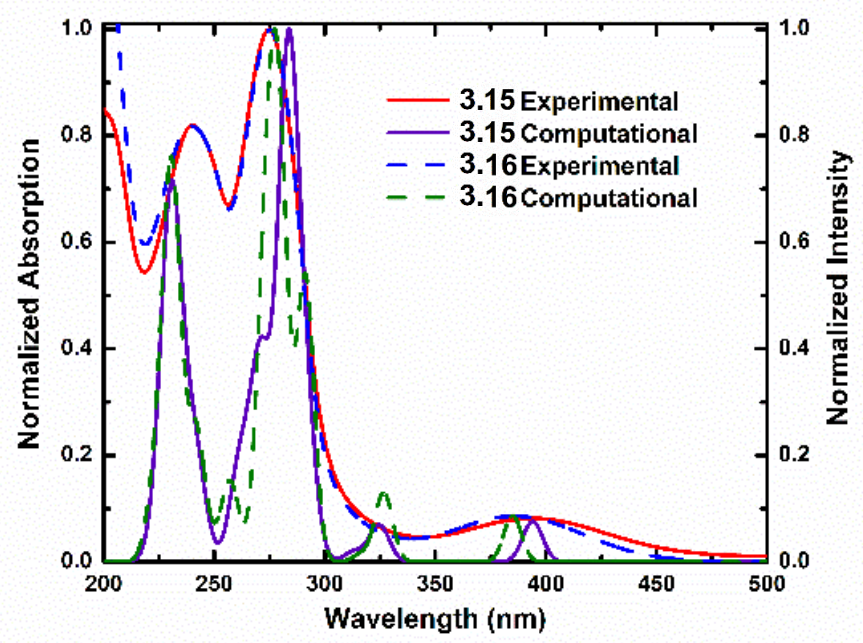

Figure 3-21. Experimental absorption spectra of **3.15** (red solid line) and **3.16** (blue dashed line) in MeCN, as well as TD DFT calculated absorption spectra of **3.15** (purple solid line) and **3.16** (green dashed line).

Table 3-3. TD DFT optical transitions[a] for **3.15** and **3.16**, calculated at the B3LYP/6-311+G(2d,p) level of theory on geometry optimized structures with Gaussian 09 software.[30]

k	**3.15**		**3.16**	
	E (eV)	*f*	E (eV)	*f*
1	3.1469	0.0276	3.2206	0.0273
2	3.8194	0.0250	3.7961	0.0408
3	3.9578	0.0071	3.9157	0.0046
4	4.2397	0.0429	4.2561	0.1391
5	4.2852	0.0829	4.2670	0.0293
6	4.3775	0.2499	4.4441	0.0153
7	4.3898	0.0703	4.4444	0.2303
8	4.5744	0.1362	4.5399	0.1592
9	4.7329	0.0581	4.8148	0.0405
10	4.7701	0.0093	4.8729	0.0097
11	5.0354	0.0025	5.0133	0.0012
12	5.0839	0.0041	5.0669	0.0013
13	5.0906	0.0043	5.0793	0.0003
14	5.1081	0.0093	5.0827	0.084
15	5.1274	0.0200	5.0834	0.0002
16	5.1886	0.0501	5.1349	0.0686
17	5.3649	0.1191	5.3638	0.1637
18	5.3779	0.1082	5.4066	0.0727
19	5.4587	0.0232	5.5428	0.0277
20	5.5231	0.0153	5.5823	0.0111

Table 3-4. Selected TD DFT transitions for **3.15**. Transitions shown are those with the greatest calculated oscillator strength, as well as the HOMO to LUMO transition. Calculations were performed at the B3LYP/6-311+G(2d,p) level of theory with acetonitrile solvation using Gaussian 09 software.[30]

Calculated λ (nm)	Transitions	Oscillator Strength (*f*)
394	HOMO → LUMO	0.0276
283	HOMO-6 → LUMO HOMO-5 → LUMO HOMO-4 → LUMO HOMO-3 → LUMO HOMO-2 →LUMO HOMO-1 → LUMO HOMO → LUMO+1	0.2499
271	HOMO-6 → LUMO HOMO-5 → LUMO HOMO-4 → LUMO HOMO-3 → LUMO HOMO-2 → LUMO HOMO-1 → LUMO HOMO → LUMO+2	0.1362
231	HOMO-8 → LUMO HOMO-5 → LUMO+1 HOMO-4 → LUMO+1 HOMO-2 → LUMO+1 HOMO → LUMO+4	0.1191
230	HOMO-8 → LUMO HOMO-5 → LUMO+1 HOMO-4 → LUMO+1 HOMO-2 → LUMO+1 HOMO → LUMO+4	0.1082

Table 3-5. Selected TD DFT transitions for **3.16**. Transitions shown are those with the greatest calculated oscillator strength, as well as the HOMO to LUMO transition. Calculations were performed at the B3LYP/6-311+G(2d,p) level of theory with acetonitrile solvation using Gaussian 09 software.[30]

Calculated λ (nm)	Transitions	Oscillator Strength (*f*)
385	HOMO → LUMO	0.0273
291	HOMO-6 → LUMO HOMO-4 → LUMO+1 HOMO-3 → LUMO HOMO-2 → LUMO+1	0.1391
279	HOMO-5 → LUMO HOMO-3 → LUMO HOMO-1 → LUMO	0.2303
273	HOMO-5 → LUMO HOMO-4 → LUMO HOMO-2 → LUMO HOMO → LUMO+2	0.1592
231	HOMO-8 → LUMO HOMO-5 → LUMO+1 HOMO-4 → LUMO+1 HOMO-2 → LUMO+1	0.1637

Table 3-6. Comparative table for the measured molar coefficients of extinction[a] with the corresponding calculated oscillator strengths[b] for **3.15** and **3.16**.

	λ (nm)	ε ($\mu M^{-1}cm^{-1}$)	Calculated λ (nm)	*f*
3.15	240	0.0161	230	0.1082
			231	0.1191
	275	0.0196	271	0.1362
			283	0.2499
	390	0.0018	394	0.0276
3.16	240	0.0164	231	0.1637
	275	0.0195	273	0.1592
			279	0.2303
			291	0.1391
	390	0.0019	385	0.0273

[a] Optical measurements were performed on dilute MeCN solutions. [b] TD DFT/B3LYP/6- 311+G(2d,p) level of theory on geometry optimized structures where *f* = oscillator strength using Gaussian 09 software[30].

3.9 Sulfur Arylation

The preparation of *S*-alkylated **Py$_2$TTA** derivatives established a flexible and general route for functionalization of thiatriazines post-ring formation. One natural progression of this is extending to more complex examples, such as functionalization using aromatic substituents. As alkylation occurs at the sulfur atom in the **TTA** ring, the tridentate terpy-like pocket remains free to coordinate with a variety of metals. It can therefore be envisioned that sulfur functionalization with heteroaromatic substituents (e.g., ***S*-pyridyl-Py$_2$TTA**, ***S*-pyrimidyl-Py$_2$TTA**, ***S*-furyl-Py$_2$TTA**) could facilitate the development of novel ligand systems, thus facilitating the development of interesting coordination complexes, extended coordination polymers and networks.

3.9.1 Arylation Attempts using Aryl Halides

Initial attempts at aromatic functionalization of **TTA** followed similar procedures to that of the alkyl iodide alkylations described above. While typical S_NAr reactions do not proceed when employing simple aryl halides, the reaction with chlorobenzene was used as a starting point to access the reactivity of $\mathbf{Py_2TTA^-}$ towards such aromatic electrophiles. Treatment of **Py_2TTAH** with NaH, followed by the addition of chlorobenzene did not lead to a reaction, even after several days. The chloride (as opposed to the iodide) was chosen for the S_NAr reactions, as it has been shown that more electronegative halogens tend to be better leaving groups.[31] Several reaction conditions were tried in an attempt to arylate with chlorobenzene, such as using differing amounts of chlorobenzene (from 1.5 equivalents to using it as the reaction solvent) as well as running the reaction at reflux and room temperatures. In all of the variations, however, the major product after a H_2O/DCM work up was unreacted starting material (i.e., **Py_2TTAH**).

3.9.2 Arylation *via* 1-chloro-2,4-dinitrobenzene

As attempts to directly substitute aromatic groups onto the **TTA** ring proved unsuccessful, 1-chloro-2,4-dinitrobenzene ($Cl(NO_2)_2Ph$) was considered as it is one of the few aryl halides which facilitates heteroatomic arylation reactions (e.g., arylation of pyridine).[32, 33] This can be rationalized by the two nitro groups, which are ortho and

para directors and should lead to resonance stabilization of the negative charge in the intermediate (Figure 3-22).[32] Following nucleophilic addition, which results in a dinitrophenyl pyridinium salt, the compound is then able to undergo a process known as the Zinke reaction, swapping the dinitrophenyl substituent for any desired aromatic group (Scheme 3-6).[33]

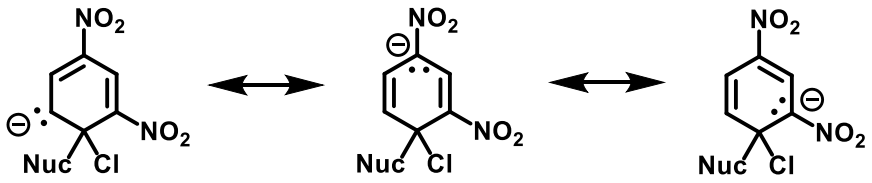

Figure 3-22. Resonance stabilization of the negative charge formed in the reaction intermediate of $S_NAr$ylation using $Cl(NO_2)_2Ph$. (adapted from reference [32], © W. W. Norton & Company, Inc, 2010.)

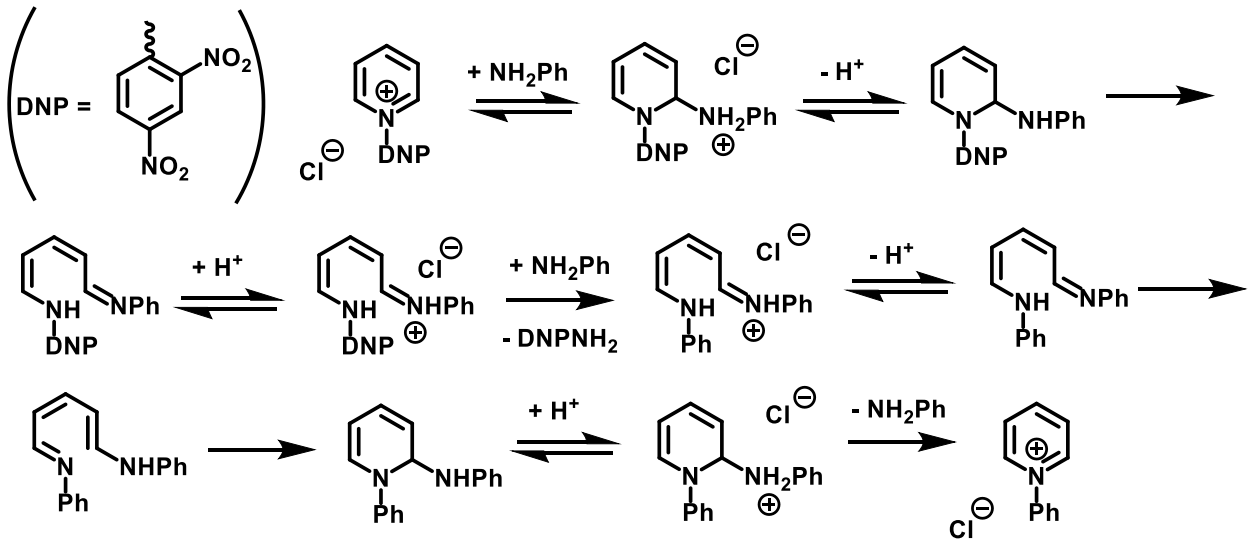

Scheme 3-6. Mechanism of the Zincke reaction. (adapted from reference [33])

Unfortunately, the mechanism of the Zincke reaction relies on a nitrogen exchange with the amine, and therefore does not allow for an analogous reaction using the sulfur of the **TTA** ring. Nevertheless, arylation of $\mathbf{Py_2TTA^-}$ with $Cl(NO_2)_2Ph$ was still

considered, as a proof of concept towards *S*-arylation, with the expected product to be **3.20** (Scheme 3-7). To that end, **Py$_2$TTAH** was deprotonated with NaH, then Cl(NO$_2$)$_2$)Ph was added and the reaction was subsequently refluxed in THF. After 48 hours, the reaction was cooled to RT, filtered and the filtrate was evaporated under reduced pressure. Upon analysis *via* ^{1}H NMR spectroscopy, the spectrum revealed an increased number of signals in the aromatic region, which may be attributed to *S*-arylation. The crude product, however, contained multiple impurities. This method was not pursued any further, as it was simultaneously found that hypervalent iodine compounds were more effective at arylation and provided a product with fewer impurities.

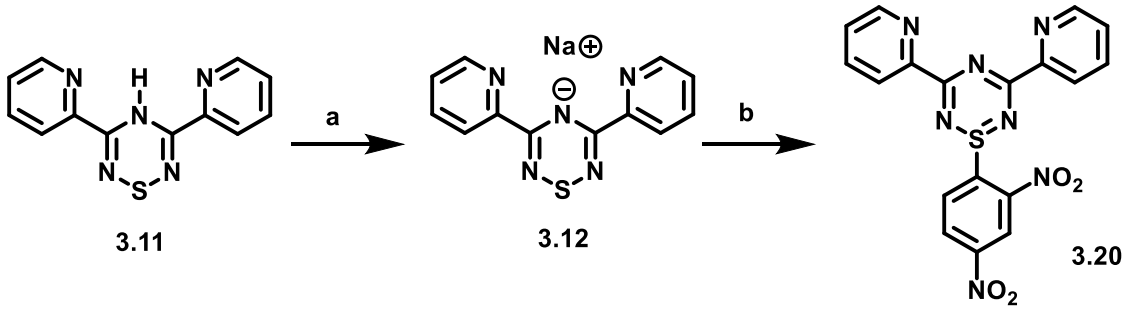

Scheme 3-7. Proposed synthesis of **3.20**, using Cl(NO$_2$)$_2$Ph. Reagents and conditions: (a) NaH; THF (b) Cl(NO$_2$)$_2$Ph.

3.9.3 Hypervalent Iodine as an Electrophile

Hypervalent iodine has been shown to be an effective electrophile in the arylation of heteroatoms, offering a more direct synthesis for *N*-arylation reactions compared with the Zincke reaction.[34] When used for arylation reactions, hypervalent

iodine consists of a positive iodonium ion bridging two aryl groups, with a negative counterion. These iodonium ions can be symmetric or asymmetric with respect to their aryl groups, of which there are many literature procedures for the synthesis of different carbocycle variations,[34, 35] and a few procedures for heterocyclic hypervalent iodonium complexes.[36] There are also examples in the literature of hypervalent iodonium effectively arylating chalcogens.[37, 38]

For the arylation of **Py$_2$TTAH**, diphenyliodonium triflate ([IPh$_2$][OTf]) was chosen and synthesized as described in literature.[35] The hypervalent iodonium reagent was then used as an electrophile, reacting with **Py$_2$TTA**$^-$ to form a rusty brown mixture. After ~20 hours, the reaction was poured onto hexanes affording a pale yellow solid. After stirring with hexanes for several hours, the reaction was filtered to give a crude yield of 107%. The ^{1}H NMR spectrum (Figure 3-23) revealed four distinct aromatic signals that integrate to two protons each, and one additional aromatic signal comprised of overlapping peaks that integrates to five protons, therefore suggesting the formation of 3,5-*bis*(2-pyridyl)-*S*-phenyl-1,2,4,6-thiatriazine (***S*-Ph-Py$_2$TTA**; **3.21**; Scheme 3-8). The ^{1}H NMR spectrum of the crude product was relatively clean, with only one small aromatic impurity and a small number of solvent peaks present in the aliphatic region.

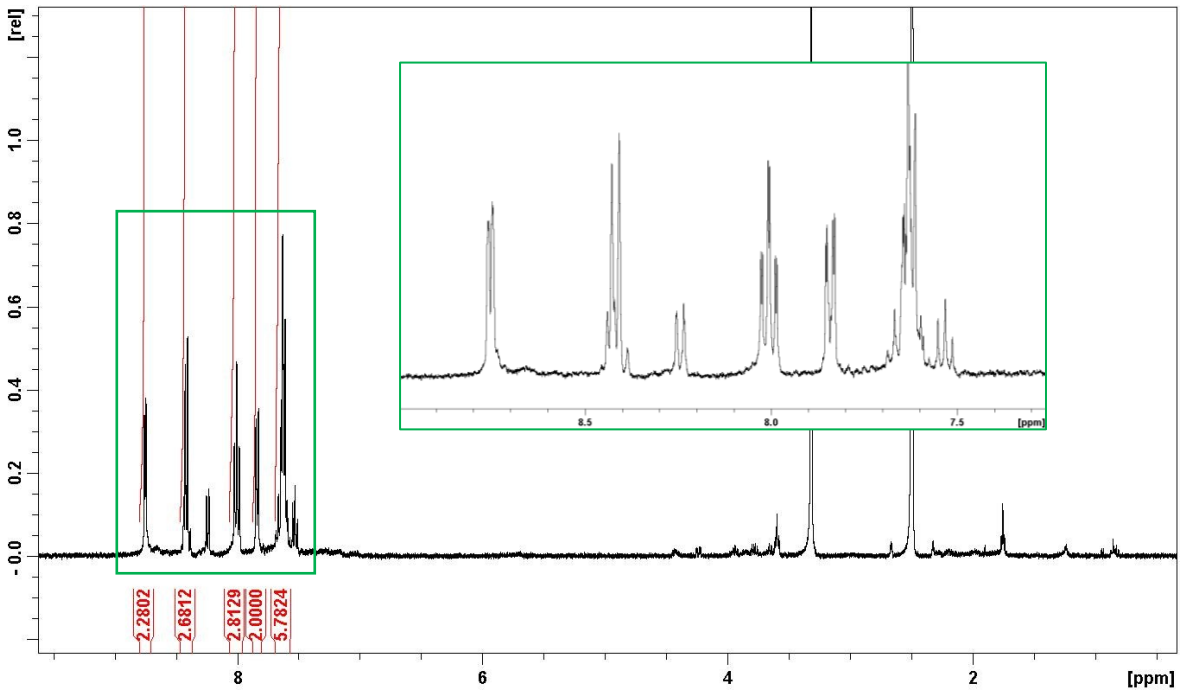

Figure 3-23. ^{1}H NMR spectrum of ***S*-Ph-Py$_2$TTA** in DMSO-d$_6$.

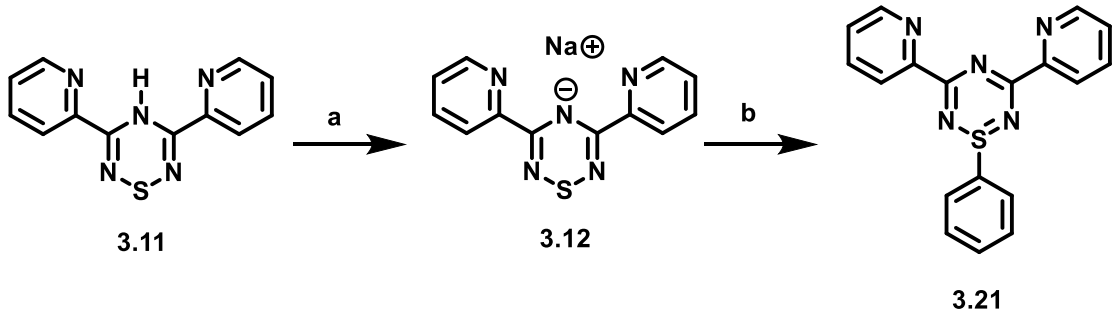

Scheme 3-8. Synthesis of ***S*-Ph-Py$_2$TTA**. Reagents and conditions: (a) NaH, THF (b) [IPh$_2$][OTf]; THF.

Assignment of the major product for this reaction as **3.21** was further supported by 2D COSY NMR studies (Figure 3-24), which revealed two separate spin systems; one for the phenyl ring bonded to the sulfur atom, and the other defining the equivalent pyridyl rings. In addition, the COSY NMR spectrum enabled assignment of the overlapping signals at 7.5 to 7.7 ppm in the ^{1}H NMR spectrum; the para-protons of the

two pyridyl rings (b in Figure 3-24) as well as the meta and para protons of the phenyl ring (f,g in Figure 3-24).

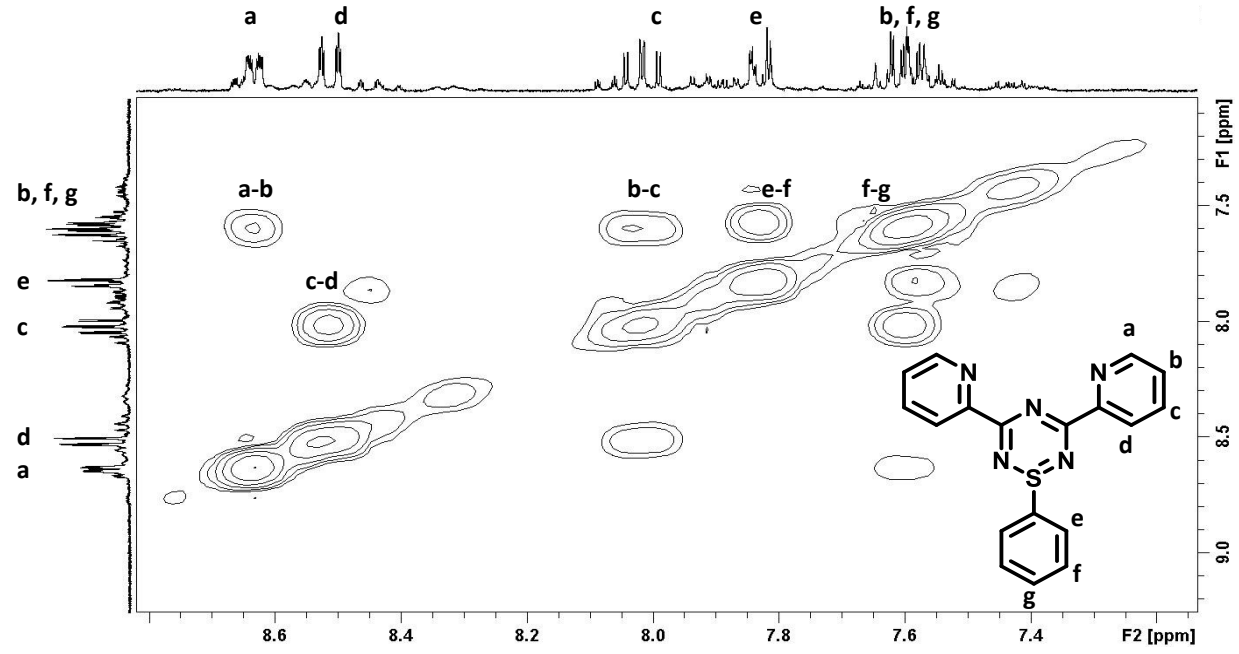

Figure 3-24. COSY proton correlation NMR spectrum of ***S*-Ph-Py$_2$TTA** in DMSO-d$_6$, outlining adjacent proton coupling peaks. Note that the f-g correlation signal may be hidden by the diagonal peak.

3.10 Conclusions

To summarize, this chapter presented a flexible and general route for the preparation of *S*-alkyl-thiatriazines, which can proceed *via* two synthetic pathways; either through cationic or anionic intermediates. Crystallographic analysis combined with spectroscopic studies of the intermediates and final products of the alkylation reactions demonstrated the stability of the **TTA** ring through cationic, neutral, and anionic states. In addition, promising initial work towards a synthetic route for sulfur arylation of thiatriazines was also presented, employing diaryliodonium salts. ^{1}H and

COSY NMR analysis of the product obtained suggests the desired product ***S*-Ph-Py$_2$TTA** was achieved through this route. Overall, the research presented in this chapter lays the groundwork for future development of a wide range of more complex examples of *S*-functionalized thiatriazines.

3.11 Future Work

The work presented in this chapter is an important finding, and holds potential in the design of novel heterocyclic compounds that can be targeted for applications ranging from mesogens in liquid crystalline materials to ionic liquids and electroactive substrates. Taking advantage of the fact that alkylation occurs at the sulfur atom in the **TTA** ring, leaving the tridentate coordination pocket free to bond to a variety of metals, facilitates the development of novel ligand systems. Furthermore, *S*-functionalization could be used to create novel tethered **TTA** systems, or liquid crystalline materials using long alkyl chains.

Another logical next step would involve the preparation of the *S*-pyrimidyl derivative, which would facilitate multimetallic coordination. Furthermore, changing the 3- and 5- substituent from a pyridyl to pyrimidyl ring (i.e., **Prm$_2$TTA**) would change the bidentate chelating pockets to tridentate (Figure 3-25). Such ligand systems have significant potential towards the development of extended coordination polymers and networks.

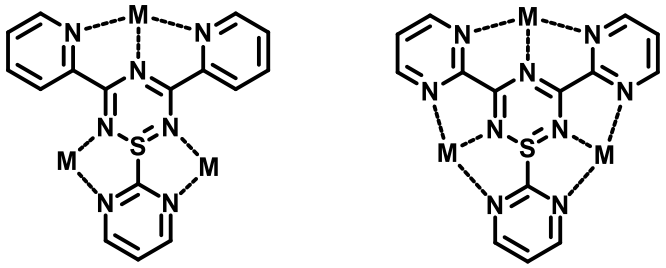

Figure 3-25. Potential metal coordination pockets with the inclusion of a heterocycle on the sulfur atom with pyridyl (left) and pyrimidyl (right) substituents at the 3- and 5- positions.

3.12 Experimental Details

3.12.1 General Procedures

The reagents sodium hydride (60% dispersion in mineral oil, Alfa Aesar) methyl iodide (Alfa Aesar), ethyl iodide (Sigma-Aldrich), triethyloxonium tetrafluoroborate (Sigma-Aldrich), and methyl trifluorosulfonate (methyl triflate, Synquest Labs Inc.) were obtained commercially and used as received. THF and DCM were dried by passing them through activated alumina on a J.C. Meyer solvent purification system and stored over 4Å Molecular sieves. All other solvents were reagent grade. 3,5-*bis*(2-pyridyl)-4-hydro-1,2,4,6-thiatriazine (**Py_2TTAH**)[26] and diphenyliodonium triflate [IPh_2][OTf][35] were prepared as outlined in the literature. All reactions were performed under an atmosphere of dry nitrogen unless otherwise stated. Melting points were taken using a Mel-Temp apparatus and are uncorrected. ^{1}H NMR, ^{13}C NMR, and COSY NMR spectra were run in MeCN-d_3 or DMSO-d_6 solutions at room temperature on Bruker Avance 400 MHz or Bruker Avance 300 MHz spectrometers. IR spectra of solid

samples were recorded on an Agilent Technologies Cary 630 FT-IR spectrometer. UV-visible spectra were measured using an Agilent Cary 5000 UV-Vis-NIR spectrophotometer in the range 200 – 1200 nm. Solution absorption measurements were completed using MeCN solutions with standard 10 mm pathlength cuvettes.

3.12.2 Crystal Growth

Yellow blocks of **[Na(*μ*-I)(*S*-Et-Py$_2$TTA)]$_\infty$** suitable for X-ray analysis were recrystallized *via* vapour diffusion of Et_2O into a saturated solution of DCM. Small yellow crystals of **[Na(*μ*-I)(*S*-Me-Py$_2$TTA)]$_\infty$** suitable for X-ray analysis were recrystallized *via* vapour diffusion of Et_2O into a saturated solution of MeCN. Bright yellow block-like crystals of **[*S*-Et-Py$_2$TTAH][BF$_4$]** suitable for X-ray analysis were grown *via* slow evaporation of the reaction filtrate. Yellow block-like crystals of [3,5-*bis*(*N*-methyl-2-pyridinium)-*S*-methyl-1,2,4,6-thiatriazine][OTf]$_2$ suitable for X-ray analysis were grown *via* vapour diffusion of chloroform into a saturated solution of acetone. Yellow needles of ***S*-Et-Py$_2$TTA** suitable for X-ray analysis were grown through recrystallization from hexanes.

3.12.3 Computational Chemistry

All calculations were carried out using the Gaussian09 program package.[30] The geometries of the studied compounds were investigated using the hybrid density functional B3LYP with the 6-311+G(2d,p) basis set. Optimized structures were used to

examine the orbital energies and frontier molecular orbital probabilities. The calculated UV-vis spectra and excitation energies were determined using TD DFT which employed the optimized B3LYP ground states. The solvent model and solvent was MeCN, and twenty excited states were considered.

3.12.4 Synthetic Procedures

[Na(μ-I)(*S*-Et-Py$_2$TTA)]$_\infty$ (3.13). Under an inert atmosphere, 60% sodium hydride (0.164 g, 4.11 mmol) was added to a solution of **Py$_2$TTAH** (1 g, 3.92 mmol) in THF (25 mL), resulting in the evolution of hydrogen gas and a dark green solution. After 30 minutes, ethyl iodide (1.22 g, 7.83 mmol) was added and, after stirring for 17 hours, the resulting orange precipitate was filtered and dried in air. Yield 1.22 g (2.82 mmol, 72%). Yellow blocks suitable for X-ray analysis were recrystallized by vapour diffusion of Et_2O into a saturated solution of DCM. Dec. > 150°C. ^{1}H NMR (δ, MeCN-d3): 8.56 (2H, ddd, J = 4.8, 1.7, 0.9 Hz, Ar), 8.40 (2H, ddd, J = 8.0, 1.1, 1.0 Hz, Ar), 7.98 (2H, ddd, J = 8.0, 7.6, 1.7 Hz, Ar), 7.55 (2H, ddd, J = 7.6, 4.8, 1.2 Hz, Ar), 3.23 (2H, q, J = 7.4 Hz), 1.37 (3H, t, J = 7.5 Hz). ^{13}C NMR (δ, MeCN-d3): 170.50, 153.85, 150.24, 138.99, 128.09, 124.86, 46.89, 5.81. IR ν_{max} (cm^{-1}): 3047 (w), 1587 (w), 1571 (w), 1529 (s), 1467 (w), 1437 (m), 1396 (w), 1375 (s), 1352 (m), 1335 (s), 1287 (m), 1268 (w), 1257 (m), 1145 (m), 1086 (m), 1048 (m), 1001 (s), 903 (w), 837 (w), 822 (m), 775 (s), 761 (s), 746 (s), 725 (s), 716 (m), 710 (w), 705 (w), 700 (w), 695 (s), 690 (m), 685 (m), 681 (m), 675 (w) , 670 (m), 665 (m), 660 (m), 655 (m).

[Na(*μ*-I)(*S*-Me-Py$_2$TTA)]$_\infty$ (3.14). Under an inert atmosphere, 60% sodium hydride (0.164 g, 4.11 mmol) was added to a solution of **Py$_2$TTAH** (1 g, 3.92 mmol) in THF (20 mL), resulting in the evolution of hydrogen gas and a dark green solution. After 30 minutes, methyl iodide (1.11 g, 7.83 mmol) was added and, after stirring for 16 hours, the resulting yellow precipitate was filtered and dried in air. Yield 1.38 g (3.30 mmol, 84%). Pure material was obtained by vapour diffusion of Et_2O into a saturated solution of MeCN. Dec. > 155°C. ^{1}H NMR (δ, MeCN-d3): 8.56 (2H, ddd, J = 4.8, 1.7, 0.9 Hz, Ar), 8.41 (2H, ddd, J = 7.8, 1.1, 1.0 Hz, Ar), 7.99 (2H, ddd, J = 7.8, 7.7, 1.7 Hz, Ar), 7.56 (2H, ddd, J = 7.6, 4.8, 1.2 Hz, Ar), 2.86 (3H, s). ^{13}C NMR (δ, MeCN-d3): 170.32, 154.01, 150.30, 139.03, 128.12, 124.94, 35.96. IR ν_{max} (cm^{-1}): 3049 (w), 3008 (w), 1588 (w), 1575 (w), 1528 (m), 1504 (m), 1442 (w), 1431 (w), 1399 (m), 1379 (s), 1333 (m), 1292 (m), 1253 (m), 1177 (w), 1146 (w), 1115 (m), 1090 (w), 1051 (w), 1044 (m), 1016 (w), 1002 (m), 983 (m), 938 (w), 911 (w), 843 (w), 828 (w), 791 (s), 757 (s), 728 (s), 699 (m), 669 (w).

***S*-Et-Py$_2$TTA (3.15) *via* [Na(*μ*-I)(*S*-Et-Py$_2$TTA)]$_\infty$.** **3.13** (1.19g, 2.74 mmol) was dissolved in a water/THF mixture (7:3), extracted into DCM, dried over $MgSO_4$, filtered and the solvent removed under reduced pressure. The resulting brown residue was dried *in vacuo.* Solvent/antisolvent recrystallization with DCM/hexanes afforded **3.15** as pure yellow crystals (yield 0.75 g, 2.65 mmol, 96%). MP: 125-126°C. ^{1}H NMR (δ, MeCN-d3): 8.72 (2H, ddd, J = 4.7, 1.8, 0.9 Hz, Ar), 8.39 (2H, ddd, J = 7.9, 1.2, 0.9 Hz, Ar), 7.91 (2H, ddd, J = 7.9, 7.6, 1.8 Hz, Ar), 7.50 (2H, ddd, J = 7.6, 4.7, 1.3 Hz, Ar), 3.13 (2H, q, J = 7.5),

1.32 (3H, t, J = 7.4). ^{13}C NMR (δ, MeCN-d3): 171.68, 155.49, 150.41, 137.67, 126.99, 124.65, 45.54, 5.99. IR ν_{max} (cm^{-1}): 3051 (w), 3011 (w), 2965 (w), 2952 (w), 2922 (w), 2907 (w), 1574 (w), 1513 (m), 1451 (w), 1437 (w), 1424 (w), 1396 (s), 1379 (s), 1374 (s), 1332 (s), 1285 (m), 1250 (s), 1174 (m), 1112 (m), 1080 (w), 1053 (w), 1043 (m), 1022 (m), 994 (m), 968 (m), 910 (w), 898 (w), 841 (w), 822 (m), 812 (w), 793 (m), 775 (s), 752 (s), 737 (s), 725 (s), 693 (m), 681 (m), 674 (w), 669 (w), 660 (w), 655 (w).

***S*-Et-Py$_2$TTA (3.15) *via* [*S*-Et-Py$_2$TTAH][BF$_4$]**. Under an inert atmosphere, 60% sodium hydride (0.0169 g, 0.424 mmol) was added to a stirring slurry of **3.15** (0.150 g, 0.404 mmol) in THF (10 mL). After 16 hours, then reaction mixture was quenched with water, extracted into DCM, dried over $MgSO_4$, filtered and the solvent removed under reduced pressure. The resulting yellow residue was dried *in vacuo* (yield 0.11g, 0.388 mmol, 96%). Recrystallization from hexanes afforded pure yellow crystals suitable for X-ray analysis. Spectroscopic data were identical to that of material prepared *via* **[Na(*μ*-I)(*S*-Et-Py$_2$TTA)]$_\infty$**.

***S*-Me-Py$_2$TTA (3.16) *via* [Na(*μ*-I)(*S*-Me-Py$_2$TTA)]$_\infty$. 3.14** (1.33 g, 3.17 mmol) was dissolved in a water/THF mixture (7:3), extracted into DCM, dried over $MgSO_4$, filtered and the solvent removed under reduced pressure. The resulting dark yellow residue was dried *in vacuo*. Solvent/antisolvent recrystallization with THF/hexanes afforded **3.18** as pure yellow needles (yield 0.85 g, 3.14 mmol, 99%). MP: 146-147°C. ^{1}H NMR (δ,

MeCN-d3): 8.71 (2H, ddd, J = 4.7, 1.8, 0.9 Hz, Ar), 8.42 (2H, ddd, J = 7.9, 1.2, 0.9 Hz, Ar), 7.91 (2H, ddd, J = 7.9, 7.6, 1.8 Hz, Ar), 7.50 (2H, ddd, J = 7.6, 4.7, 1.2 Hz, Ar), 2.76 (3H, s). ^{13}C NMR (δ, MeCN-d3): 171.31, 155.47, 150.41, 137.70, 127.01, 124.74, 34.78. IR ν_{max} (cm^{-1}): 3048 (w), 2983 (w), 2899 (w), 1583 (w), 1502 (s), 1458 (m), 1438 (m), 1414 (m), 1375 (s), 1348 (m), 1327 (s), 1296 (m), 1282 (m), 1250 (m), 1141 (w), 1108 (m), 1188 (w), 1041 (w), 994 (m), 989 (m), 902 (w), 845 (w), 826 (w), 815 (w), 771 (m), 755 (s), 733 (m), 698 (m), 664 (w).

***S*-Me-Py$_2$TTA (3.16) *via* [*S*-Me-Py$_2$TTAH][OTf].** Under an inert atmosphere, 60% sodium hydride (0.015 g, 0.375 mmol) was added to a stirring slurry of **3.16** (0.150 g, 0.358 mmol) in THF (5 mL). After 16 hours, then reaction mixture was quenched with water, extracted into DCM, dried over $MgSO_4$, filtered and the solvent removed under reduced pressure. The resulting yellow residue was dried *in vacuo* (yield 0.051g, 0.188 mmol, 52%). Solvent/antisolvent recrystallization with THF/hexanes afforded pure yellow needles. Spectroscopic data were identical to that of material prepared *via* **[Na(*μ*-I)(*S*-Me-Py$_2$TTA)]$_\infty$**.

[*S*-Et-Py$_2$TTAH][BF$_4$] (3.17). Under an inert atmosphere, triethyloxonium tetrafluoroborate (78 mg, 0.411 mmol) was added to a solution of **Py$_2$TTAH** (0.1 g, 0.391 mmol) in DCM (10 mL). After 24 hours, the resulting mixture was filtered. Upon slow evaporation of the purple filtrate, large yellow crystals suitable for XRD were obtained,

which crystallized alongside starting material. The yellow crystals were washed with DCM to remove the unreacted starting material. Yield 0.026 g (0.07 mmol, 18%) Dec. > 193°C. ^{1}H NMR (δ, MeCN-d3): 12.30 (1H, br), 8.85 (2H, ddd, J = 4.8, 1.5, 0.9 Hz, Ar), 8.34 (2H, ddd, J = 7.9, 1.1, 1.0 Hz, Ar), 8.14 (2H, ddd, J = 7.8, 7.7, 1.7 Hz, Ar), 7.82 (2H, ddd, J = 7.7, 4.8, 1.1 Hz, Ar), 3.71 (2H, q, J = 7.3 Hz), 1.53 (3H, t, J = 7.3 Hz). ^{13}C NMR (δ, MeCN-d3): 158.54, 150.57, 145.61, 139.96, 130.77, 124.48, 49.47, 5.89. IR ν_{max} (cm^{-1}): 3271 (m), 3059 (w), 2986 (w), 2940 (w), 2923 (w), 2852 (w), 1661 (s), 1638 (m), 1617 (w), 1585 (m), 1571 (m), 1560 (s), 1541 (m), 1534 (m), 1508 (w), 1470 (m), 1460 (s), 1451 (s), 1419 (s), 1395 (s), 1383 (s), 1357 (m), 1305 (w), 1285 (w), 1257 (w), 1161 (w), 1086 (m), 1063 (s), 1048 (s), 1031 (s), 1005 (s), 996 (s), 809 (m), 798 (s), 766 (m), 738 (s), 697 (s).

[*S*-Me-Py$_2$TTAH][OTf] (3.18). Under an inert atmosphere, methyl triflate (0.169 g, 1.03 mmol) was added to a solution of **Py$_2$TTAH** (0.25 g, 0.979 mmol) in DCM (15 mL). After 24 hours, **3.16** was filtered off, washed with DCM, and dried under reduced pressure. Yield: 0.3757 g (0.895 mmol, 91.5%). Dec. > 221**°C**. ^{1}H NMR (δ, MeCN-d3): 12.37 (1H, br), 8.86 (2H, ddd, J = 4.8, 1.7, 1.0 Hz, Ar), 8.33 (2H, ddd, J = 7.8, 1.1, 1.0 Hz, Ar), 8.14 (2H, ddd, J = 7.8, 7.7, 1.6 Hz, Ar), 7.82 (2H, ddd, J = 7.7, 4.8, 1.2 Hz, Ar), 3.43 (3H, s). ^{13}C NMR (δ, MeCN-d3): 158.16, 150.60, 145.68, 139.91, 130.77, 124.42, 40.45. IR ν_{max} (cm^{-1}): 3237 (m), 2991 (m), 2905 (m), 1651 (s), 1585 (m), 1572 (m), 1560 (s), 1463 (s), 1450 (m), 1406 (s), 1354 (w), 1313 (w), 1297 (w), 1251 (s), 1226 (s), 1169 (s), 1145 (s), 1092 (m), 1043 (w), 1029

(s), 1010 (m), 998 (s), 944 (w), 910 (w), 805 (m), 768 (m), 758 (w), 741 (s), 705 (s), 692 (s), 672 (w), 660 (w).

Synthesis of *S*-Ph-Py$_2$TTA (3.21). Under an inert atmosphere, 60% sodium hydride (0.01 g, 0.22 mmol) was added to a solution of **Py$_2$TTAH** (0.05 g, 0.21 mmol) in THF (5 mL), resulting in the evolution of hydrogen gas and a dark green solution. After 30 minutes, [IPh$_2$][OTf] (0.1 g, 0.23 mmol) was added and, after stirring for 20 hours, the resulting yellow precipitate was filtered, rinsed with hexanes and dried in air. Yield 0.048 g (0.144 mmol, 68%) ^{1}H NMR (δ, MeCN-d3): 8.75 (2H, ddd, J = 4.6, 1.5, 0.6 Hz, Ar), 8.41 (2H, ddd, J = 7.9, 1.1, 1.0 Hz, Ar), 8.00 (2H, ddd, J = 7.7, 7.7, 1.8 Hz, Ar), 7.84 (2H, dd, J = 7.6, 1.8 Hz, Ar), 7.67-7.58 (5H, mult). IR ν_{max} (cm^{-1}): 3669 (w), 3485 (w), 1606 (w), 1587 (w), 1524 (m), 1467 (w), 1445 (w), 1378 (m), 1349 (w), 1332 (w), 1258 (s), 1232 (s), 1192 (m), 1171 (s), 1091 (w), 1037 (s), 1002 (m), 908 (w), 838 (w), 779 (w), 748 (m), 729 (m), 688 (w).

3.13 References

1. M. P. Cava, M. V. Lakshmikantham, R. Hoffmann and R. M. Williams, *Tetrahedron*, 2011, **67**, 6771-6797.

2. M. E. Cinar and T. Ozturk, *Chemical Reviews*, 2015, **115**, 3036-3140.

3. B. F. Abdel-Wahab and S. Shaaban, *Synthesis-Stuttgart*, 2014, **46**, 1709-1716.

4. F. A. Davis, *Journal of Organic Chemistry*, 2006, **71**, 8993-9003.

5. A. K. Boudalis, C. P. Raptopoulou, A. Terzis and S. P. Perlepes, *Polyhedron*, 2004, **23**, 1271-1277.

6. C. Wang, H. Dong, W. Hu, Y. Liu and D. Zhu, *Chemical Reviews*, 2012, **112**, 2208-2267.

7. A. W. Cordes, P. J. Hayes, P. D. Josephy, H. Koenig, R. T. Oakley and W. T. Pennington, *Journal of the Chemical Society-Chemical Communications*, 1984, 1021-1022.

8. P. J. Hayes, R. T. Oakley, A. W. Cordes and W. T. Pennington, *Journal of the American Chemical Society*, 1985, **107**, 1346-1351.

9. R. T. Boere, R. T. Oakley, R. W. Reed and N. P. C. Westwood, *Journal of the American Chemical Society*, 1989, **111**, 1180-1185.

10. K. L. M. Harriman, A. A. Leitch, S. A. Stoian, F. Habib, J. L. Kneebone, S. I. Gorelsky, I. Korobkov, S. Desgreniers, M. L. Neidig, S. Hill, M. Murugesu and J. L. Brusso, *Dalton Transactions*, 2015, **44**, 10516-10523.

11. C. Y. Ang, R. T. Boere, L. Y. Goh, L. L. Koh, S. L. Kuan, G. K. Tan and X. Yu, *Chemical Communications*, 2006, 4735-4737.

12. C. Y. Ang, S. L. Kuan, G. K. Tan, L. Y. Goh, T. L. Roemmele, X. Yu and R. T. Boere, *Canadian Journal of Chemistry*, 2015, **93**, 181-195.

13. N. J. Yutronkie, I. A. Kuehne, I. Korobkov, J. L. Brusso and M. Murugesu, *Chemical Communications*, 2016, **52**, 677-680.

14. A. Stoller, W. Kunz, H. Zondler, C. Kuethy and J. Wenger, *WO Pat.*, 9808845-A1, 1998.

15. A. Stoller and W. Kunz, *WO Pat.*, 9725319-A, 1997.

16. H. Zondler and A. Stoller, *WO Pat.*, 9725318-A; EP876358-A, 1997.

17. L. C. Peng, F. Xiang, E. Roberts, Y. Kawagoe, L. C. Greve, K. Kreuz and D. P. Delmer, *Plant Physiology*, 2001, **126**, 981-992.

18. N. J. Yutronkie, A. A. Leitch, I. Korobkov and J. L. Brusso, *Crystal Growth & Design*, 2015, **15**, 2524-2532.

19. M. Haake, H. Fode and K. Ahrens, *Zeitschrift Fur Naturforschung Section B-a Journal of Chemical Sciences*, 1973, **B 28**, 539-540.

20. J. Goerdeler and D. Loevenich, *Chemische Berichte-Recueil*, 1954, **87**, 1079-1082.

21. J. Goerdeler and B. Wedekind, *Chemische Berichte-Recueil*, 1962, **95**, 147-153.

22. W. Ried and M. A. Jacobi, *Chemische Berichte-Recueil*, 1988, **121**, 383-386.

23. R. Appel and G. Vollmer, *Chemische Berichte-Recueil*, 1970, **103**, 2555-2561.

24. Y. G. Shermolovich, V. S. Talanov, V. V. Pirozhenko and L. N. Markovskii, *Zhurnal Organicheskoi Khimii*, 1982, **18**, 2539-2547.

25. A. D. Stoller, *Journal of Heterocyclic Chemistry*, 2000, **37**, 583-595.

26. A. A. Leitch, I. Korobkov, A. Assoud and J. L. Brusso, *Chemical Communications*, 2014, **50**, 4934-4936.

27. N. J. Yutronkie, A. A. Leitch, I. Korobkov and J. L. Brusso, *Crystal Growth & Design*, 2015, **15**, 2524-2532.

28. D. Vofsi and A. V. Tobolsky, *Journal of Polymer Science Part a-General Papers*, 1965, **3**, 3261-3273.

29. J. S. Hrkach and K. Matyjaszewski, *Macromolecules*, 1990, **23**, 4042-4046.

30. M. J. Frisch, G. W. Trucks, H. B. Schlegel, G. E. Scuseria, M. A. Robb, J. R. Cheeseman, G. Scalmani, V., Barone, B. Mennucci, G. A. Petersson, H. Nakatsuji, M. Caricato, X. Li, H. P. Hratchian, A. F. Izmaylov, J., Bloino, G. Zheng, J. L. Sonnenberg, M. Hada, M. Ehara, K. Toyota, R. Fukuda, J. Hasegawa, M. Ishida, T., Nakajima, Y. Honda, O. Kitao, H. Nakai, T. Vreven, J. J. A. Montgomery, J. E. Peralta, F. Ogliaro, M., Bearpark, J. J. Heyd, E. Brothers, K. N. Kudin, V. N.

Staroverov, R. Kobayashi, J. Normand, K., Raghavachari, A. Rendell, J. C. Burant, S. S. Iyengar, J. Tomasi, M. Cossi, N. Rega, J. M. Millam, M., Klene, J. E. Knox, J. B. Cross, V. Bakken, C. Adamo, J. Jaramillo, R. Gomperts, R. E. Stratmann, O., Yazyev, A. J. Austin, R. Cammi, C. Pomelli, J. W. Ochterski, R. L. Martin, K. Morokuma, V. G., Zakrzewski, G. A. Voth, P. Salvador, J. J. Dannenberg, S. Dapprich, A. D. Daniels, O. Farkas, J. B., Foresman, J. V. Ortiz, J. Cioslowski and D. J. Fox, *Gaussian 09, Revision A.02*, Gaussian, Inc., Wallingford CT, 2009.

31. J. Clayden, N. Greeves, S. Warren and P. Wothers, *Organic Chemistry*, Oxford University Press, 2007.

32. M. Jones Jr and S. A. Fleming, *Organic Chemistry*, Norton, Fourth Edition edn., 2010.

33. W. C. Cheng and M. J. Kurth, *Organic Preparations and Procedures International*, 2002, **34**, 585-608.

34. E. A. Merritt and B. Olofsson, *Angewandte Chemie-International Edition*, 2009, **48**, 9052-9070.

35. M. Bielawski, M. Zhu and B. Olofsson, *Advanced Synthesis & Catalysis*, 2007, **349**, 2610-2618.

36. M. Bielawski, J. Malmgren, L. M. Pardo, Y. Wikmark and B. Olofsson, *Chemistryopen*, 2014, **3**, 19-22.

37. M. Hori, T. Kataoka, H. Shimizu, M. Ikemori and Y. Aoyama, *Journal of the Chemical Society-Perkin Transactions 1*, 1988, 1209-1217.

38. E. Honda, T. Iwamura, S. Watanabe and T. Kataoka, *Heterocycles*, 2000, **53**, 1997-2008.

Chapter 4 – Iron Coordination with Thiatriazine Ligands

4.1 Introduction

The study of transition metal complexes is a broad field of research, with applicability in a wide range of areas including catalysis, magnetism, dyes and pigments, medicinal and biological applications, to name a few.[1-5] The geometry and electronic configurations of metal complexes are, in general, what gives rise to the variety of properties these applications rely on. Therefore, the design of metal complexes with different metals and ligands has received much attention over recent decades in order to influence the geometry, electronic properties, and long range order of these systems.

Presently, the use of thiatriazine (**TTA**) rings as ligands in metal coordination has not been explored in great depth. Boeré and coworkers reported the first example of a thiatriazine ligand coordinated to a metal ion. As described in more detail in Chapter 1, this was achieved through coordination of thiatriazinyl radicals with a chromium cyclopentadienyl precursor.[6, 7] More recently, Brusso and coworkers employed 3,5-*bis*(2-pyridyl)-4-hydro-1,2,4,6-thiatriazine (**Py_2TTAH**; **4.1**) as a ligand, with coordination to transition metal and lanthanide ions.[8-10] In these reports, the **Py_2TTAH** starting material deprotonates and the metal ion coordinates in the tridentate pocket of the **Py_2TTA** ligand.

With respect to the transition metal complexes, Harriman *et al.* reported a family of coordination compounds isolated following reactions between the **Py_2TTA** ligand and iron halides. Of this family, two similar compounds containing chloride (**[Fe(Py_2TTA)Cl_2]**; **4.2**) and bromide (**[Fe(Py_2TTA)Br_2]**; **4.3**) ancillary ligands were isolated, as well as a coordination polymer containing μ-bridging fluoride ions (**[Fe(μ-F)(1-oxo-Py_2TTA)F]$_\infty$**; **4.4**; Scheme 4-1).[8, 9] Considering **4.2** in greater detail, the oxidation state of the iron is likely Fe(III), with an anionic **Py_2TTA^-** ligand and two chloride ions. This assignment is based on single crystal XRD analysis, which revealed the bond lengths within the **TTA** ring were consistent with discrete single or double bonds, consistent with the ligand in the anionic state. However, the ligand is planar, which is indicative of the aromatic radical form. Consequently, consideration of both Mössbauer and magnetic susceptibility studies supports the identification of the ligand in the anionic form coordinated to an Fe(III) centre. Conversely, theoretical studies revealed delocalization of electron density between the **TTA** ring and Fe centre, which could suggest some radical character in the ligand. Overall, these results leads to the conclusion that the formal oxidation state of the iron centre is Fe(III), although computational studies may be indicative of a small amount of mixed valency in the system.[8, 9]

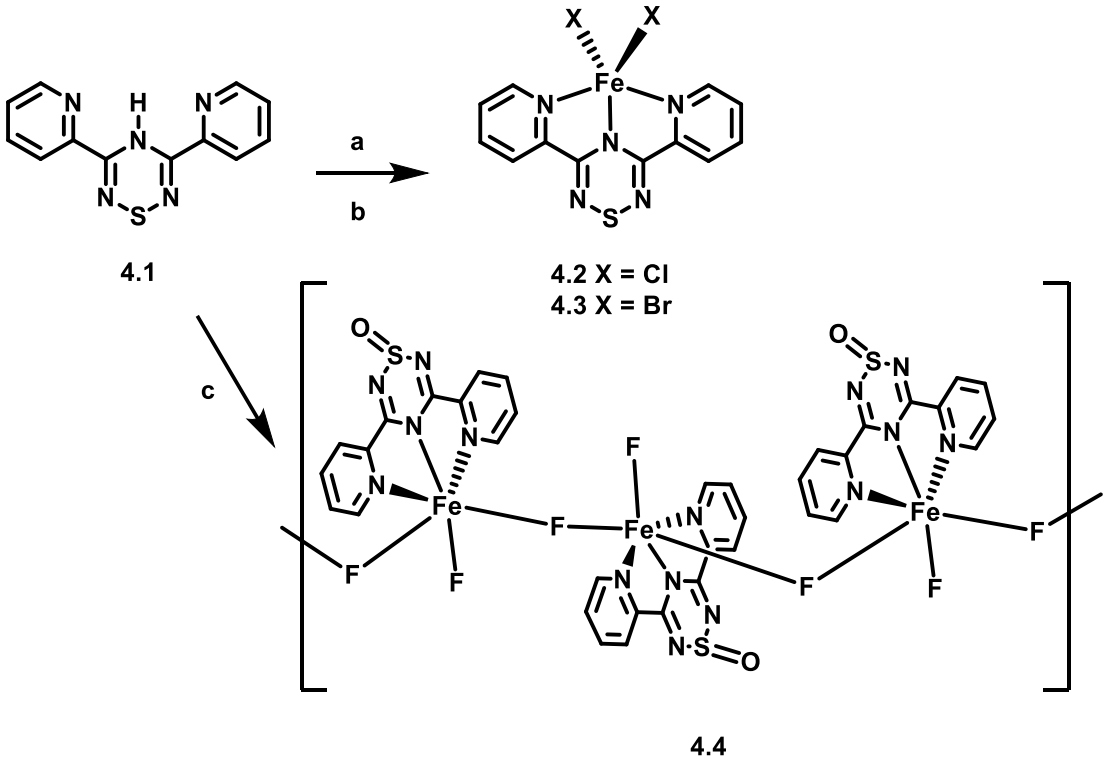

Scheme 4-1. Synthesis of iron halide complexes with **Py$_2$TTAH**. Reagents and conditions: (a) $FeCl_3$, DMF/MeOH (b) $FeBr_3$, MeCN/$CHCl_3$ (c) FeF_3, DMF/MeOH/Et_2O.[9]

4.1.1 Scope of this Chapter

This chapter reports the synthesis and crystallographic analysis of two iron coordination complexes with thiatriazine based ligands. The first compound employs 3,5-*bis*(2-pyridyl)-*S*-methyl-1,2,4,6-thiatriazine (***S*-Me-Py$_2$TTA**; **4.5**) as a tridentate ligand coordinated to an Fe(III) ion, with three chloride anions filling the remainder of the octahedral coordination sphere. The second complex contains two tridentate **Py$_2$TTA** ligands coordinated to an Fe(II) centre in an octahedral manner. While neither of these species is fully characterized, preliminary results are provided herein.

4.2 Sulfur Functionalized TTA Systems as Ligands for Coordination

As one of the anticipated future applications of *S*-functionalized **Py$_2$TTA** systems is metal coordination, the simplest *S*-substituted molecule, ***S*-Me-Py$_2$TTA**, was used for proof-of-concept coordination. Iron trichloride was chosen as the metal salt for comparative purposes with the previously reported complex **4.2**. Thus, any changes in reactivity could be attributed to the change in the ligand employed. As such, the synthesis closely mirrored that of **4.2**. More specifically, using liquid-liquid diffusion (toluene-methanol), a solution of ***S*-Me-Py$_2$TTA** in toluene was layered under a solution of $FeCl_3$ in methanol under ambient conditions in a 2:1 ratio. After 3 days, X-ray quality orange-red crystals of **Fe(*S*-Me-Py$_2$TTA)Cl$_3$** (**4.6**) were obtained (Scheme 4-2).

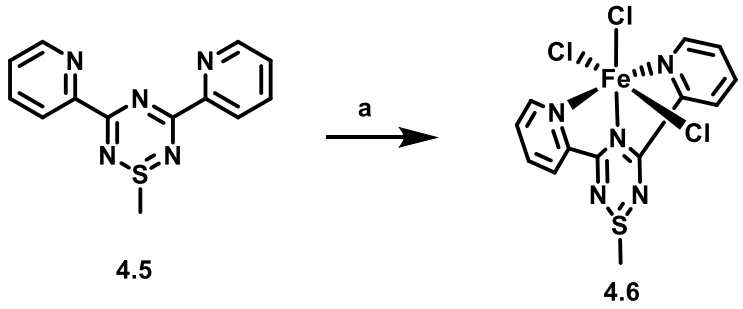

Scheme 4-2. Synthesis of **4.6**. Reagents and conditions: (a) $FeCl_3$; Toluene/MeOH.

Single crystal X-ray diffraction (XRD) revealed crystals of **4.6** belong to the monoclinic space group $P2_1/n$, and consist of four discrete molecules in the unit cell. The coordination complex is best described as a distorted six coordinate meridial iron complex, with three chloride ions and a neutral, tridentate ***S*-Me-Py$_2$TTA** ligand

completing the coordination sphere (Figure 4-1). The distortion from octahedral can be observed by considering the bond lengths and angles around the metal centre, as outlined in Table 4-1. Between the discrete molecules, a number of close contacts exist that are within or are nominally larger than the sum of the Van der Waals radii (Table 4-1 and Figure 4-2). The numerous close contacts between the pyridyl and **TTA** rings show that intermolecular communication may be possible for similar *S*-functionalized systems, which is ideal for molecular materials applications.

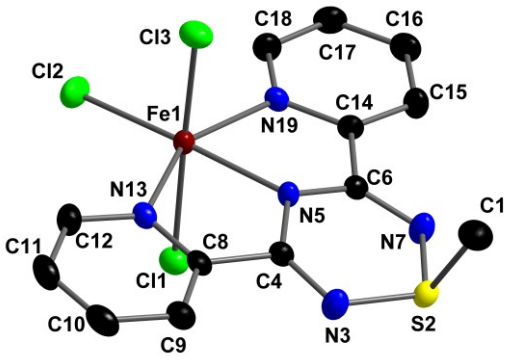

Figure 4-1. Asymmetric unit of compound **4.6** using 50% thermal ellipsoids. Hydrogen atoms removed for clarity.

Table 4-1. Bond lengths between iron and adjacent atoms, as well as close contacts that are within or nominally larger than the sum of the Van der Waals separation for **4.6**.

Fe Bond Lengths		**Ligand Close Contacts**		**Chloride Close Contacts**	
Bond	Distance (Å)	Contact	Distance (Å)	Contact	Distance (Å)
Fe1 – Cl1	2.427(7)	N7 – N7	3.083(3)	Cl1 – S2	3.399(7)
Fe1 – Cl2	2.247(7)	N7 – S2	3.188(2)	Cl1 – H1a	2.935(5)
Fe1 – Cl3	2.341(7)	S2 – C6	3.311(2)	Cl1 – H12	2.812(5)
Fe1 – N5	2.105(2)	S2 – C14	3.476(2)	Cl1 – H17	2.935(5)
Fe1 – N13	2.141(2)	C8 – C10	3.427(3)	Cl2 – S2	3.438(9)
Fe1 – N19	2.144(2)	C9 – C9	3.499(3)	Cl2 – H1a	2.806(9)
		C9 – C15	3.488(3)	Cl2 – C1	3.499(3)
		C9 – C16	3.476(3)	Cl2 – C16	3.474(3)
				Cl2 – C17	3.385(3)
				Cl3 – H1c	2.763(6)
				Cl3 – H10	2.959(6)

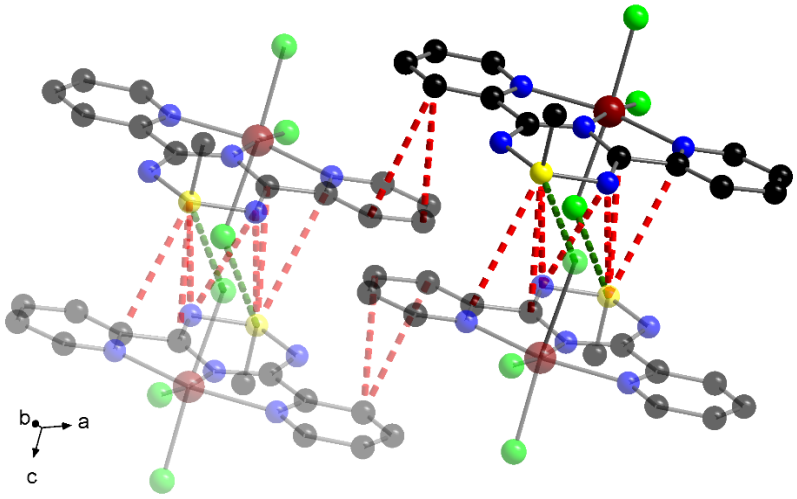

Figure 4-2. Close contacts in **4.6** between **Py$_2$TTA** ligands showing **TTA–TTA** and Py–Py interactions (red) and S–Cl interactions (dark green). Cl–H contacts not shown and hydrogen atoms removed for clarity.

4.3 Work Towards a *bis* Tridentate Thiatriazine System

To date, metal centres with two **TTA** ligands (i.e., ***bis*(TTA)** complexes) have not been reported. Such a compound would be synthetically interesting, and may also lead to properties such as spin crossover characteristics, as seen with similar tridentate ligands that coordinate in an ML_2 fashion with transition metals such as iron and cobalt.[11-17] As all previous coordination complexes using **Py_2TTA** derivatives have thus far resulted in a single ligand coordinated, it was envisioned that if the ligands were more susceptible to coordination, *bis*-complexation may be realized. To that end, deprotonation of **Py_2TTAH** with sodium hydride (NaH) prior to complexation would afford the anionic species, which may facilitate coordination, thus affording the ***bis*(Py_2TTA)** species.

In order to ensure that the presence of the sodium ion does not interfere with the subsequent coordination of a 3d-metal ion, the previously reported complex **4.2** was prepared starting from **Py_2TTA^-** (**4.7**), as outlined in Scheme 4-3.[8] To that end, **Py_2TTAH** was deprotonated with NaH, and solid $FeCl_3$ was added, affording a dark black-blue mixture from the green mixture. After stirring for two hours, the reaction mixture was left to stand under an atmosphere of nitrogen for four days. Black powdery solids were then filtered off (97% yield), and analyzed by infrared spectroscopy (IR). The IR spectrum of this compound was found to match perfectly with the IR spectrum of the

previously reported complex **4.2**. This therefore suggests that the sodium atom does not inhibit iron coordination in the tridentate pocket of the **Py$_2$TTA** framework.

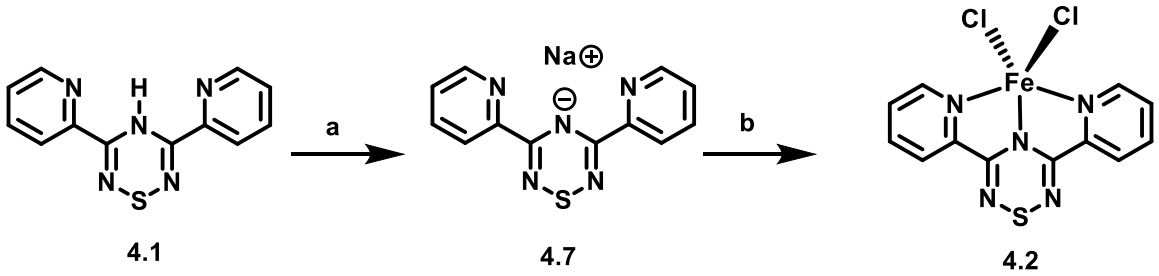

Scheme 4-3. Synthesis of **4.2** *via* **4.7**. Reagents and conditions: (a) NaH, THF (b) $FeCl_3$.

Since the sodium ion did not appear to hinder coordination, work to isolate a ***bis*(Py$_2$TTA)** complex was undertaken. Initial reactions involved the addition of solid $FeCl_2$ to a solution of **Py$_2$TTA$^-$** in THF in a 1:2 molar ratio under an inert atmosphere. After stirring for 5 minutes, the green mixture changed to a brownish coloured solution, which was subsequently left to stand under an atmosphere of static nitrogen. After four days, several black cubic crystals were isolated and analyzed by IR spectroscopy and single crystal XRD, and found to be compound **4.8** (**[Fe(Py$_2$TTA)$_2$]·THF**; Scheme 4-4).

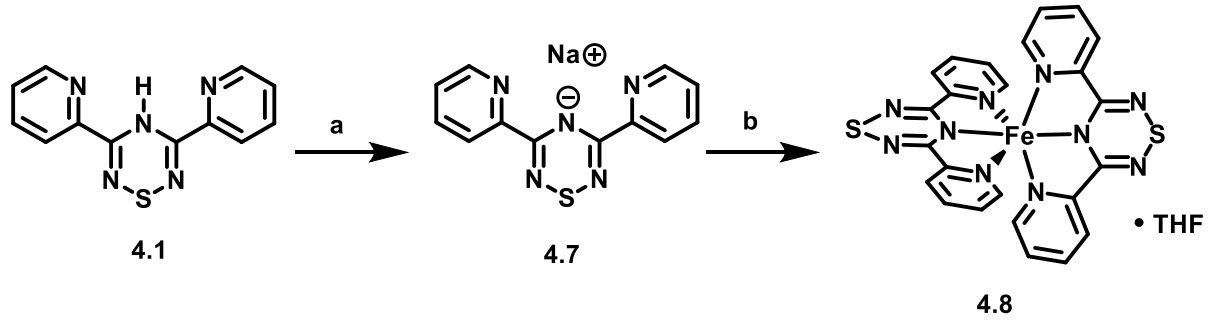

Scheme 4-4. Synthesis of compound **4.8**. Reagents and Conditions: (a) NaH; THF (b) $FeCl_2$; THF.

The coordination environment of **[Fe(Py$_2$TTA)$_2$]·THF**, with atom labeling, is shown in Figure 4-3. The geometry of the iron centre is best described as a distorted octahedral (Table 4-2), completed by two tridentate **Py$_2$TTA**$^-$ ligands. Within the **TTA** ring, the bond lengths are consistent with discrete single and double bonds, indicative of anti-aromatic character of the anionic ligand (Table 4-3). Therefore, by charge balance the iron centre would formally have a 2^+ charge. The iron-nitrogen bond lengths of 2.075(4) Å (Fe1 – N4) and 2.194(2) Å (Fe1 – N6) are consistent with what is typically reported for high spin Fe(II) systems.[18] As compounds similar to **4.8** have been shown to exhibit spin crossover properties (*vide supra*), this predicted high spin environment at 200 K may change to a low spin centre upon a decrease in temperature; however, further characterization is needed to verify this hypothesis.

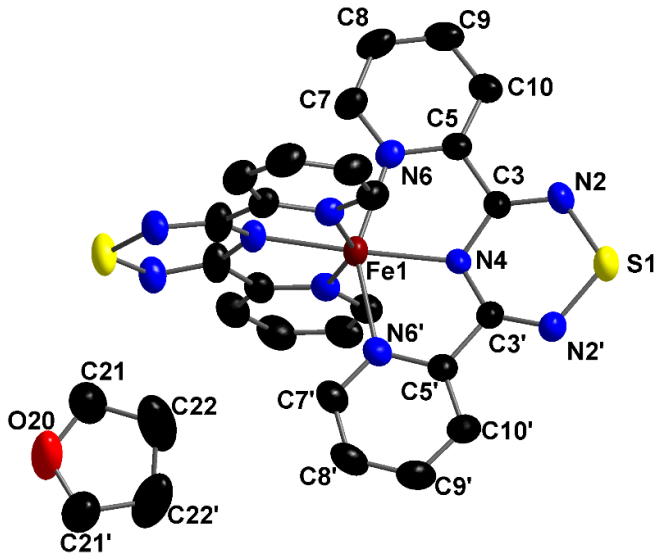

Figure 4-3. The iron coordination environment of **[Fe(Py$_2$TTA)$_2$]·THF**, **4.8**, with 50% thermal ellipsoids. Hydrogen atoms removed for clarity. Atom labels are identical for both **Py$_2$TTA** ligands, and thus are only shown on one side.

Table 4-2. N—Fe—N angles in **4.8** displaying the degree of distortion in the octahedral system. Atom labels are based on those shown in Figure 4-3.

Atom Angle	Ideal Angle (°)	Measured Angle (°)
N6 – Fe1 – N6′	180	150.259(7)
N6 – Fe1 – N4	90	74.912(2) [a]
		75.472(2) [a]

[a] The two angles are listed in order to account for the distortion in the complex.

Table 4-3. Bond lengths of the **TTA** ring of **4.8**, showing the discrete single and double bond character, indicative of the anionic ligand.

Bond	Bond Length (Å)
N4 – C3	1.375(2)
C3 – N2	1.298(1)
N2 – S1	1.709(9)

XRD analysis revealed that crystals of **[Fe(Py$_2$TTA)$_2$]·THF** belong to the tetragonal space group $I\bar{4}$. As indicated by the body-centred space group, molecules of **4.8** are arranged with one iron complex in the centre of the unit cell, and one at each vertex of the rectangular prism (Figure 4-4, top). When viewed down the *c* axis, it can be seen that the angles of the **Py$_2$TTA** ligands do not lie along the axis of the unit cell (Figure 4-4, bottom). There are two unique close contacts between the **Py$_2$TTA** ligands of neighbouring molecules, between S1 with C9 and C10 of the adjacent pyridyl ring (3.425(4) and 3.355(4) Å, respectively).

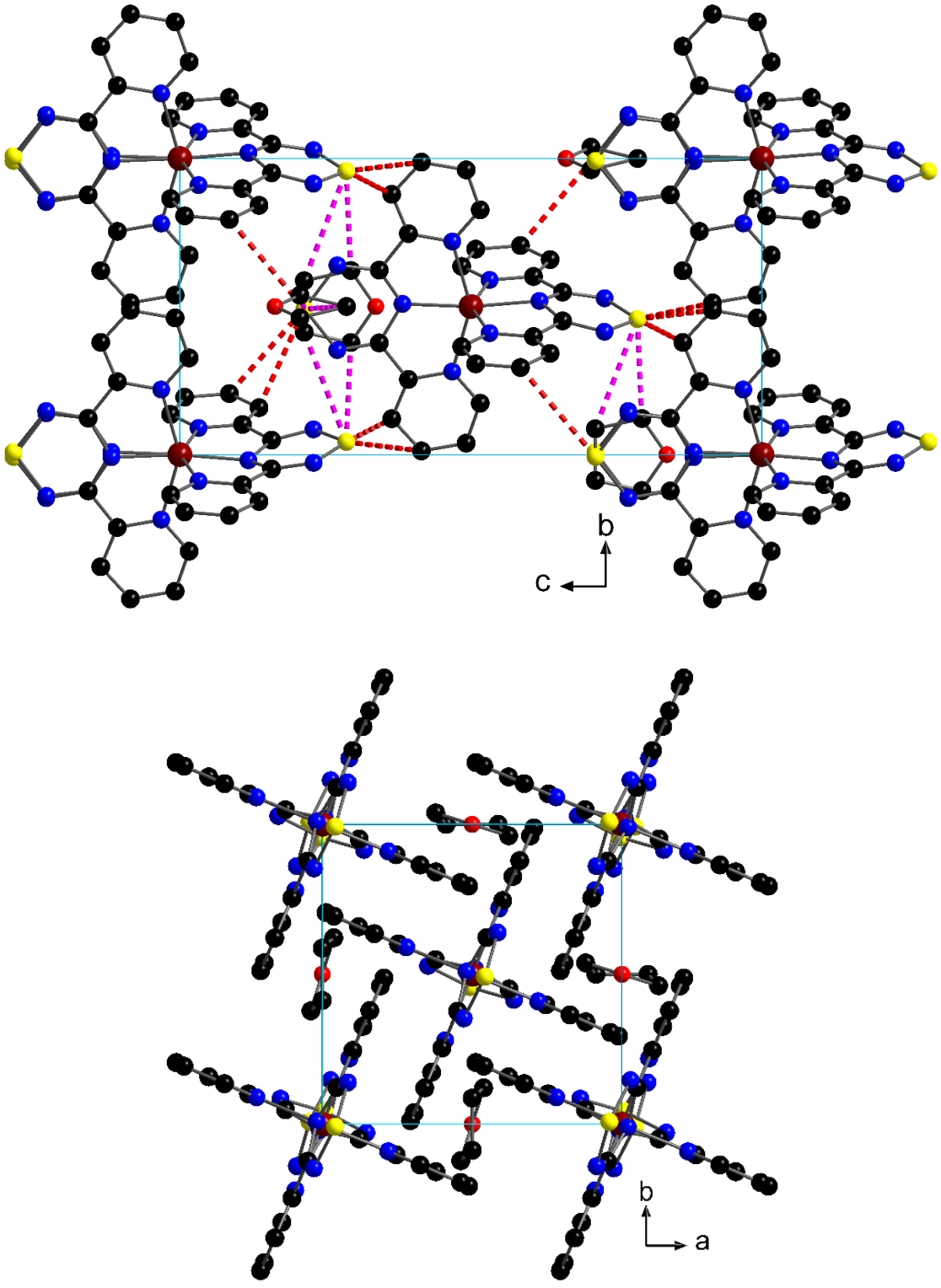

Figure 4-4. Two views of the unit cell and short contacts of **[Fe(Py$_2$TTA)$_2$]·THF**. Hydrogen atoms are removed for clarity. Top: View along the *a* axis. Short contacts to the THF solvent molecules are shown in purple, and short contacts between the **Py$_2$TTA** ligands are shown in red. Bottom: View down the *c* axis showing the angled **Py$_2$TTA** ligands around the central iron. Hydrogen atoms removed for clarity.

The co-crystallized THF molecules reside in four of the six faces of the unit cell (in the *ac* and the *bc* faces), which results in a total of two complete THF molecules per unit cell (i.e., four half THF molecules are in the unit cell, one on each of the rectangular faces). These THF molecules are offset from the centre of the unit cell face such that they are aligned with the **TTA** rings of the central **[Fe(Py$_2$TTA)$_2$]** molecule, such that they interact with the faces of the **TTA** rings, as can be seen by looking at the position of the THF molecules in Figure 4-4 (top). Two short contacts within or nominally larger than the Van der Waals radii exist between the **TTA** ligands and the THF molecules, between S1 and the C21 and C22 atoms of THF (3.031(8) and 3.544(1) Å).

There is 50 % disorder in the N—S—N fragment of the **TTA** ring, with the sulfur atom located 0.388(1) Å either above or below the mean plane of the ring. In addition, there is 50 % disorder in the THF molecules in the crystal, with the oxygen atom of THF facing either towards or away from the centre of the unit cell. The THF molecule also rotates such that the face of the THF ring is either aligned with the *ac* or the *bc* crystallographic planes (as shown by the THF molecules in bottom image of Figure 4-4). Due to this disorder, variations in the close contacts between the sulfur atom and the THF molecule occur. An example of this is shown in Figure 4-4 (top), where the THF molecule in the bottom right side is interacting with the central **[Fe(Py$_2$TTA)$_2$]** molecule (purple contacts), while the THF molecule at the top right side is interacting with the **[Fe(Py$_2$TTA)$_2$]** molecules on the top right vertices instead.

Unfortunately, extensive attempts to reproduce these crystals have thus far been unsuccessful. One possible explanation for this could be an instability of the complex, as all attempts to reproduce these crystals resulted in black powders which did not match spectroscopically with compound **4.8**, suggesting possible degradation of the product. Nevertheless, this complex is noteworthy as the first example of a ***bis*(TTA)** complex, and may hold the potential for spin crossover properties. Therefore, further research into an alternate synthetic route for further characterization should be performed.

4.4 Conclusions

In conclusion, two different iron complexes have been identified, and the crystal structures of each have been described. XRD analysis revealed that **Fe(*S*-Me-Py$_2$TTA)Cl$_3$**, compound **4.6**, was comprised of a distorted octahedral Fe(III) centre coordinated to the tridentate neutral ***S*-Me-Py$_2$TTA** ligand, with chloride ligands completing the coordination sphere and balancing the charge. Additionally, compound **[Fe(Py$_2$TTA)$_2$]·THF** (**4.8**) was described, and is a pseudo-octahedral Fe(II) system, with two tridentate **Py$_2$TTA$^-$** ligands surrounding the iron centre. Based on the Fe-N distances, both complexes are predicted to be high spin. While neither of these compounds have been fully characterized, they represent an important first step towards the use of the **Py$_2$TTA** family of molecules as a ligand system.

4.5 Future Work

The focus of research stemming from the work presented here should aim at developing new *S*-functionalized **Py$_2$TTA** ligands. For example, synthesizing **TTA** rings with long alkyl chains on the sulfur atom may lead to liquid crystalline properties, which upon metal coordination could produce metallomesogens. Alternately, the incorporation of heterocycles as substituents from the sulfur could facilitate multi-metallic coordination, which suggests the possibility of extended networks or polymeric species.

Future work for **4.8** entails reproducing this material. This may be possible by adding an anti-solvent into the reaction mixture, as only a few crystals were obtained using the method described in section 4.3. Alternately, if the irreproducibility of these crystals is a result of instability, perhaps more stringent anaerobic conditions, such as a glovebox or degassing the solvent may yield a reliable synthetic route. Once the synthesis of **[Fe(Py$_2$TTA)$_2$]·THF** is successfully repeated, analysis including magnetic measurements, optical spectroscopy (e.g., UV-vis studies) and computational studies should be carried out to probe the physical and electronic properties of the complex.

4.6 Experimental Details

4.6.1 General Procedures

The reagents sodium hydride (60% dispersion in mineral oil, Alfa Aesar), iron(II) chloride (Strem Chemicals), and iron(III) chloride (Aldrich) were obtained commercially and used as received. THF was dried by passing them through activated alumina on a J.C. Meyer solvent purification system and stored over 4Å Molecular sieves. All other solvents were reagent grade. 3,5-*bis*(2-pyridyl)-4-hydro-1,2,4,6-thiatriazine (**Py_2TTAH**) was prepared as outlined in the literature.[19] ***S*-Me-Py_2TTA** was prepared as outlined in Chapter 3. IR spectra of solid samples were recorded on an Agilent Technologies Cary 630 FT-IR spectrometer. Detailed synthetic procedures are not included, as the compounds have not been fully characterized.

4.6.2 Crystal Growth

Red crystals of **4.6**, suitable for X-ray analysis, were grown *via* slow liquid-liquid diffusion of saturated solutions toluene into MeOH. X-ray quality black crystals of **4.8** were grown *in situ* from a concentrated THF solution. Additional crystallographic details are described in the Appendix.

4.7 References

1. K. P. Jensen, B. O. Roos and U. Ryde, *Journal of Inorganic Biochemistry*, 2005, **99**, 45-54.

2. A. Bencini, F. Bartoli, C. Caltagirone and V. Lippolis, *Dyes and Pigments*, 2014, **110**, 169-192.

3. C. Cook, F. Habib, T. Aharen, R. Clerac, A. G. Hu and M. Murugesu, *Inorganic Chemistry*, 2013, **52**, 1825-1831.

4. G. C. Vougioukalakis and R. H. Grubbs, *Chemical Reviews*, 2010, **110**, 1746-1787.

5. F. Trudu, F. Amato, P. Vanhara, T. Pivetta, E. M. Pena-Mendez and J. Havel, *Journal of Applied Biomedicine*, 2015, **13**, 79-103.

6. C. Y. Ang, R. T. Boere, L. Y. Goh, L. L. Koh, S. L. Kuan, G. K. Tan and X. Yu, *Chemical Communications*, 2006, 4735-4737.

7. C. Y. Ang, S. L. Kuan, G. K. Tan, L. Y. Goh, T. L. Roemmele, X. Yu and R. T. Boere, *Canadian Journal of Chemistry*, 2015, **93**, 181-195.

8. K. L. M. Harriman, A. A. Leitch, S. A. Stoian, F. Habib, J. L. Kneebone, S. I. Gorelsky, I. Korobkov, S. Desgreniers, M. L. Neidig, S. Hill, M. Murugesu and J. L. Brusso, *Dalton Transactions*, 2015, **44**, 10516-10523.

9. K. L. M. Harriman, I. A. Kuhne, A. A. Leitch, I. Korobkov, R. Clerac, M. Murugesu and J. L. Brusso, *Inorganic Chemistry*, 2016, 11340-11344.

10. N. J. Yutronkie, I. A. Kuehne, I. Korobkov, J. L. Brusso and M. Murugesu, *Chemical Communications*, 2016, **52**, 677-680.

11. A. Santoro, L. J. K. Cook, R. Kulmaczewski, S. A. Barrett, O. Cespedes and M. A. Halcrow, *Inorganic Chemistry*, 2015, **54**, 682-693.

12. R. Boca, P. Baran, M. Boca, L. Dlhan, H. Fuess, W. Haase, W. Linert, B. Papankova and R. Werner, *Inorganica Chimica Acta*, 1998, **278**, 190-196.

13. S. Hayami, N. Motokawa, A. Shuto, R. Moriyama, N. Masuhara, K. Inoue and Y. Maeda, *Polyhedron*, 2007, **26**, 2375-2380.

14. T. Sato, K. Nishi, S. Iijima, M. Kojima and N. Matsumoto, *Inorganic Chemistry*, 2009, **48**, 7211-7229.

15. A. Abherve, M. Clemente-Leon, E. Coronado, C. J. Gomez-Garcia and M. Lopez-Jorda, *Dalton Transactions*, 2014, **43**, 9406-9409.

16. R. Pritchard, C. A. Kilner and M. A. Halcrow, *Chemical Communications*, 2007, 577-579.

17. F. Habib, O. R. Luca, V. Vieru, M. Shiddiq, I. Korobkov, S. I. Gorelsky, M. K. Takase, L. F. Chibotaru, S. Hill, R. H. Crabtree and M. Murugesu, *Angewandte Chemie-International Edition*, 2013, **52**, 11290-11293.

18. J. Olguin and S. Brooker, *Coordination Chemistry Reviews*, 2011, **255**, 203-240.

19. A. A. Leitch, I. Korobkov, A. Assoud and J. L. Brusso, *Chemical Communications*, 2014, **50**, 4934-4936.

Chapter 5 – Incorporation of Boron into Thiatriazine Precursor Frameworks

5.1 Introduction

In the field of materials chemistry, organic luminescent materials have been used in many applications, such as luminescent dyes for lasers or biological labelling, organic light emitting devices (OLEDs), and optical sensors to name a few.[1, 2] Of small organic luminescent materials, one of the more widely known chromophores is the BODIPY framework, **5.1** (Chart 5-1).[1] To that end, research into BODIPY and its derivatives has received much attention in recent years, with over 6000 papers published since 1990.[1] The most common applications of BODIPY derivatives involve their use as fluorescent dyes in biological labelling, as BODIPY can be easily modified for either hydrophobic or hydrophilic environments. BODIPY derivatives tend to display high quantum yields, which may be partially explained by the lack of self-quenching due to minimal intermolecular interactions. While this is ideal for fluorescent imaging, OLEDs require good intermolecular communication for charge transfer properties.

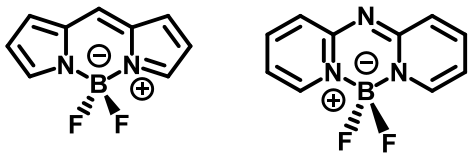

Chart 5-1. The BODIPY core, **5.1** and the aza-BODIPY core, **5.2**, both of which have been extensively functionalized from the aromatic carbon atoms.

[1] Source: Web of Science Search for "BODIPY", June 6, 2016

Increasing intermolecular communication may be achieved through the inclusion of heteroatoms into an extended π-conjugated framework, as described in detail in Chapter 1. To that end, the incorporation of BF_2 moieties into heterocyclic rings such as triazine, creating boratriazine rings (e.g., the central ring of **5.2**) is of interest. While the majority of examples of boratriazines contain extended conjugated frameworks (such as aza-BODIPY compounds, **5.2**), significantly fewer examples of non-fused systems have been reported, most of which have not received a great deal of attention, likely due to their publication in small Russian language journals (Chart 5-2; **5.3**-**5.7**).[3-13] While none of the previous unfused boratriazine rings have been substituted with heteroaromatic substituents, such functionalization may lead to enhanced intermolecular interactions, and thus electronic communication. Therefore, the addition of pyridyl substituents to the boratriazine ring holds much appeal. To that end, *N*-2-pyridylimidoyl-2-pyridylamidine (**5.7**) is an ideal candidate for boron incorporation reactions, as it is similar to the starting materials employed in the synthesis of reported boratriazine frameworks.[11]

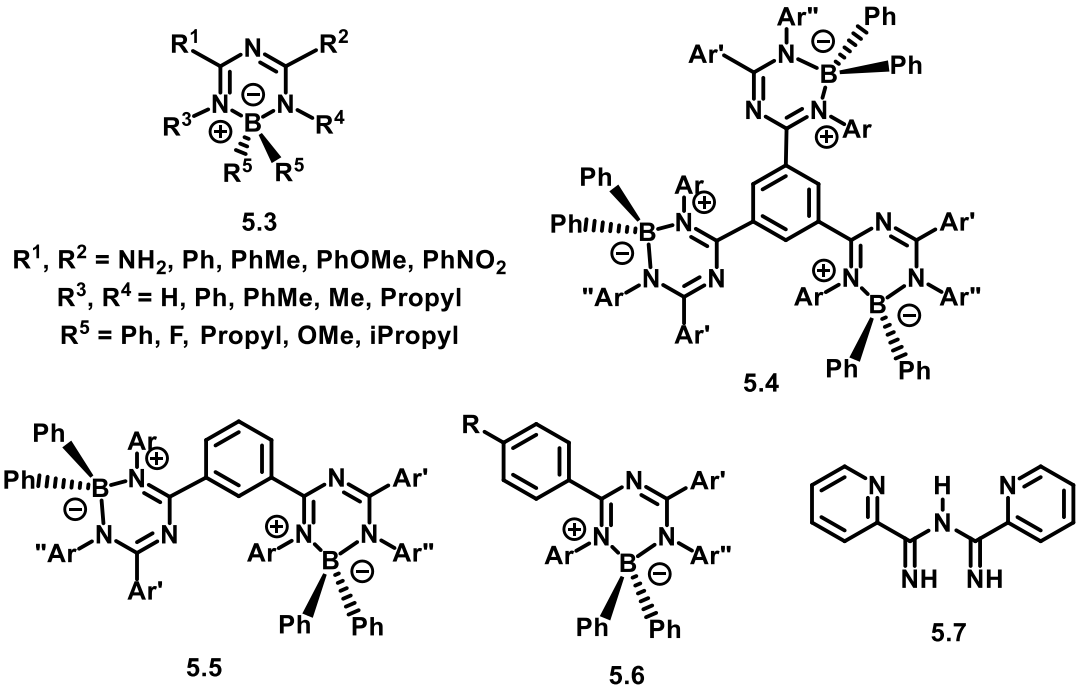

Chart 5-2. Previous reported unfused boratriazine systems (**5.3**-**5.6**) as well as *N*-2-pyridylimidoyl-2-pyridylamidine (**5.7**).

Due to the numerous nitrogen atoms and chelating environments, there are several possible sites in which a BF_2 fragment could coordinate with **5.7**. As such, it is important to consider the different coordination environments and geometries typically observed in boron complexes. Boron atoms commonly adopt either three coordinate trigonal planar configurations, or four coordinate anionic tetrahedral geometries, such as BF_3 and BF_4^- respectively. In 1984, however, Lee and Martin provided compelling evidence for pentavalent coordination.[14] Through ^{11}B NMR spectroscopy, the authors observed a symmetrical boron complex with significant upfield shifts in the ^{11}B signals, attributed to pentavalent boron with E-C-E pincer ligands (**5.8**; Chart 5-3).[14] Since then,

five other examples of pentavalence have been reported (**5.9**-**5.13**), and the crystal structures of these compounds confirmed the pentacoordinate boron environments.[15-20]

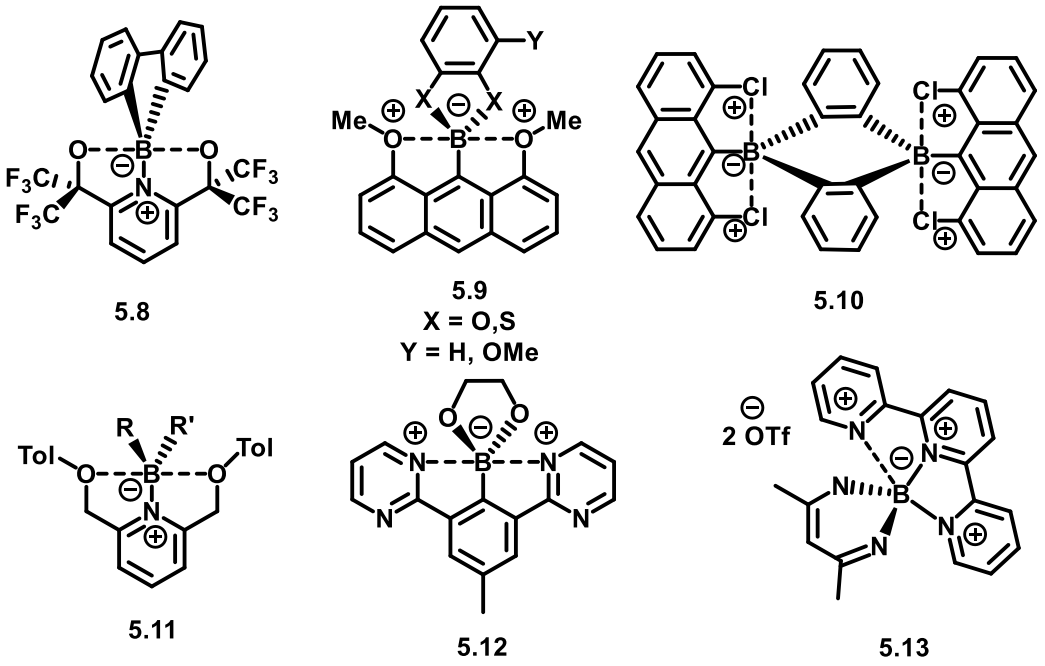

Chart 5-3. Previously reported pentavalent boron compounds.[14-20]

While a pentacoordinate structure is an unlikely product using **5.7** as a starting material due to the presence of multiple bidentate coordination pockets, pentavalence with similar structures to **5.12** or **5.13** may be possible with 5-*bis*(2-pyridyl)-4-hydro-1,2,4,6-thiatriazine (**Py$_2$TTAH**; **5.14**). In **5.14**, there are two possible coordination sites for boron depending on the orientation of the pyridyl rings (Chart 5-4). While either coordination site would be of interest, the pentacoordinate complex (**5.15**) would not only represent another example in a class of rare compounds, but it would also leave the N—S—N portion of the TTA ring free to engage in intermolecular interactions.

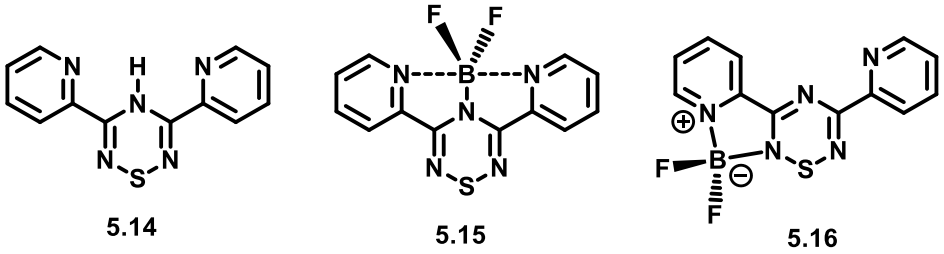

Chart 5-4. **Py$_2$TTAH** (**5.14**) and its possible boron coordination sites highlighting **5.15** and **5.16**.

5.1.1 Scope of this Chapter

This chapter reports the work carried out towards the synthesis of boron complexes with **5.7** and **5.14**, as well as characterization studies of the resulting products through ^{1}H, ^{11}B, and ^{19}F NMR spectroscopy. Also presented are the preliminary results from UV-vis and fluorescence spectroscopy and DFT calculations on promising derivatives isolated.

5.2 Reactions of Boron Trifluoride with *N*-2-pyridylimidoyl-2-pyridylamidine

Initial attempts to coordinate BF_2 to **5.7** followed closely with methods reported for similar compounds.[21] First, **5.7** was reacted with triethylamine for 30 minutes at room temperature in tetrahydrofuran (THF), and then boron trifluoride etherate ($BF_3{\cdot}OEt_2$) was added dropwise. The solution was then refluxed for 24 hours before precipitating the product with water. The cream coloured solid was isolated by filtration and analyzed for purity using IR, ^{1}H, ^{11}B, and ^{19}F NMR spectroscopic techniques. Chart 5-5 shows potential products from this reaction, which are considered in further detail below in order to identify the obtained product.

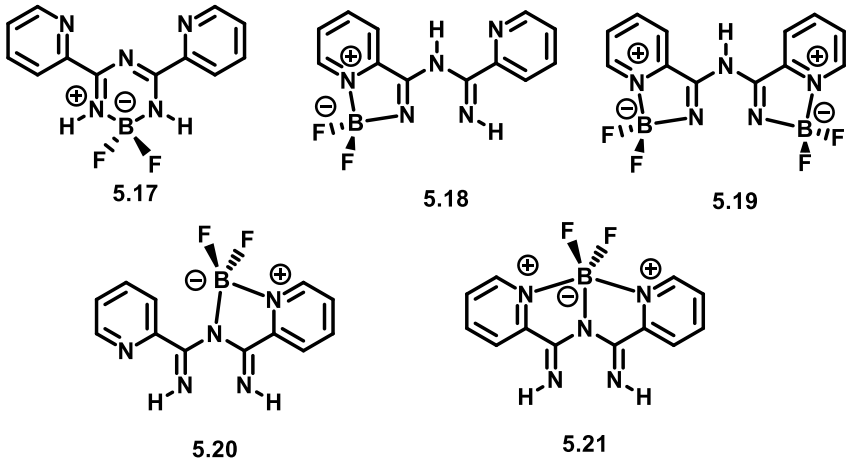

Chart 5-5. Potential products from the reaction between **5.7** and $BF_3{\cdot}OEt_2$.

The ^{1}H NMR spectrum (Figure 5-1) indicated one major product was formed, along with a minor side product. The major product displayed symmetric pyridyl peaks, therefore limiting the potential products to **5.17**, **5.19** or **5.21**. Furthermore, an NH signal was present in both the IR and ^{1}H NMR spectra, which integrated to two. This suggests that compound **5.19** is unlikely to be the final product, as there would only be one NH proton. The minor product is unidentifiable by ^{1}H NMR due to the overlapping signals with the major product; however, the integration of peaks in this product are very small, thus should not interfere significantly with the interpretation of the major product.

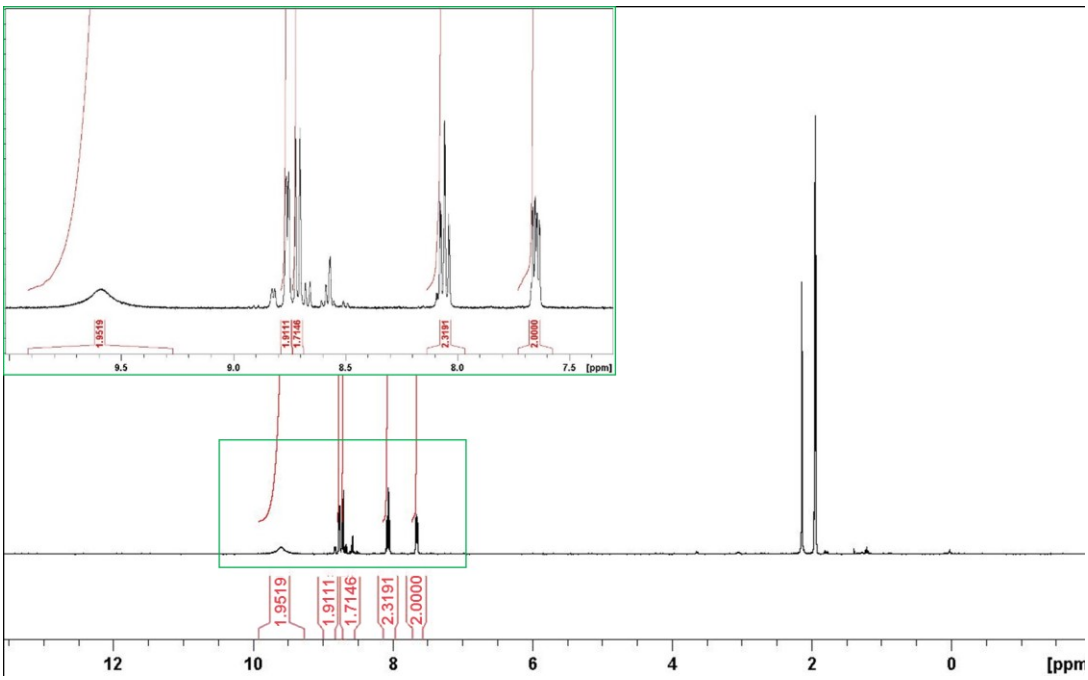

Figure 5-1. ^{1}H NMR spectrum of the solid isolated from the reaction between **5.7** and $BF_3{\cdot}OEt_2$, in MeCN-d_3.

Comparing the remaining possible products (i.e., **5.17** and **5.21**), it is more likely that the boron fragment would coordinate in a bidentate fashion (i.e., between the imine nitrogen atoms as in **5.17**), as opposed to formation of the pentavalent compound **5.21**. This assessment is based on literature, where pentacoordinate boron complexes are rare, and require a single, stabilized coordination site. Therefore, it is reasonable to assume the boron atom would fill the bidentate pocket of **5.7**, generating the more favorable tetrahedral geometry. Thus, based on the ^{1}H NMR spectrum, the most likely product from the reaction between **5.7** and $BF_3{\cdot}OEt_2$ is **5.17**.

Further support of this assignment is provided by ^{11}B NMR analysis (Figure 5-2). To that end, Lee and Martin postulated that pentacoordinate boron would display downfield shifts around -20 ppm or lower in the ^{11}B NMR spectrum, while

tetracoordinate boron tends to display shifts around or above 0 ppm.[14] As shown in Figure 5-2, the ^{11}B NMR spectrum of the product from the reaction between **5.7** and $BF_3{\cdot}OEt_2$ contains a peak at 0 ppm, which is consistent with a tetracoordinate geometry, as would be expected for **5.17**. This signal is a triplet with a 1:2:1 ratio, indicative of coupling to two equivalent fluorine atoms. This coupling is also detected in the ^{19}F NMR spectrum; however, here it is observed as a quartet with a 1:1:1:1 ratio. The differences in splitting patterns between the ^{11}B and ^{19}F NMR spectra can be attributed to the spin multiplicity of these atoms (3/2 for ^{11}B and 1/2 for ^{19}F). In addition to the major BF_2 peaks, a second set of signals were present in both the ^{11}B and ^{19}F NMR spectra, suggesting the minor product observed in the ^{1}H NMR spectrum also contained a BF_2 moiety. It can be concluded that the major product is **5.17**, however, despite best attempts, pure compound still remains elusive.

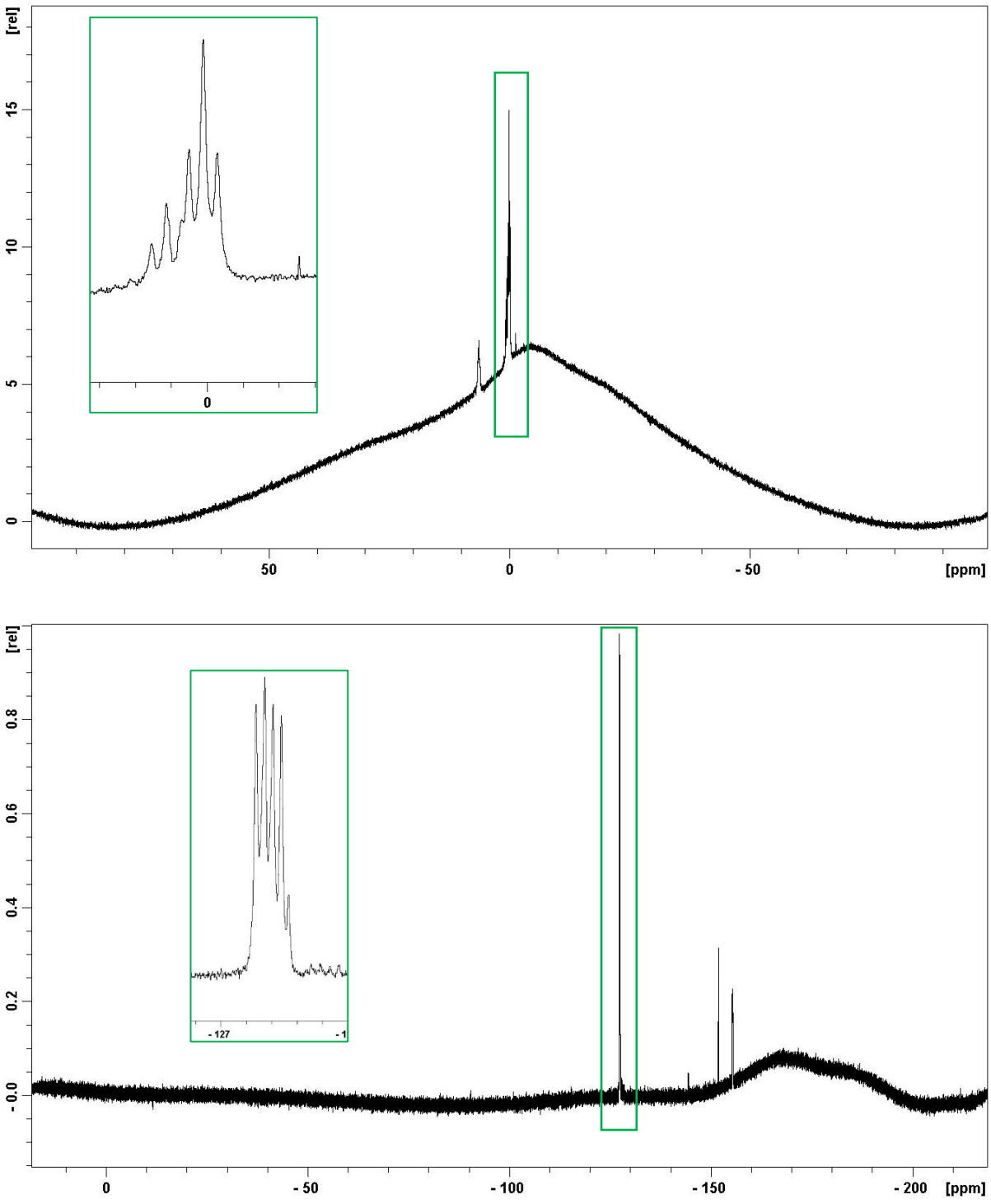

Figure 5-2. ^{11}B (top) and ^{19}F (bottom) NMR spectra of **5.17** in MeCN-d_3. The broad peak in the baseline of the ^{11}B spectrum is attributed to the borosilicate glass of the NMR tube. The broad peak in the baseline of the ^{19}F spectrum is due to a poor signal to noise ratio due to the limited solubility of **5.17** in MeCN-d_3.

5.2.1 Theoretical and UV-vis Spectroscopy Studies

Qualitative solution state UV-vis and fluorescence studies were carried out on MeCN solutions of **5.17**; the results of which are shown in Figure 5-3. The UV-vis spectrum contains four peaks with maxima at 240, 280, 310 and 323 nm, which is consistent with the clear, colourless solution observed, as **5.17** does not absorb in the visible region. Photoluminescent studies on the same MeCN solution were carried out at an excitation wavelength of 310 nm, and showed a maximum emission peak of 393 nm, consistent with the purple fluorescence observed when the solution was exposed to 254 nm UV light (see Figure 5-3 inset).

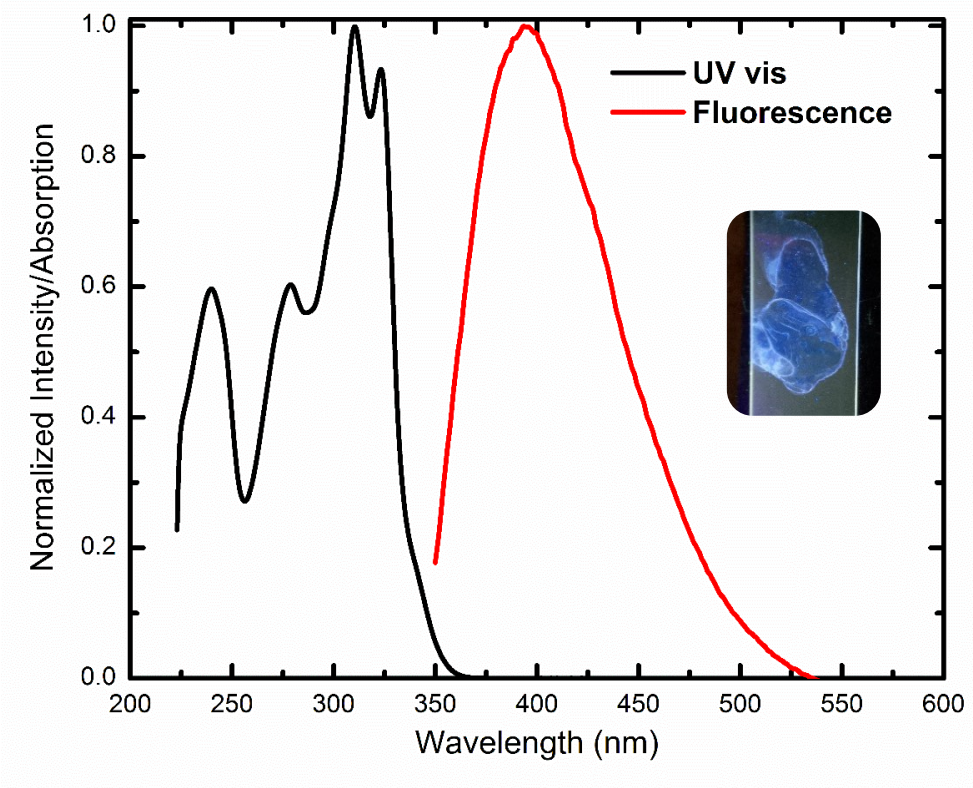

Figure 5-3. Normalized experimental absorption (black) and fluorescence (red) spectra measured on MeCN solutions of **5.17**. Inset: Purple fluorescence of **5.17** in DCM, drop-cast onto a slide and the solution observed under 254 nm UV light.

As pure compound has yet to be obtained, these results were qualitative and not performed in a concentration dependant quantitative method, thus the quantum yield has not been calculated. Nonetheless, both the Stokes shift and the HOMO/LUMO gap were evaluated. The calculated Stokes shift of 70 nm (0.684 eV) is slightly smaller than other six membered rings containing carbon, nitrogen, and BF_2 (e.g., difluoro-boron[2,2-*bis*(2-phenyldiazenyl)acetonitrilato]),[22] which is indicative of compound **5.17** having a slightly more ridged structure.

Using the edge of absorption of the highest wavelength peak (i.e., 345 nm), the HOMO/LUMO energy gap was calculated to be 3.59 eV, which is slightly larger (~ 0.5 eV) than the similar compounds reported (e.g., difluoro-boron[2,2-*bis*(2-phenyldiazenyl)acetonitrilato]).[22] In order to rationalize the HOMO/LUMO energy gap, DFT calculations using the B3LYP/6-311+G(2d,p) level of theory were performed on compound **5.17**. The geometry optimized structure is shown in Figure 5-4, along with the calculated HOMO and LUMO electron density probability diagrams. Interestingly, the geometry optimized structure shows a symmetric molecule with the pyridyl rings twisted out of the plane of the boratriazine ring by 43°, with the nitrogen atoms of the pyridyl substituents and the central nitrogen forming a terpy-like pocket. As can be seen in Figure 5-4c, a significant amount of the electron density in the HOMO resides on the boratriazine ring, with a node bisecting the six membered ring between the N—B—N and C—N—C portions. The remainder of the electron density resides on the fluorine

atoms and around the nitrogen atoms of the pyridyl substituents, with nodes between the pyridyl and boratriazine rings. The LUMO, alternately, does not contain nodes between the three rings; instead, the electron density is distributed across all three of the rings in the molecule. The LUMO contains two perpendicular nodes in the boratriazine ring; one bisecting the six membered ring between the N—B—N and C—N—C sections as in the HOMO, and the second running along the centre of the ring through the boron and central nitrogen atoms. The energies of the HOMO and LUMO were calculated to be -7.31 and -2.42 eV, respectively, resulting in a HOMO-LUMO gap of 4.89 eV. While this gap is slightly larger than the 3.59 eV gap found through experimental spectroscopic techniques, solvent effects might explain this difference, as DFT calculations were performed in the gas phase.

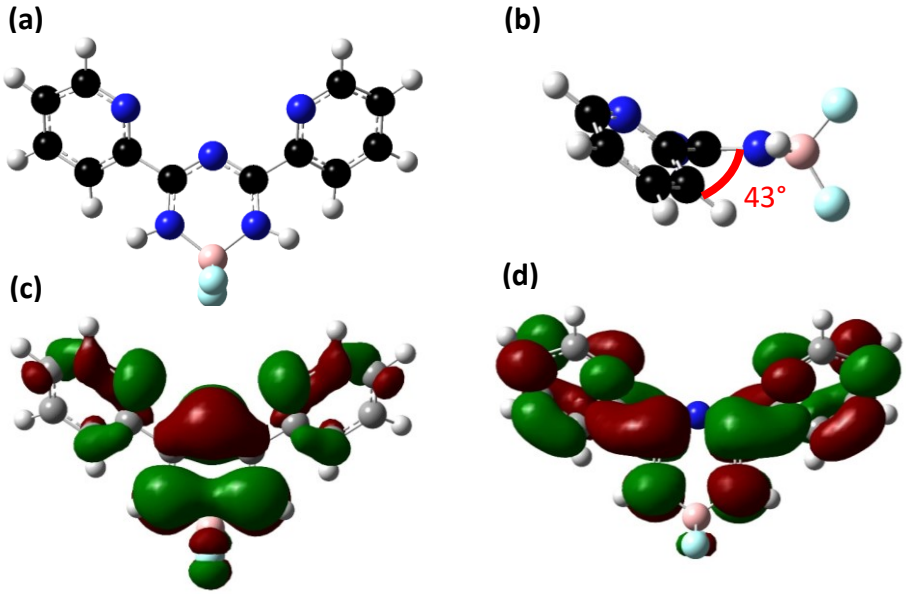

Figure 5-4. (a) Geometry optimized structure of **5.17** calculated at the B3LYP/6-311+G(2d,p) level of theory with Gaussian 09 software. (b) Side view of the geometry optimized structure of **5.17** highlighting the 43° twist angle between the pyridyl substituents and the central boratriazine ring. (c) Highest occupied molecular orbital probability diagram calculated using Gaussview05 software. (d) Lowest unoccupied molecular orbital probability diagram calculated using GaussView 5.0 software.[23]

5.3 Reactions of Boron Trifluoride with Py_2TTAH

In addition to **5.7**, **Py_2TTAH** (**5.14**) was also employed as a ligand for boron coordination, as it has the potential to coordinate to boron in a tridentate fashion, leading to a pentavalent environment. Contrary to **5.7** where the boron was most likely to coordinate between the two imine nitrogen atoms, in **Py_2TTAH** this site is occupied by a sulfur atom. Therefore, the more likely coordination pockets are with the pyridyl nitrogen atoms in either a bidentate or tridentate manner, as illustrated in Chart 5-4 (page 122). While either coordination environment may be achievable, compound **5.15**, in which the rarer 5-coordinate environment is obtained due to coordination of boron in

the tridentate pocket of **Py$_2$TTA**, is more desirable. This is due to the novelty of the coordination, as well as the expected increase in rigidity, which may lead to higher fluorescence quantum yields by diminishing rotational quenching.[24]

5.3.1 Synthetic Work using Sodium Hydride

The solvent most commonly used for BF_2 reactions is toluene; however, in order to incorporate boron into the terpy-like coordination pocket of **Py$_2$TTAH**, deprotonation prior to treatment with $BF_3{\cdot}OEt_2$ is necessary. As outlined in Chapter 2, sodium hydride (NaH) effectively deprotonates **Py$_2$TTAH**. Unfortunately, NaH is insoluble in toluene, and therefore reactions in THF were initially carried out. To that end, under inert conditions at both room temperature and reflux conditions, the addition of $BF_3{\cdot}OEt_2$ into the dark green **Py$_2$TTA$^-$** mixture resulted in an immediate colour change to dark purple, similar to the colour of the starting material **Py$_2$TTAH**. ^{1}H NMR analysis of an aliquot of this solution confirmed the presence of **Py$_2$TTAH**.

As reactions between **Py$_2$TTAH** and $BF_3{\cdot}OEt_2$ did not react in THF, it was postulated that the higher reflux temperature of toluene was necessary for the boron coordination reaction. Since deprotonation *via* NaH could not be achieved in toluene, exchanging solvents between the deprotonation reaction and the addition of the $BF_3{\cdot}OEt_2$ was considered. A direct solvent switch (evaporating all of the THF to dryness, and then adding toluene) unfortunately resulted in a very messy ^{1}H NMR spectrum,

with countless overlapping signals in the aromatic region (Figure 5-5). Nevertheless, ^{19}F NMR experiments suggested the presence of a BF_2 group present, based on the expected peak shifts and splittings, as outlined above in section **5.2**.

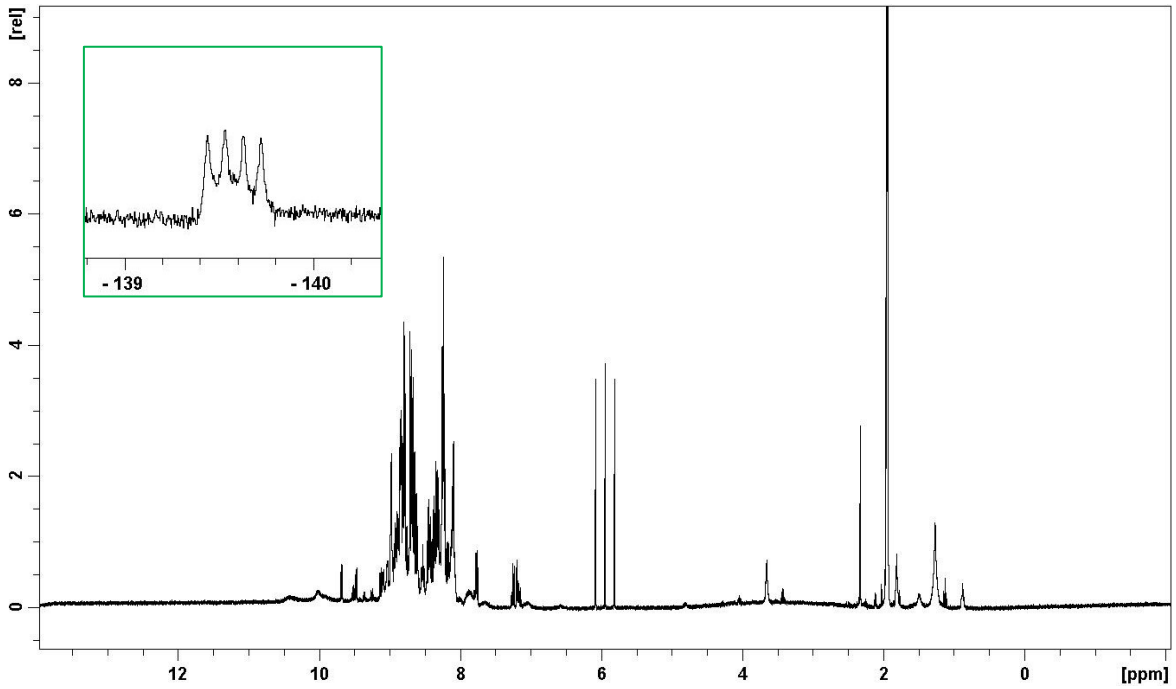

Figure 5-5. ^{1}H NMR spectrum of the reaction between **Py_2TTA^-** and $BF_3{\cdot}OEt_2$ with a direct solvent switch from THF to toluene in MeCN-d_3. Inset: Portion of the ^{19}F NMR for the same reaction, quartet indicative of a BF_2 complex formed.

In an effort to synthesize a cleaner crude product, reactions using either a gradual solvent switch, or THF/toluene mixtures were considered. In the gradual solvent switch, the THF was evaporated to approximately half of the starting volume, then toluene was added to return the mixture to the initial volume. This mixture was subsequently evaporated down to half its volume. This process was repeated several times in order for the resulting solution to consist of mainly toluene. In the reactions using mixtures, varying amounts of toluene were added to the THF solution following

deprotonation and prior to the addition of $BF_3{\cdot}OEt_2$. Unfortunately, all of these variations resulted in unsuccessful reactions, with the major product identified as unreacted starting material **Py_2TTAH**, even upon refluxing the reactions for several days.

5.3.2 Synthetic Work with Drier Conditions

As all attempts at incorporating a BF_2 moiety into the tridentate pocket of **Py_2TTA**$^-$ resulted in a reformation of the protonated starting material, methods for removing proton sources from the reaction were considered. First, the $BF_3{\cdot}OEt_2$ was distilled to remove trace amounts of water. Additionally, reactions were carried out in which an auxiliary base (i.e., triethylamine) was added, such that the base would act as a proton scavenger. Unfortunately, these changes did not improve the reaction and only starting material was identified. Experiments were also attempted with the addition of sodium sulfate (Na_2SO_4) to the reaction mixture, as the drying agent should remove any residual water. In this case, a small by-product of BF_2 containing product was formed, as evidenced by the ^{11}B and ^{19}F NMR spectra (Figure 5-6); however, attempts to separate this compound from the starting material *via* column chromatography resulted in the isolation of only **Py_2TTAH**. This may be attributed to decomposition of the BF_2 complex on silica, which is consistent with what has been reported for similar compounds that require neutral alumina as opposed to silica for purification by chromatography.[25] As

the isolated BF_2 compound was only a minor product of the reaction, it was decided to further optimize the yield before further attempts to isolate and purify it.

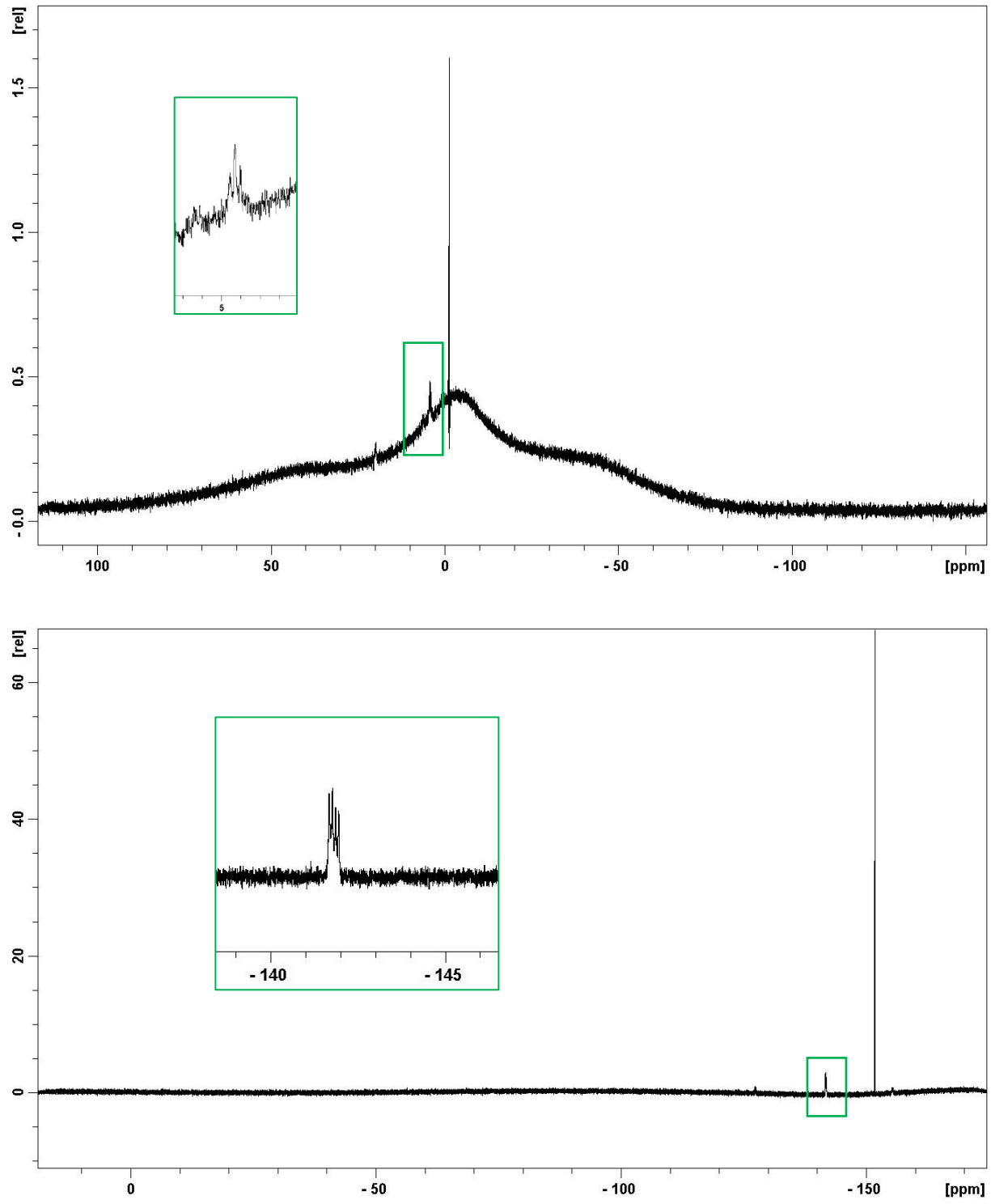

Figure 5-6. ^{11}B (top) and ^{19}F (bottom) NMR spectra of the reaction between **Py_2TTAH** and $BF_3{\cdot}OEt_2$ with $NaSO_4$ added to the reaction mixture, in MeCN-d_3. The broad peak in the baseline of the ^{11}B spectrum is attributed to the borosilicate glass of the NMR tube.

5.3.3 Removal of the Sodium Atom

It was postulated that the numerous impurities seen in previous reactions may be due to the sodium atom occupying the tridentate pocket, similar to what was seen in in the sodium/iodide coordination polymers described in Chapter 3, and therefore hindering reactivity towards boron incorporation. A reaction was therefore performed with **Py_2TTAH** and $BF_3{\cdot}OEt_2$ without the presence of any base. This reaction afforded a black precipitate, which formed after refluxing in toluene for 20 hours. The solid was isolated by filtration, washed with toluene and dried in air. Upon ^{1}H and ^{19}F NMR spectroscopic characterization (Figure 5-7), the black solids were found to contain a number of different fluorine signals, including a quartet at -140 ppm. This quartet is in the range expected for a conjugated BF_2 functional group, and possesses the correct 1:1:1:1 quartet splitting pattern. While this reaction led to a messy mixture of compounds (as seen by ^{1}H NMR spectroscopy), it suggests that BF_2 coordination with Py_2TTAH is possible without prior deprotonation using NaH. Although promising, this reaction requires fine-tuning and optimization to selectively synthesize and maximize the yield of the desired product.

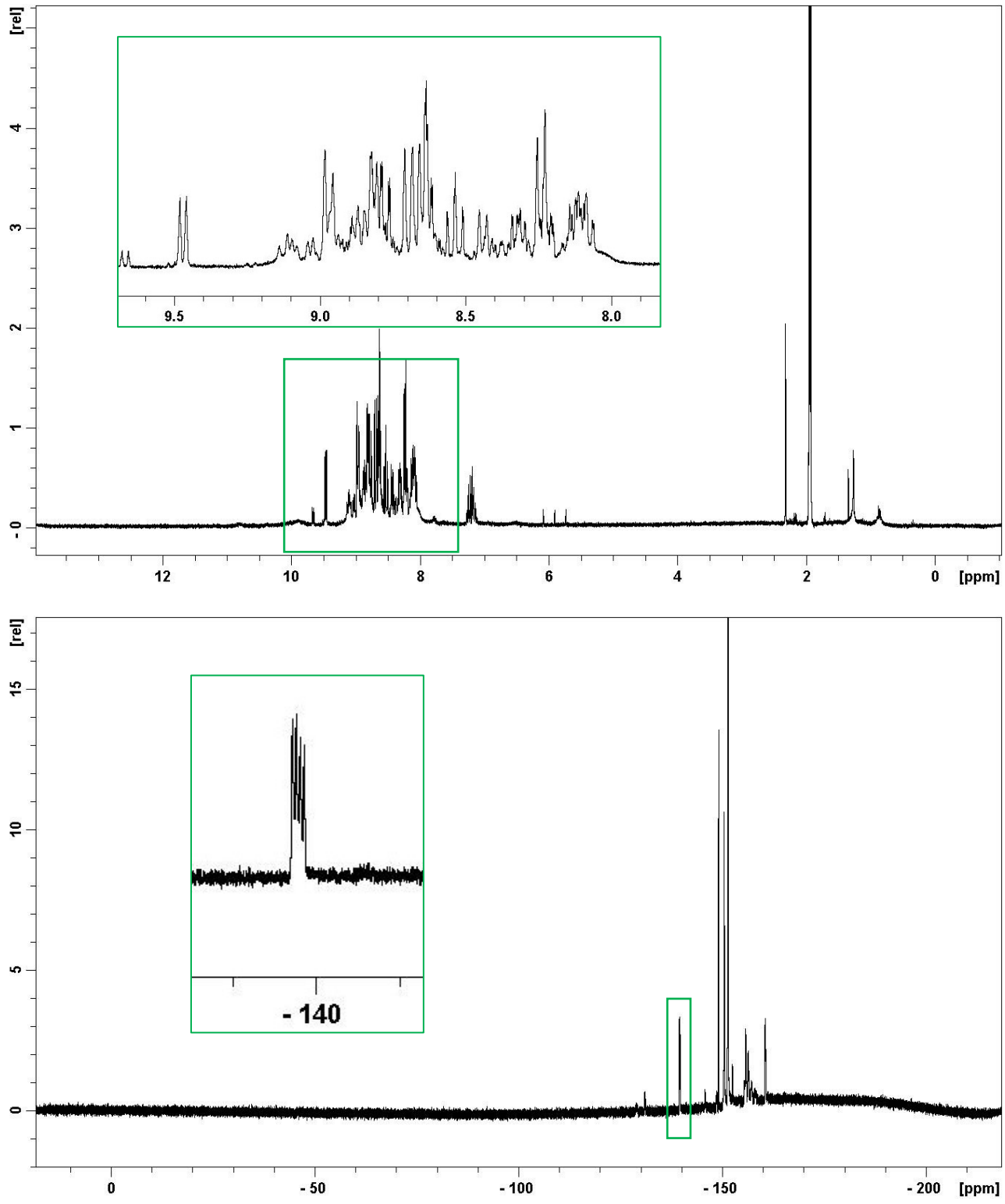

Figure 5-7. ^{1}H (top) and ^{19}F (bottom) NMR spectra of reaction with **Py_2TTAH** and $BF_3{\cdot}OEt_2$, in MeCN-d_3.

As a first step towards optimizing the reaction between **Py_2TTAH** and $BF_3{\cdot}OEt_2$ without NaH, a weaker base such as triethylamine was considered to act as a proton scavenger, thus preventing reformation of **Py_2TTAH**. To that end, a mixture of **Py_2TTAH**, $BF_3{\cdot}OEt_2$, and triethylamine was refluxed in toluene for 24 hours. Upon cooling to room temperature, the reaction mixture was quenched with H_2O, extracted into DCM and then the organic layer was evaporated down to a solid residue. The crude material was dissolved in DCM, and then filtered through a neutral alumina plug. A yellow residue was obtained upon evaporation of the solvent, and analyzed by NMR spectroscopy. Upon examination of the ^{1}H, ^{11}B, and ^{19}F NMR spectra, the chemical shifts of the major product from this reaction matched the shifts of **5.17** (Figures 5-8 [^{1}H], 5-9 [^{11}B], and 5-10 [^{19}F]). This therefore indicates that the reaction between **Py_2TTAH** and $BF_3{\cdot}OEt_2$ affords the same product as the reaction between **5.7** and $BF_3{\cdot}OEt_2$. As such, in the former reaction, the sulfur atom in **Py_2TTAH** must be replaced with the BF_2 moiety in order to create a boratriazine ring. Upon exposing the solid obtained from the reaction with **Py_2TTAH** to 254 nm UV light, a weak purple fluorescence was observed. As well, a small impurity was seen in the ^{1}H NMR spectrum (Figure 5-8) from the reaction between **Py_2TTAH** and $BF_3{\cdot}OEt_2$, but not in the ^{11}B and ^{19}F spectra (Figures 5-9 and 5-10, respectively), indicating that this impurity does not contain a BF_2 moiety.

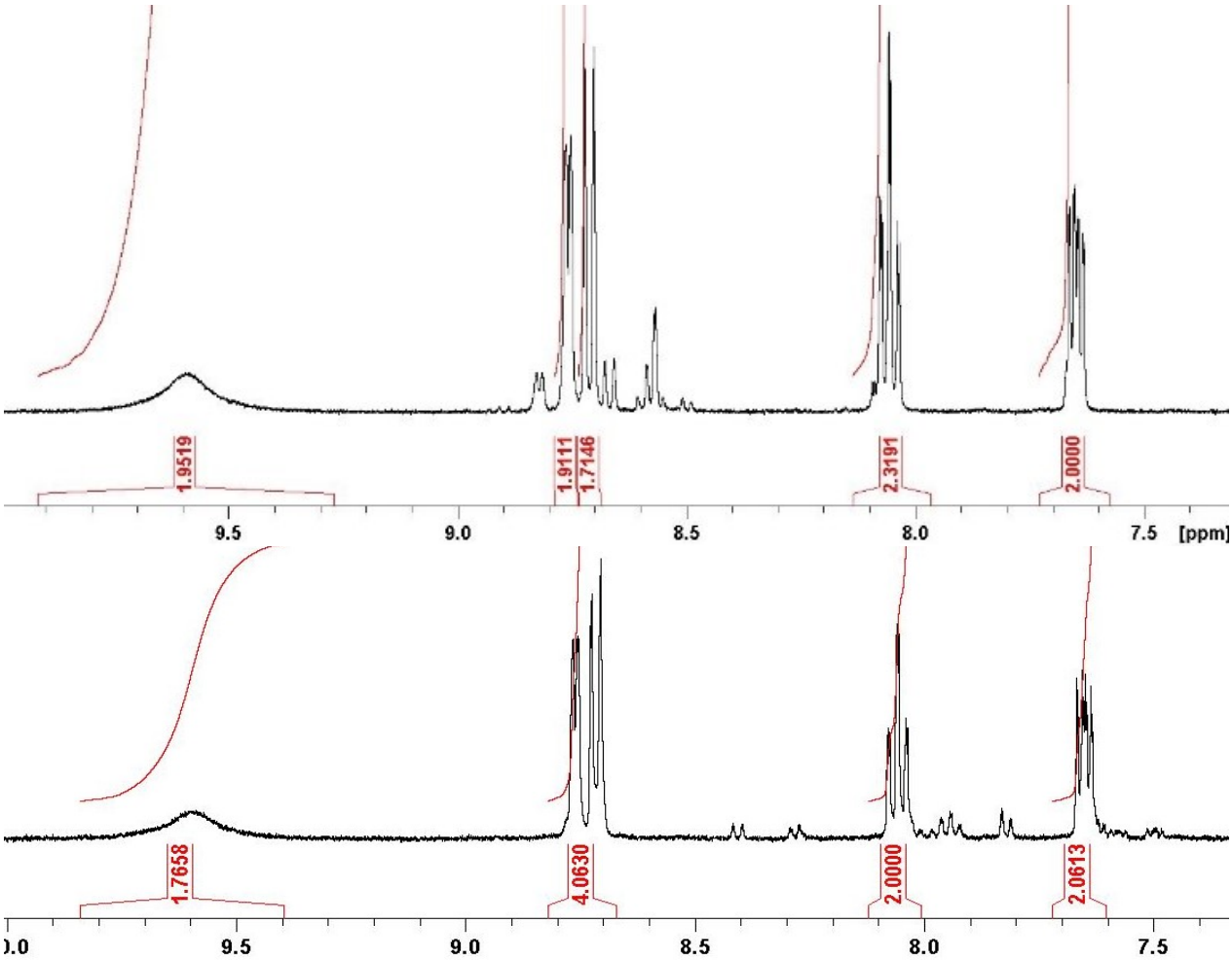

Figure 5-8. ^{1}H NMR comparisons of **5.17** synthesized *via* **5.7** (top) and the product from the reaction of **Py$_2$TTAH** with $BF_3{\cdot}OEt_2$, following purification through neutral alumina (bottom), both in MeCN-d_3. Only the aromatic region is shown as the full spectrum is shown in Figure 5-3.

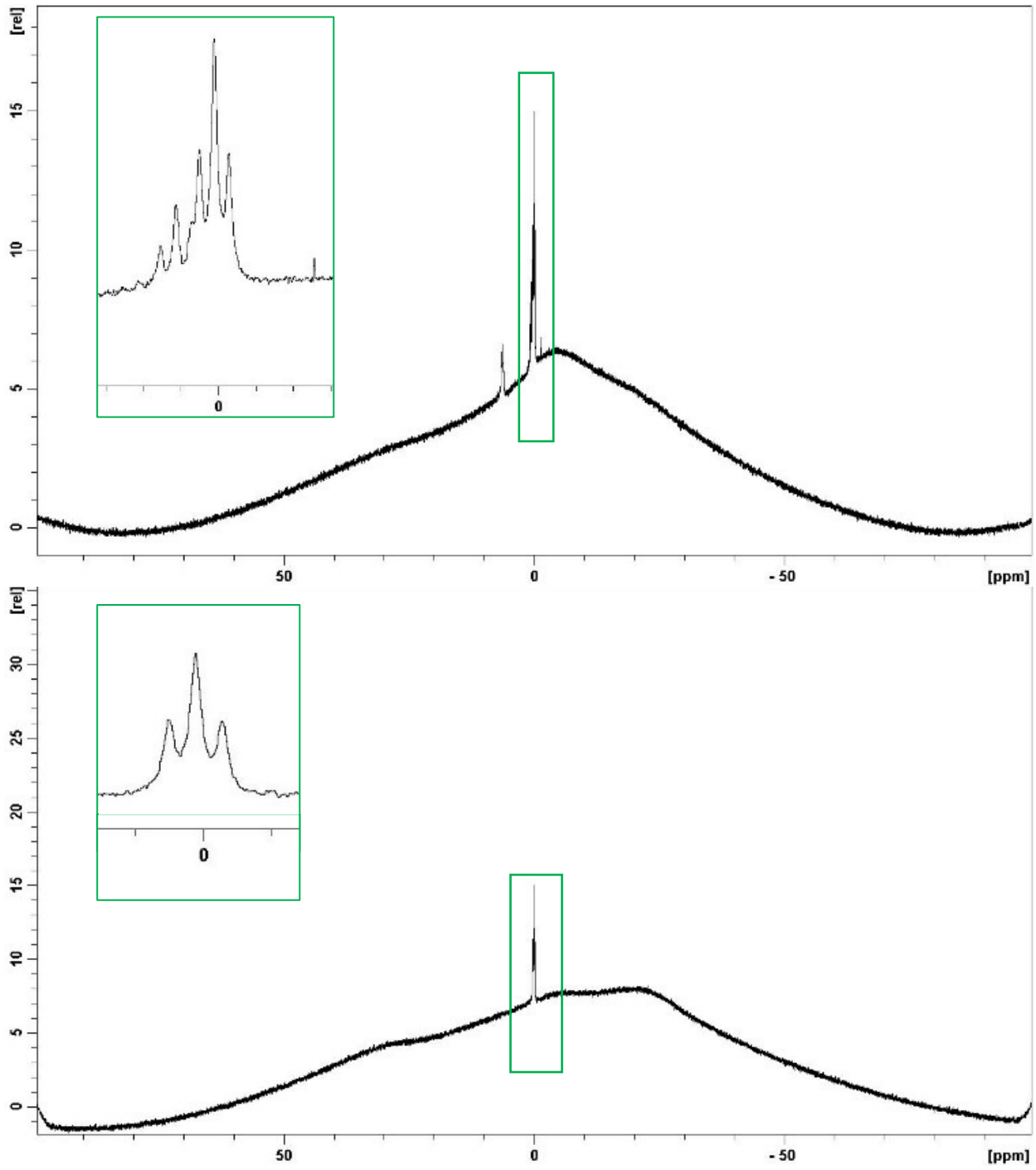

Figure 5-9. ^{11}B NMR comparisons of **5.17** synthesized *via* **5.7** (top) and the product from the reaction of **Py_2TTAH** with $BF_3{\cdot}OEt_2$, following purification through neutral alumina (bottom), both in MeCN-d_3. Insets are the region with the BF_2 peak. The broad peak in the baseline of the ^{11}B spectrum is attributed to the borosilicate glass of the NMR tube.

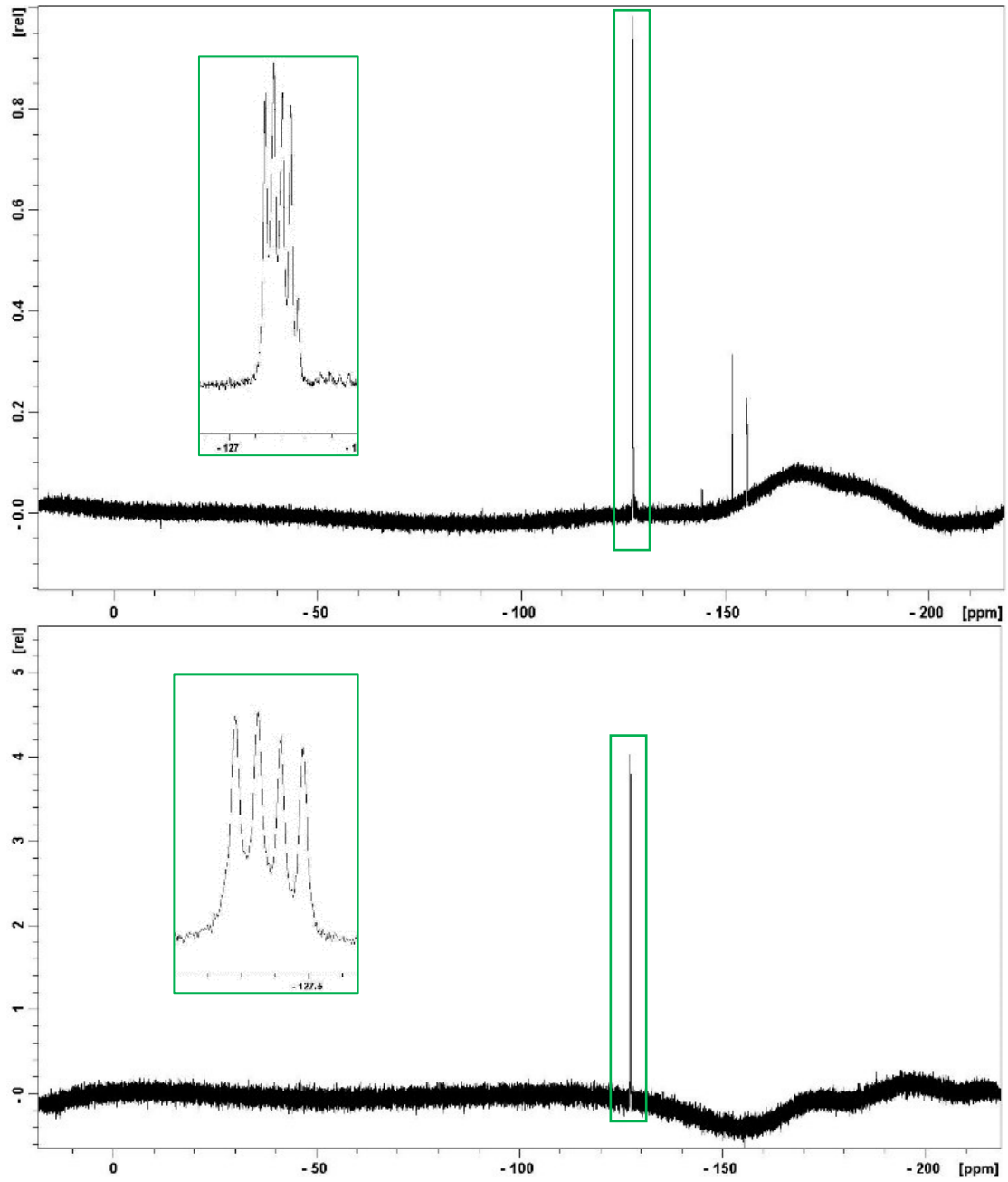

Figure 5-10. ^{19}F NMR comparisons of **5.17** synthesized *via* **5.7** (top) and the product from the reaction of **Py$_2$TTAH** with $BF_3{\cdot}OEt_2$, following purification through neutral alumina (bottom), both in MeCN-d_3. Insets are the region with the BF_2 peak. The broad peak in the baseline of the ^{19}F spectrum is due to a poor signal to noise ratio due to the limited solubility of **5.17** in MeCN-d_3.

5.4 Conclusions

In conclusion, this chapter reports the synthesis and characterization of a BF_2 containing compound, most likely a boratriazine ring, *via* two different synthetic routes; starting from either **5.7** or **Py_2TTAH**. Analysis was carried out using NMR spectroscopy on multiple nuclei, absorption and fluorescence spectroscopy, as well as theoretical DFT computations. The spectroscopic studies revealed that a symmetrical BF_2 containing complex was formed, with the most likely structure being the boratriazine **5.17**. While further purification and characterization is still required, it is clear that the inclusion of BF_2 functional groups into triazine rings holds potential for future studies as a fluorescent material.

5.5 Future Work

The next step in the analysis of compound **5.17** is purification, and obtaining crystals suitable for X-ray diffraction analysis. By studying the solid state packing of this molecule, its potential for future applications in materials chemistry can be explored, as the extent of orbital overlap between neighbouring molecules is of great importance to charge transport devices. Therefore, measuring the close contacts in the molecule through single crystal XRD analysis may elucidate whether **5.17** may be a promising candidate for such applications.

Considering the possibility of boron coordination in the tridentate pocket of **Py_2TTAH**, pentacoordinate coordination may yet be possible. Looking at the chemical shift of the ^{19}F quartet observed in Figures 5-6 and 5-7, this signal occurs at a much lower chemical shift (~ -140 ppm) compared with the peak from complex **5.17** (~ -127 ppm), suggesting a different compound was formed from the reactions in toluene that yielded a minor BF_2 containing product. It is therefore possible that with the right conditions, deprotonation of the central **TTA** nitrogen followed by pentacoordinate BF_2 incorporation may be possible.

Finally, boron coordination studies could be expanded into pyrimidyl derivatives of both the imidoyl amidine and thiatriazine starting materials. The replacement of pyridyl substituents with pyrimidyl heterocycles would allow for multiple coordination sites and the potential for multi-boron complexes. Furthermore, through functionalization of the imine nitrogen atoms in **5.7**, or by changing the substituents attached to the boron atom, the molecular orbital energies and properties of the molecules can be fine-tuned.

5.6 Experimental Details

5.6.1 General Procedures

The reagents sodium hydride (60% dispersion in mineral oil, Alfa Aesar) and triethylamine (Sigma-Aldrich) were obtained commercially and used as received.

$BF_3{\cdot}OEt_2$ was distilled over calcium hydride. THF and toluene were dried by passing them through activated alumina on a J.C. Meyer solvent purification system and stored over 4Å Molecular sieves. All other solvents were reagent grade. *N*-2-pyridylimidoyl-2-pyridylamidine (**5.7**) and 3,5-*bis*(2-pyridyl)-4-hydro-1,2,4,6-thiatriazine (**Py_2TTAH**; **5.14**) were prepared as outlined in the literature.[26] All reactions were performed under an atmosphere of dry nitrogen unless otherwise stated. ^{1}H NMR, ^{11}B NMR, and ^{19}F NMR spectra were run in MeCN-d_3 solutions at room temperature on Bruker Avance 400 MHz or Bruker Avance 300 MHz spectrometers. IR spectra of solid samples were recorded on an Agilent Technologies Cary 630 FT-IR spectrometer. UV-visible spectra were measured using an Agilent Cary 5000 UV-Vis-NIR spectrophotometer in the range 200 – 1200 nm. Fluorescence spectra were obtained using a Varian Cary Eclipse fluorescence spectrometer. Solution absorption and emission measurements were completed using MeCN solutions with standard 10 mm pathlength cuvettes.

5.6.2 Computational Chemistry

All calculations were carried out using the Gaussian09 program package.[23] The geometries of the studied compounds were investigated using the hybrid density functional B3LYP with the 6-311+G(2d,p) basis set. Optimized structures were used to examine the orbital energies and frontier molecular orbital probabilities.

5.6.3 Synthetic Details

5.17 ***via*** **5.7**. In an inert atmosphere, triethylamine (337 mg, 3.33 mmol) was added to a stirring slurry of **5.7** in THF (10 mL). After 30 minutes, $BF_3{\cdot}OEt_2$ was added *via* syringe. The resulting yellowy mixture was refluxed for 24 hours before quenching with H_2O. The resulting precipitate was filtered, washed with cold THF and dried in air. Crude yield: 137 mg (0.503 mmol, 45%). ^{1}H NMR (δ, MeCN-d3): 9.59 (2H, s, br), 8.76, (2H, ddd, J = 4.7, 1.7, 0.8 Hz, Ar), 8.71 (2H, ddd, J = 7.9, 1.0, 1.0 Hz, Ar), 8.06 (2H, ddd, J = 7.8, 7.7, 1.7 Hz, Ar), 7.65 (2H, ddd, J = 7.6, 4.7, 1.1 Hz, Ar). ^{11}B NMR (δ, MeCN-d3): 0.05 (t, J = 25.7 Hz). ^{19}F NMR (δ, MeCN-d3): -127.9 (q, J = 25.2 Hz). IR ν_{max} (cm^{-1}): 3100 (w), 1596 (m), 1575 (m), 1526 (s), 1496 (m), 1456 (m), 1434 (m), 1319 (m), 1288 (m), 1187 (m), 1151 (m), 1056 (s), 1010 (s), 918 (w), 899 (w), 871 (w), 805 (m), 774 (m), 724 (m), 675 (w).

5.17 ***via*** **Py_2TTAH.** Under an inert atmosphere, triethylamine (145 mg, 1.43 mmol) was added to a stirring solution of **Py_2TTAH** (250 mg, 0.98 mmol) in toluene (10 mL). After 30 minutes, $BF_3{\cdot}OEt_2$ was added *via* syringe. The mixture was stirred at reflux for 24 hours before quenching with H_2O. The product was extracted into DCM, dried over Na_2SO_4, filtered, and the solvent removed under reduced pressure, resulting in a black solid. Crude yield: 0.3 g. Partial purification was achieved by short-column chromatography on neutral alumina (DCM) yielding a yellow residue after the solvent was removed under reduced pressure. Yield < 10%. Spectroscopic data were identical to those for material prepared *via* **5.7**.

5.7 References

1. S. Mukherjee and P. Thilagar, *Journal of Materials Chemistry C*, 2016, **4**, 2647-2662.
2. A. Loudet and K. Burgess, *Chemical Reviews*, 2007, **107**, 4891-4932.
3. J. E. Milks, J. H. Polevy and G. W. Kennerly, *Journal of the American Chemical Society*, 1962, **84**, 2529-2534.
4. V. A. Dorokhov, G. A. Stashina, V. M. Zhulin and B. M. Mikhailov, *Doklady Akademii Nauk Sssr*, 1981, **258**, 351-353.
5. Mikhailo.Bm, V. A. Dorokhov and Seredenk.Vi, *Doklady Akademii Nauk Sssr*, 1971, **199**, 1328.
6. Mikhailo.Bm, V. A. Dorokhov and Seredenk.Vi, *Zhurnal Obshchei Khimii*, 1973, **43**, 862-867.
7. Mikhailo.Bm, V. A. Dorokhov and Lavrinov.Li, *Zhurnal Obshchei Khimii*, 1974, **44**, 1888-1891.
8. B. M. Mikhailov, V. A. Dorokhov and V. I. Seredenko, *Bulletin of the Academy of Sciences of the Ussr Division of Chemical Science*, 1978, **27**, 1205-1210.
9. B. M. Zolotarev, O. S. Chizhov, V. A. Dorokhov, L. I. Lavrinovich and B. M. Mikhailov, *Bulletin of the Academy of Sciences of the Ussr Division of Chemical Science*, 1978, **27**, 1140-1143.
10. I. Hager, R. Frohlich and E. U. Wurthwein, *European Journal of Inorganic Chemistry*, 2009, 2415-2428.
11. C. Glotzbach, N. Godeke, R. Frohlich, C. G. Daniliuc, S. Saito, S. Yamaguchi and E. U. Wurthwein, *Dalton Transactions*, 2015, **44**, 9659-9671.
12. S. A. Tikhonov and V. I. Vovna, *Journal of Structural Chemistry*, 2015, **56**, 446-453.
13. V. G. Gerasimova, A. I. Razgonov and V. I. Tsarev, *Izvestiya Vysshikh Uchebnykh Zavedenii Khimiya I Khimicheskaya Tekhnologiya*, 1992, **35**, 31-35.
14. D. Y. Lee and J. C. Martin, *Journal of the American Chemical Society*, 1984, **106**, 5745-5746.

15. M. Yamashita, Y. Yamamoto, K. Akiba and S. Nagase, *Angewandte Chemie-International Edition*, 2000, **39**, 4055-4058.

16. M. Yamashita, Y. Yamamoto, K. Y. Akiba, D. Hashizume, F. Iwasaki, N. Takagi and S. Nagase, *Journal of the American Chemical Society*, 2005, **127**, 4354-4371.

17. C. D. Dou, S. Saito and S. Yamaguchi, *Journal of the American Chemical Society*, 2013, **135**, 9346-9349.

18. J. Y. Nakatsuji, Y. Moriyama, S. Matsukawa, Y. Yamamoto and K. Y. Akiba, *Main Group Chemistry*, 2007, **5**, 277-285.

19. G. P. McGovern, D. Zhu, A. J. A. Aquino, D. Vidovic and M. Findlater, *Inorganic Chemistry*, 2013, **52**, 13865-13868.

20. Y. Hirano, S. Kojima and Y. Yamamoto, *Journal of Organic Chemistry*, 2011, **76**, 2123-2131.

21. S. M. Barbon, V. N. Staroverov, P. D. Boyle and J. B. Gilroy, *Dalton Transactions*, 2014, **43**, 240-250.

22. S. M. Barbon, P. A. Reinkeluers, J. T. Price, V. N. Staroverov and J. B. Gilroy, *Chemistry-a European Journal*, 2014, **20**, 11340-11344.

23. M. J. Frisch, G. W. Trucks, H. B. Schlegel, G. E. Scuseria, M. A. Robb, J. R. Cheeseman, G. Scalmani, V., Barone, B. Mennucci, G. A. Petersson, H. Nakatsuji, M. Caricato, X. Li, H. P. Hratchian, A. F. Izmaylov, J., Bloino, G. Zheng, J. L. Sonnenberg, M. Hada, M. Ehara, K. Toyota, R. Fukuda, J. Hasegawa, M. Ishida, T., Nakajima, Y. Honda, O. Kitao, H. Nakai, T. Vreven, J. J. A. Montgomery, J. E. Peralta, F. Ogliaro, M., Bearpark, J. J. Heyd, E. Brothers, K. N. Kudin, V. N. Staroverov, R. Kobayashi, J. Normand, K., Raghavachari, A. Rendell, J. C. Burant, S. S. Iyengar, J. Tomasi, M. Cossi, N. Rega, J. M. Millam, M., Klene, J. E. Knox, J. B. Cross, V. Bakken, C. Adamo, J. Jaramillo, R. Gomperts, R. E. Stratmann, O., Yazyev, A. J. Austin, R. Cammi, C. Pomelli, J. W. Ochterski, R. L. Martin, K. Morokuma, V. G., Zakrzewski, G. A. Voth, P. Salvador, J. J. Dannenberg, S. Dapprich, A. D. Daniels, O. Farkas, J. B., Foresman, J. V. Ortiz, J. Cioslowski and D. J. Fox, *Gaussian 09, Revision A.02*, Gaussian, Inc., Wallingford CT, 2009.

24. D. L. Pavia, G. M. Lampman, G. S. Kritz and J. R. VyVyan, *Introduction to Spectroscopy*, Cengage Learning, Stamford, CT, 5th Edition edn., 2015.

25. S. M. Barbon, J. T. Price, U. Yogarajah and J. B. Gilroy, *Rsc Advances*, 2015, **5**, 56316-56324.

26. A. A. Leitch, I. Korobkov, A. Assoud and J. L. Brusso, *Chemical Communications*, 2014, **50**, 4934-4936.

Chapter 6 – Conclusions

6.1 Conclusions

This thesis describes the synthesis and study of post-functionalized thiatriazine (**TTA**) compounds. The **TTA** ring is attractive to investigate due to the large number of heteroatoms in the system and its redox stability.[1] Post-functionalization of the **TTA** core is of particular interest, as it provides a facile route for the tunability of chemical properties, thus enabling the synthesis of a variety of candidates for molecular materials. To that end, post-functionalization of 3,5-*bis*(2-pyridyl)-4-hydro-1,2,4,6-thiatriazine (**Py_2TTAH**) and its precursor materials have been achieved *via* alkylation and arylation, as well as through iron coordination and boron incorporation.

Chapter 2 describes alkylation work performed in pursuit of a biradical species based on the *bis*-*N*-bridgehead-1,2,5-thiadiazolium dication, an intermediate in the synthesis of **Py_2TTAH**. While alkylation of **Py_2TTAH** was achieved, it was found that alkylation occurred on the sulfur atom instead of the desired nitrogen. While the biradical synthesis continues to elude us, the discovery of sulfur-functionalization has elucidated the reactivity of these systems and suggested new methods for tuning their properties.

The proclivity of the sulfur atom towards alkylation was analyzed and explored further in Chapter 3. It was found that neutral *S*-alkylated species could be isolated *via*

both cationic and anionic routes, depending on the electrophilicity of the alkylating agent. The neutral species, as well as the isolable intermediates, were characterized by single crystal X-ray diffraction and absorption spectroscopy, and the findings were compared to computational results obtained through theoretical DFT calculations. In addition to *S*-alkylated derivatives, work has also been extended to the addition of aryl groups. The synthesis of ***S*-Ph-Py$_2$TTA** has been demonstrated through reactions with hypervalent iodine electrophiles. The synthetic procedure developed here is anticipated to provide a versatile route towards further aryl functionalization, such as the addition of a heterocycle at the sulfur position.

Chapter 4 details the synthesis and characterization of two iron coordination complexes with the tridentate **Py$_2$TTA** framework. The first was an Fe(III) system with a tridentate ***S*-Me-Py$_2$TTA** ligand. This complex demonstrates that functionalized **TTA** rings are suitable candidates for future studies. The second complex described was an Fe(II) centre coordinated by two tridentate **Py$_2$TTA$^-$** ligands. While reproducibility issues were encountered, the crystal structures obtained represent chemically intriguing systems, which deserves further study.

Functionalization of **Py$_2$TTAH** and its precursor *N*-2-pyridylimidoyl-2-pyridylamidine was further explored using a boron difluoride moiety, as discussed in Chapter 5. The reaction between boron trifluoride etherate and either *N*-2-

pyridylimidoyl-2-pyridylamidine or **Py_2TTAH** afforded the same boratriazine product, which was found to fluoresce purple under UV light, an attractive property for future investigations into material applications.

Overall, this thesis provides the groundwork for a number of interesting and exciting methods for the post-functionalization of **Py_2TTAH**. These methods, and the resulting compounds, are the first steps in the development of more complex **TTA** derivatives. The post-functionalization of **TTA** rings, as described in this thesis, holds significant potential for future studies into molecular materials due to the versatile synthetic routes and the possibilities for chemical tunability of the final products. This thesis outlines preliminary studies that can be used as a starting point for future functionalization towards liquid crystalline materials, metal coordination, and optoelectronic applications such as solar cells or OLEDs, to name a few.

6.2 References

1. R. T. Boere, A. W. Cordes, P. J. Hayes, R. T. Oakley, R. W. Reed and W. T. Pennington, *Inorganic Chemistry*, 1986, **25**, 2445-2450.

Appendix – Crystallographic Details

A.1 Crystallographic Details from Chapter 3

Data collection results for compounds **3.13**, **3.14**, **3.15**, **3.17** and **3.19** represent the best data sets obtained in several trials for each sample. The crystals were mounted on thin glass fibers using paraffin oil. Prior to data collection crystals were cooled to 200(2) K (3.13, 3.14, 3.17, and 3.19) and 258(2) K (3.15). Data was collected on Bruker AXS SMART and KAPPA single crystal diffractometers equipped with sealed Mo tube sources (wavelength 0.71073 Å) and APEX II CCD detectors. Raw data collection and processing was performed with the APEX II software package from BRUKER AXS.[1] Diffraction data for **3.13** and **3.17** were collected with a sequence of 0.3° ω scans at 0, 90, 180 and 270° in φ in order to ensure adequate data redundancy. Initial unit cell parameters were determined from 60 data frames with 0.3° ω scan each, collected at the different sections of the Ewald sphere. Diffraction data for **3.14**, **3.15** and **3.19** were collected with a sequence of 0.5° ω and φ scans. Semi-empirical absorption corrections based on equivalent reflections were applied.[2] Systematic absences in the diffraction data-set and unit-cell parameters were consistent with triclinic $P\bar{1}$ (№2) for **3.13** and **3.19**, orthorhombic $P2_12_12_1$ (№19) for **3.15** and **3.17**, and orthorhombic *Pbca* (№61) for **3.14**. Solutions in the centrosymmetric space groups for **3.13**, **3.14** and **3.17** yielded chemically reasonable and computationally stable results of refinement. However, data for compounds **3.15** and **3.17** suggested non-centrosymmetric chiral space groups for

the structural model. The structures were solved by direct methods, completed with difference Fourier synthesis, and refined with full-matrix least-squares procedures based on F^2.

Solving structural model for **3.13** revealed one dimeric unit associated by two symmetry related iodine atoms I(1) and I(1A). Dimeric unit is located on one of the inversion centers of the space group.

The structural model of **3.14**, similar to **3.13** contains symmetry related sodium [Na(1) and Na(1A)] and iodine [I(1) and I(1A)] atoms surrounding the centre of inversion, with four bridging ligands extending away from the inversion centre.

For **3.15** the Flack x parameter is -0.05(3), which supports the chosen absolute structural configuration.

Structural model of **3.17** consists of two oppositely charged fragments located in the general positions of the asymmetric unit. Refinement of the structure in the chiral space group settings yield -0.02(3) Flack x parameter, suggesting that a correct absolute structural configuration was chosen for the structural model.

The structural model of **3.19** indicated three charged fragments in the asymmetric unit, one dication and two anions. One of triflate anions was modelled as disordered over three positions with 0.435(1):0.435(1):0.131(2) occupancy ratio.

Restraints, mainly for the S-C-F angle (S-F distance), C-F distance, and S-C distance were applied to make the molecule symmetrical and set its geometry equal for all three positions. 'Enhanced' rigid-bond restraints were also introduced for atom ADPs. Constraints for sulfur and oxygen atoms were applied, equalizing ADPs for the first two positions.

Structural models were successfully refined with a full set of anisotropic thermal motion parameters for all non-hydrogen atoms. All hydrogen atom positions were calculated based on the geometry of related non-hydrogen atoms. All hydrogen atoms were treated as idealized contributions during the refinement. All scattering factors are contained in several versions of the SHELXTL program library, with the latest version used being v.6.12.[3]

Table A-1. Crystallographic data and selected collection parameters for **3.13** (**[Na(*μ*-I)(*S*-Et-Py$_2$TTA)]$_\infty$**), **3.14** (**[Na(*μ*-I)(*S*-Me-Py$_2$TTA)]$_\infty$**), **3.15** (***S*-Et-Py$_2$TTA**), **3.17** (**[*S*-Et-Py$_2$TTA][BF$_4$]**), and **3.19** (3,5-*bis*(*N*-methyl-2-pyridinium)-*S*-methyl-1,2,4,6-thiatriazine dication).

Parameters	**3.13**	**3.14**	**3.15**	**3.17**	**3.19**
Empirical formula	$C_{14}H_{13}IN_5NaS$	$C_{13}H_{11}IN_5NaS$	$C_{14}H_{13}N_5S$	$C_{14}H_{14}BF_4N_5S$	$C_{17}H_{17}F_6N_5O_6S_3$
Formula weight	433.24	419.22	283.35	371.17	597.53
Crystal system	triclinic	orthorhombic	orthorhombic	orthorhombic	triclinic
Space group	$P\bar{1}$	*Pbca*	$P2_12_12_1$	$P2_12_12_1$	$P\bar{1}$
a (Å)	10.1629(3)	16.9522(14)	5.799(3)	9.9995(2)	8.938(4)
b (Å)	10.3262(3)	9.6979(7)	14.641(9)	10.0313(2)	11.927(5)
c (Å)	10.3488(3)	18.6808(13)	16.056(10)	16.1233(4)	12.900(5)
α (deg)	109.4798(8)	90	90	90	96.902(19)
β (deg)	116.3682(8)	90	90	90	108.004(18)
γ (deg)	102.2525(9)	90	90	90	107.987(17)
V (Å$_3$)	829.69(4)	3071.1(4)	1363.2(14)	1617.30(6)	1208.1(8)
Z	2	8	4	4	2
D_{calc} (mg/m3)	1.734	1.813	1.381	1.524	1.643
T (K)	200(2)	200(2)	258(2)	200(2)	200(2)
μ (mm^{-1})	2.084	2.249	0.234	0.250	0.398
θ range for data collection (deg)	2.313 to 28.43	2.403 to 28.060	1.882 to 28.089	2.397 to 28.28	2.198 to 34.352
no. of total reflections	8711	23517	11126	14055	25311
no. of unique reflections	4062	3698	3294	3960	9183
R_{int}	0.0109	0.2779	0.0331	0.0279	0.0202
R1, WR_2 (on F_2)	0.0167, 0.0434	0.0640, 0.0989	0.0419, 0.0933	0.0424, 0.1191	0.0485, 0.1266

A.2 Crystallographic Details from Chapter 4

Data collection results for compounds **4.6** and **4.8** represent the best data sets obtained in several trials for each sample. The crystals were mounted on thin glass fibers using paraffin oil. Prior to data collection, crystals were cooled to 200(2)K. Data was collected on Bruker AXS SMART and KAPPA single crystal diffractometers equipped with sealed Mo tube sources (wavelength 0.71073 Å) and APEX II CCD detectors. Data collection and processing were performed with the Bruker APEX II software package.[1] Semi-empirical absorption corrections based on equivalent reflections were applied.[4] The structure was solved by direct methods and refined with full-matrix least-squares procedures using SHELXL[5] and WinGX.[6] All non-hydrogen atoms were refined anisotropically. The positions of hydrogen atoms were calculated based on the geometry of related non-hydrogen atoms.

The structural model for **4.6** revealed 4 molecules contained within the unit cell. These molecules surround an inversion centre in the middle of the unit cell.

Based on the structural model for **4.8**, the main molecule and the THF molecule lie on 4-fold rotoinversion axes. Both are disordered over two positions with equal occupancies (0.5 : 0.5).

Table A-2. Crystallographic data and selected collection parameters for **4.6** (**Fe(*S*-Me-Py$_2$TTA)Cl$_3$**) and **4.8** (**[Fe(Py$_2$TTA)$_2$]·THF**).

Parameters	**4.6**	**4.8**
Empirical formula	$C_{13}H_{11}Cl_3FeN_5S$	$C_{28}H_{24}FeN_{10}OS_2$
Formula weight	431.53	636.54
Crystal system	monoclinic	tetragonal
Space group	$P2_1/n$	$I\bar{4}$
a (Å)	8.6072(3)	8.9344(12)
b (Å)	18.1628(7)	8.9344(12)
c (Å)	11.2827(4)	17.560(2)
α (deg)	90	90
β (deg)	107.765(2)	90
γ (deg)	90	90
V (Å$_3$)	1679.73	1401.7(4)
Z	4	2
D_{calc} (mg/m3)	1.706	1.508
T (K)	200(2)	200(2)
μ (mm^{-1})	1.503	0.730
θ range for data collection (deg)	2.202 to 27.895	2.320 to 28.460
no. of total reflections	27754	8638
no. of unique reflections	3994	1757
R_{int}	0.0543	0.0207
R1, WR_2 (on F_2)	0.0305, 0.0656	0.0254, 0.0640

A.3 References

1. W. Bruker, *APEX Spftware Suite*, AXS, Madison, 2005.
2. R. H. Blessing, *Acta Crystallographica Section A*, 1995, **51**, 33-38.
3. G. M. Sheldrick, *Acta Crystallographica Section A*, 2008, **64**, 112-122.
4. G. M. Sheldrick, *SADABS, Program for Empirical X-ray Absorption Correction*, Bruker-Nonius, 2004.
5. G. M. Sheldrick, *Acta Crystallographica Section C-Structural Chemistry*, 2015, **71**, 3-8.
6. L. J. Farrugia, *Journal of Applied Crystallography*, 1999, **32**, 837.